THE APPLICATION OF PLANAR OPTICAL WAVEGUIDES TO ABSORPTION SPECTROMETRY IN FLOW INJECTION ANALYSIS.

by

Steven Joseph Choquette

Dissertation submitted to the Faculty of the
Virginia Polytechnic Institute and State University
in partial fulfillment of the requirements for the degree of

DOCTOR OF PHILOSOPHY

in

Chemistry

Approved:

R.E. Dessy, Chairman

T.C. Ward

J.G. Mason

J.G. Dillard

G.L. Long

January, 1988

Blacksburg, Virginia

THE APPLICATION OF PLANAR OPTICAL WAVEGUIDES TO ABSORPTION SPECTROMETRY IN FLOW INJECTION ANALYSIS.

by

Steven Joseph Choquette

Committee Chairman: Raymond E. Dessy

Chemistry

(ABSTRACT)

Attenuated total reflection techniques have been used extensively as analytical tools for the analysis of thin films and analytes imbedded in complex scattering matrices. However they have not been commonly utilized as detectors in common analytical techniques such as Flow Injection Analysis because of their relatively low sensitivity. The feasibility of using a thin film planar waveguide as an absorption sensor in the Flow Injection Analysis of Urea was investigated.

Urea was hydrolyzed to ammonia and carbon dioxide with the enzyme Urease. The ammonia produced was quantitated colorimetrically using Berthelot's reaction. The reaction product, indophenol blue, was detected using the combination planar waveguide 9.2 microliter flow cell sensor.

The planar waveguides used had 2 to 3 orders of magnitude greater sensitivity than typical internal reflection elements. The analytical working range obtained

for urea determinations was from 0 to 20 mM urea at a rate of 30 samples per hour.

A description of the investigation and the various factors involved in designing and optimizing a planar waveguide for absorption spectrometry is included.

ACKNOWLEDGEMENTS

The completion of this dissertation would not have been possible without the efforts of a number of people who have generously contributed their time, patience, and expertise. Although there are too many to acknowledge in this brief space, several deserve recognition.

, , , and coworkers in the Physics Machine Shop provided tireless advice and rescued several seemingly hopeless projects. All mechanical aspects of this project are attributable to the efforts of these men. and of the Chemistry Glass Shop also provided important assistance and were never too busy to stop and discuss ideas.

The members of the group, especially and , provided a useful forum to air and evaluate ideas, many of which have been incorporated into this project. and provided the environment in which these ideas were realized. I am also grateful to Dr. Mason for generously providing many hours of advice and sharing his experiences regarding the chemical aspects of this dissertation.

Finally I would like to thank my wife, , and my family for providing the moral and financial support necessary to complete this dissertation.

to , my inspiration, my teacher, and my father.

TABLE OF CONTENTS

LIST OF FIGURES

LIST OF TABLES

I. INTRODUCTION

Planar optical waveguides have been used in spectroscopy since the introduction of the Attenuated Total Reflection technique by Harrick[1] and Fahrenfort[2] in the early 1960's. These devices are nothing more than a thin slab of a dielectric material, such as silicon or germanium, which has a high index of refraction. Under the proper conditions, a beam can be introduced into and confined within this slab. As the beam traverses the length of the slab, it will bounce against the surface of this waveguide and interact with the surrounding media. By placing a sample on the surface and scanning the wavelength of the guided beam, these devices are able to obtain very high quality absorbance spectra of samples impossible to analyze by conventional transmission spectroscopic techniques. Such samples, as very thin films, or analytes imbedded in complex scattering matrices, are easily accommodated by this technique.

Although ATR has seen considerable use in qualitative analytical spectroscopy, it has not been as widely used as a tool for quantitative analytical spectrometry. The reason for this is that many analytical measurements occur in a flowing stream. Whether it is a chromatographic technique such as HPLC, or a analytical flow method such as Flow Injection Analysis, optical detection schemes for these

methods must fulfill two strict criteria. The first is that the optical path length must be as large as possible to increase sensitivity. The second is that the flow cell incorporating this optical path must have as small a sample volume as possible to increase resolution. Unfortunately the geometry of the typical internal reflection element conflicts with these two goals.

The optical path length, or number of interactions with the surface of the internal reflection element, can be increased in two ways. By lengthening the element, the total number of interactions with the sample is increased. This, however, is not a viable option if low sample volume is a goal for the flow cell incorporating this device. If the thickness of the slab is decreased, the total number of interactions per unit length increases. However, as the thickness of the element approaches the beam width, the guided beam will begin to interfere with itself and seriously affect the sample absorption spectra. As a consequence of this phenomena, the width of internal reflection elements are typically greater than 1 millimeter, limiting the number of interactions with the surface to approximately 10-20 interactions per centimeter. Unless a Fourier Transform instrument (FTIR) is used as a detector, the number of interactions with the sample is usually too small for use with analytical methods in flowing streams[3].

However, if the object is not to obtain a complete spectra of the sample, but simply to monitor the absorbance at a specified wavelength, under special conditions a coherent, monochromatic beam can be coupled into a thin film waveguide. These planar optic guides can be as thin as a few tenths of a micron and the corresponding number of interactions at the surface of the waveguide can vary from several hundred to several thousand per centimeter. The optical path length can therefore be effectively increased by three orders of magnitude over the standard internal reflection element. This research project will focus on the feasibility of using these thin film optical waveguides as an absorption sensor in a flowing stream.

Flow injection analysis, FIA, was chosen as a realistic analytical method under which to test these devices. In FIA a sample is injected into a carrier stream. Using the principle of controlled dispersion, it is mixed and eventually produces a measurable response. Because the dispersion is highly controlled, samples can be injected onto the FIA manifold at a uniform rate, and yet be completely resolved at the detector. This technique is applicable to a wide range of analytical methods, and was developed to permit the analysis of several hundred to several thousand samples a day. Although FIA methods do not commonly require an ultra sensitive detection scheme, they do require a detector that is durable and precise. For this

reason, an FIA method was chosen as a rigorous test of the utility of a planar waveguide sensor.

The specific analysis chosen to characterize these devices was the FIA of urea. Urea is one of the by-products of amino acid degradation in terrestrial vertebrates. Amino acids, in excess of those required for protein synthesis, are neither stored nor excreted, but rather are used as metabolic fuels. The carbon skeletons of amino acids are converted into a variety of molecules including fatty acids, ketones, and glucose. The amino groups are typically transferred to α ketoglutarate, which is then oxidatively deaminated to yield NH_4^+.[4] The NH_4^+ is then converted to urea in the liver and excreted. The synthesis of urea in the liver is the only known route of removal of NH_4+ from the body[5].

The determination of urea is important, as elevated serum levels of urea and blood ammonia are toxic and can be indications of impaired renal function[5]. The normal concentration of serum urea is between 1 and 8 millimolar, with the normal analytical working range between 1 and 20 millimolar urea[6]. Although many techniques exist for the analysis of urea, only two optical methods are currently in use. The first is a colorimetric method detecting the diazine derivative of urea formed by the reaction of diacetyl monoxime with urea. Urea is directly analyzed in this sensitive method, but the reaction product rapidly

fades and the reaction products do not follow Beer's law[6]. The more popular colorimetric technique is the use of Berthelot's reaction[6]. In this reaction ammonia is oxidatively coupled to phenol to form the dye indophenol blue. Berthelot's reaction produces linear calibration curves, is specific for ammonia, and yields a stable product. The disadvantage of applying this reaction to the analysis of urea, however, is that urea must first be hydrolyzed to ammonia with the enzyme urease, increasing the cost and complexity of the analysis. Berthelot's analysis, however, is conveniently automated and will form the basis of the technique used to test the feasibility of a planar optic waveguide as an absorption sensor in an FIA method.

II. HISTORICAL

Planar dielectric waveguides were well understood and used in microwave engineering previous to 1960[7]. However, it was not until 1964 when Osterberg and Smith[8] discovered that light coupled into plate glass with a prism, at angles close to the critical angle for total internal reflection, could be transmitted along the surface of the glass. They subsequently determined that for effective transmission of the beam, the surface of the glass necessarily had a higher index of refraction than the bulk[9]. Although they used a collimated mercury lamp rather than a laser, their set-up is regarded as the first rudimentary implementation of an optical guided-wave apparatus. In 1965 Anderson[10] combined these concepts with photolithography and produced the first thin film dielectric waveguides for use in the infrared.

The combination of the development of the laser and fiber optics promised virtually unlimited communications bandwidth. However, it soon was realized that for efficient transmission over large distances, optical repeaters would be necessary to periodically reshape and reamplify the optical signal. Although, at the time such repeaters could be built in the laboratory from conventional optical devices, Miller[11] recognized that in order to realize the advantages of fiber optic transmission, these repeaters would have to be miniaturized. He coined the term

Integrated Optics, to describe a technology whereby the optical and electrical components of such a repeater were miniaturized and placed onto a single chip. Since then considerable progress has been made in developing the two dimensional counterparts of such a repeater. Components such as planar lenses[12], electro-optical switches[13], semiconductor lasers, and beam modulators[14] are now well understood and commercially available. One of the major contributions of integrated optics has been in the area of signal processing. Through the combination of a laser source, collimating optics, waveguide, acoustic diffraction grating, and detector, a real time RF spectrum analyzer was fabricated[15] on a single substrate.

Although the major research efforts in fiber and integrated optics are directed towards communications applications, signal processor and sensor technology has benefitted greatly from the developments in these areas. Numerous fiber optic sensors have been described which measure nearly every conceivable physical phenomena, whether it be temperature, acoustic, magnetic, pressure or chemical in nature. Phase sensitive integrated optic sensors, based on the Mach Zehnder interferometer, have been described for temperature[16], pressure[17] and displacement[18] sensing. Planar optic sensors have been slower to develop, largely as a result of the much lower optical path length of these devices. The possible application of these thin film planar

optic waveguides to chemical analysis was however, not lost upon the original researchers in the field.

Attenuated total reflection techniques were becoming quite popular by the late 1960's and Midwinter, an early researcher in the field of integrated optics, appears to have been the first to recognize the possible extension of these thin film dielectric waveguides to absorption spectroscopy[19]. In his theoretical paper he described a symmetric waveguide (a waveguide surrounded by a homogeneous media) which could be covered by a thin cladding material that possessed the same index of refraction as the absorbing media. This ostensibly was to prevent attenuation of the guided beam due solely to index differences between the sample and blank solutions. The result of his calculations showed that the attenuation of the guided wave relative to the attenuation of a wave propagating in the solution alone, was a complex function of the guide properties and guided mode parameters. Nevertheless, in the limiting case of a very thin symmetric waveguide, the results indicated that half of the guided wave traveled in the waveguide, while half traveled as an evanescent wave in the rarer absorbing media. It was suggested that the propagation ratio, in this case 0.5, be used as a figure of merit for sensitivity. Although the device was not built, and no experimental data was published, Midwinter demonstrated that the device should be about 10^3 to 10^4 times more sensitive than an ATR device

and comparable in sensitivity to the transmission experiment.

One year later, Polky and Harris[20] extended the theory to include asymmetric waveguides (a guide supported on a substrate with a different index of refraction than the cladding). Their stated goal was to develop a small spectrophotometric device that could be used in the human body and sample the local environment through absorption of the evanescent wave. The theoretically determined sensitivity of their device, a thin film of a high index glass sputtered onto a microscope slide, was much lower than that predicted by Midwinter. Rather than a propagation ratio of 0.5, predicted for the symmetric guide, the theoretically calculated sensitivity of the asymmetric guide was, depending upon the guide parameters, less than .02. The sensitivities of these waveguides were experimentally determined using the dye methylene blue. The calibration curves of dye absorbance versus dye concentration were, for the most part, much steeper than anticipated, although in some cases the guides appeared saturated and would not respond to further increases in dye concentration. This behavior was attributed to the adsorption of methylene blue onto the surface of the guide. Harris and Polky concluded that both direct bulk absorption from the evanescent portion of the wave and absorption by adsorbed molecules were responsible for guide attenuation. Consequently, they

suggested that thin film waveguides could become a useful device for observing surface reactions.

Mitchell[21] expanded on Polky and Harris's work and described a planar optic device for the determination of bilirubin in whole blood. Utilizing the fact that the evanescent field penetration was on the order of 0.1 micron, he demonstrated that absorption data could be obtained for an analyte in a highly scattering media. While very little quantitative information was reported, this was the first demonstration that a thin film planar waveguide could retain some of the sampling advantages of an ATR element, while yielding a higher sensitivity.

After Mitchell's work, very little is reported on planar optic waveguide chemical sensors, as fiber optic waveguides curried the favor of the chemical community. During this time, however, several other unique applications of planar waveguides to chemical analysis were discovered. Levy[22] et al were the first to examine the Raman spectra of very thin polymer films by casting them on a substrate and using them as a planar waveguide. They reported excellent signal to noise ratios for thick films (>6 microns), but noted that for films less than 1 micron thick considerable noise and significant band broadening were present, due to interference from the substrate. Rabolt[23] and coworkers later improved the technique and were able to obtain Raman spectra of very thin polymer films and Langmuir-Blodgett[24]

monolayers. Borrowing a technique developed by Swalen[25], they sandwiched these films between the substrate and a thicker polymer, or sputtered glass waveguide. From these measurements and the polarization dependence of the Raman scattering, Rabolt was able to determine the configuration of these molecules on the surface of the waveguide. Extending these concepts, Swalen[26] and Rabolt were later able to study the Raman spectra of the interface region between two laminated polymer films.

Swalen[20] and coworkers applied the method to the determination of absorption spectra of organic molecules and monolayers. By depositing a Langmuir-Blodgett film on or under the surface of a thin film polymer waveguide, they were able to obtain excellent absorption spectra of these thin film assemblies. Although the technique produced higher absorbances than the corresponding ATR method, it was much less convenient. As a consequence of the physics of the device, the waveguide had to be retuned for each spectral data point acquired. However, because a clean separation of polarization was possible, the orientation of the molecules could be derived by an analysis of the mode structure (vide infra).

Since the inception of this study several papers have been reported describing the use of planar waveguides as chemical sensors. Tiefenthaler and Lukosz[27], using a very thin film glass waveguide describe a gas sensor, based on

the modulation of the coupling efficiency of an embossed grating coupler. Although, the calculated sensitivities are extremely low, as low as 1/10 to 1/100 of a monolayer of H_2O vapor, no experimental data, other than the effects of the author blowing on the waveguide, was presented. Bohn[28] later extended the theory to cover perturbation of the guided beam in a planar guide by a surface adlayer. This mode of operation is less sensitive than perturbing the coupling efficiency of a grating, and has calculated detection limits of ~ 2.0 nm of a material with an index difference of 0.02 index units. He also derived the energy distributions across a four layered thin film structure and described how quantitative preferential sampling could be achieved in these structures. The experimental results for the determination of polyaromatic hydrocarbons by Raman spectroscopy in these thin film structures followed in a subsequent publication[29].

The field of planar optic sensors will continue to grow as the need for robust, versatile, and integrated sensors develops. Planar optic sensors compliment their fiber optic equivalent, and offer the potential for miniaturization and integration of the source, sensing, and detection elements on the same substrate. By using current state of the art semiconductor fabrication techniques, one can easily envision the equivalent of a miniature two dimensional "spectrometer on a chip", depicted in Figure 1. Although

the current state of the art in semiconductor laser fabrication would limit this device to a narrow range of wavelengths, it is certainly possible that in the future, broadband coherent sources, in conjunction with acoustic diffraction gratings, could yield a visible spectrometer equivalent to the RF Fourier transform spectrometer described by Valette[9].

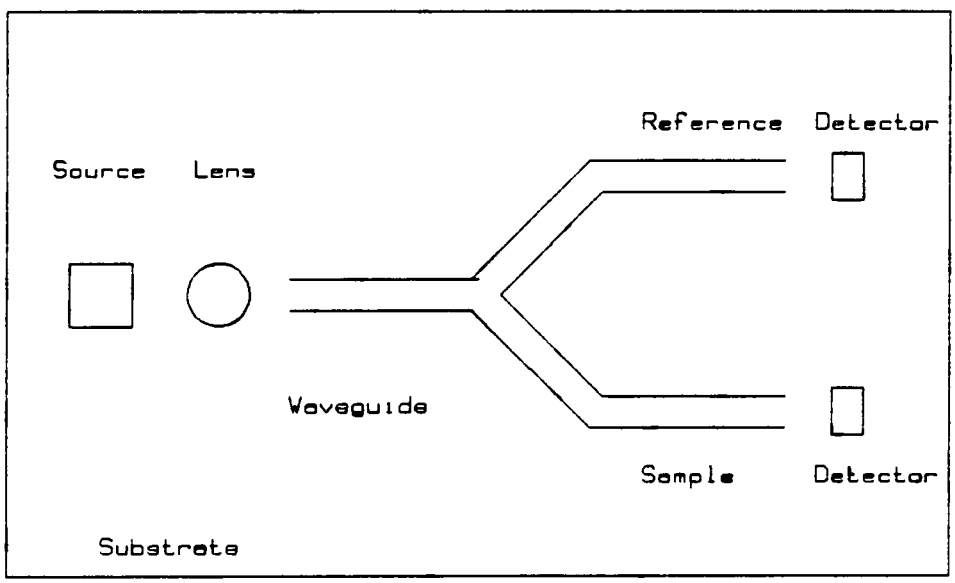

Figure 1. Integrated Optic Dual Beam Spectrometer.

III. THEORETICAL

Light propagation in a slab waveguide can be understood by first examining the behavior of a light ray at a dielectric interface. In Figure 2 a collimated, monochromatic light ray approaches the interface between two dielectrics of dissimilar indices of refraction. As the incident beam I_0 strikes the interface at an angle θ with respect the normal to the interface, a portion is reflected and a portion refracted. The angle of refraction is dependent upon the indices of the two media and obeys Snell's law

$$n_1 \mathrm{Sin}(\theta_1) = n_2 \mathrm{Sin}(\theta_2) \qquad 3.1$$

The amplitude of the reflected beam is related to the incident beam by a reflection coefficient R, which is calculated using Fresnel's formulas[30].

$$I_1 = R \cdot I_0$$

$$RTE = \frac{n_1 \mathrm{Cos}(\theta_1) - (n_2^2 - n_1^2 \mathrm{Sin}^2(\theta_1))^{\frac{1}{2}}}{n_1 \mathrm{Cos}(\theta_1) + (n_2^2 - n_1^2 \mathrm{Sin}^2(\theta_1))^{\frac{1}{2}}} \qquad 3.2$$

$$R_{TM} = \frac{n_2^2 \mathrm{Cos}(\theta_1) - n_1 (n_2^2 - n_1^2 \mathrm{Sin}^2(\theta_1)^{\frac{1}{2}}}{n_2^2 \mathrm{Cos}(\theta_1) + n_1 (n_2^2 - n_1^2 \mathrm{Sin}^2(\theta_1)^{\frac{1}{2}}} \qquad 3.2a$$

The magnitude of the reflection coefficient is polarization dependent. R_{TE} is the reflection coefficient for light polarized perpendicular to the plane of incidence (Transverse Electric) while R_{TM} is the reflection coefficient for light with the electric vector polarized parallel to the plane of incidence (Transverse Magnetic).

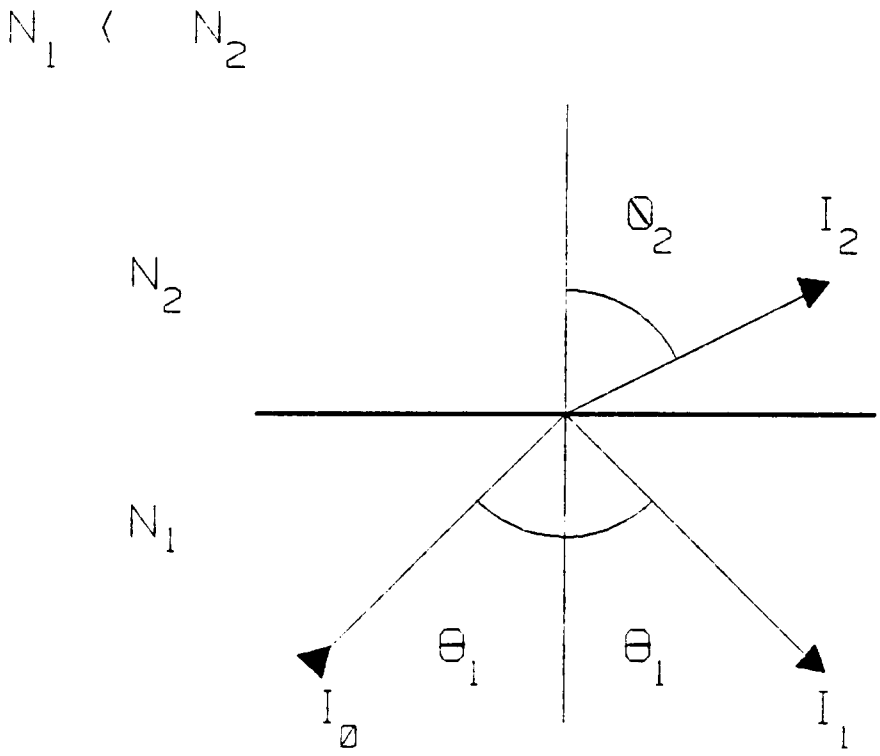

$$N_1 \sin\Theta_1 = N_2 \sin\Theta_2$$

Figure 2. Snell's Law.

The magnitude of the reflection coefficient varies according to equation 3.2 until the angle of incidence equals the critical angle, θc. At the critical angle,

$$\theta crit = Sin^{-1}(N_1/N_2) \qquad 3.3$$

$|R|$ becomes 1, and the incident beam, I_0, is totally reflected back into the denser media. For angles greater than the critical angle R is complex valued and the phase of the totally reflected beam is shifted according to[30].

$$\phi_{TE} = Tan^{-1}\left[\frac{(n_1^2 Sin^2(\theta_1) - n_2^2)^{\frac{1}{2}}}{n_1 Cos(\theta_1)}\right] \qquad 3.4$$

$$\phi_{TM} = Tan^{-1}\left[\frac{n_1^2 (n_1^2 Sin^2(\theta_1) - n_2^2)^{\frac{1}{2}}}{n_2^2 (n_1 Cos(\theta_1)}\right] \qquad 3.4a$$

The asymmetric slab waveguide is bounded by two of these dielectric interfaces. Since the dielectric on either side of the guide is different, each interface possesses a unique critical angle. Necessarily, the film index, N_f, is greater than the substrate index, N_s, which in turn is generally larger than the cladding index, N_c. Thus the critical angle at the film substrate interface, θs, is larger than θc, the critical angle at the film cladding interface. Therefore, in order for light to be confined and guided in a asymmetric waveguide, the incidence angle of the beam must be larger than the critical angles at either interface. If the incidence angle is larger than the

critical angles, θs and θc, the beam can be confined to the waveguide and will travel in a zig-zag fashion through the film. This alternating wave can be represented by two wave vectors, A and B, each of which can be decomposed into its vertical and horizontal components (Figure 3). As the horizontal components for both A and B are equal, the wave propagates at a constant speed, parallel to the film, with a propagation constant

$$\beta = kN_{film}\,Sin(\theta), \qquad 3.5$$

where $k = 2\pi/\lambda$ and β is the z component of the wavefront. The vertical component of A is an upward traveling wave while that of B is a downward traveling wave. When these are superposed they form a standing wave across the thickness of the film. As θ is changed, the directions of A and B are altered and consequently the wave velocity and standing wave pattern across the film are affected.

Sir Isaac Newton[31] was most likely the first to observe and demonstrate a standing evanescent wave for a totally internally reflected beam. From his experiments with reflected light in prisms, he concluded that the beam penetrated into the rarer media, and suggested that upon reflection the beam was slightly displaced parallel to the interface. Goos and Hänchen[32], measured this lateral shift and determined that the depth of penetration of the evanescent wave was

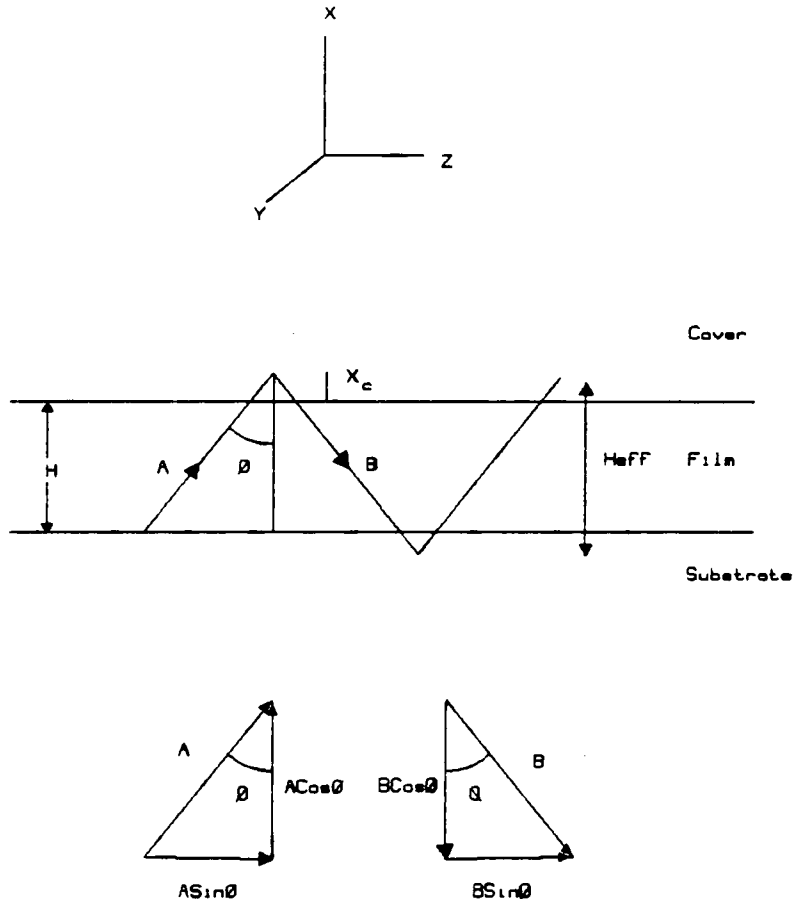

Figure 3. Ray Optics Model of a Planar Waveguide.

$$X_{TE} = k^{-1}(\beta^2/k^2 - N_r^2)^{-\frac{1}{2}} \qquad 3.6$$

$$X_{TM} = X_{TE} / \{(\beta^2/(N_r^2 k^2) + (\beta^2/N_f^2 k^2) - 1\} \qquad 3.6a$$

where N_r is the index of the rarer media. Incorporating the penetration of the totally reflected wave and its corresponding lateral shift results in the ray model of the propagation of a beam in a thin film waveguide shown in Figure 3. The waveguide is now characterized by an effective width, which is the sum of the guide thickness and the displacements of the reflected beam, due to the Goos-Hänchen shift at each interface.

If the film thickness is on the order of the wavelength of light propagating in the guide, these vectors, A and B, more accurately represent the propagation vectors (normals of the wavefront) of a plane wave traveling in the z direction, folded back upon itself between the two film surfaces.[33] The condition for propagation of this wavefront requires that these multiply reflected waves constructively interfere. If, after reflection from the top and bottom surfaces, the phase of the reflected beam differed from the incident beam by a small amount, additional reflections would eventually result in destructive interference and complete attenuation of the guided wave. The resonant condition is only satisfied when the total phase change of the beam for one complete traversal of the film, up and down, is a multiple of 2π. For a film of thickness T, the

phase change of the beam as it makes its first traversal of the film is $kN_{film}TCos(\theta)$. As the beam is totally reflected by the film cladding interface it experiences a phase shift of $-2\phi c$, as predicted by equation 3.4 . The beam is further phase shifted by $kN_{film}TCos\theta$ as it traverses the film again, and by an amount $-2\phi_s$ as it is totally reflected from the film substrate interface. The resonant condition is thus satisfied by the characteristic equation[33]

$$2kN_{film}TCos\theta - 2\phi s - 2\phi c = 2m\pi \qquad 3.7$$

where m is an integer (m = 0,1,2...n).

As a result of the phase requirements, propagation of light through the guide becomes quantized. Only certain incidence angles or paths of propagation are allowed. If the film thickness, T, is large enough the characteristic equation may be satisfied by more than one angle, and thus the guide may support more than one path or mode of propagation. Each of these modes travels with a different velocity and is characterized by a unique propagation constant, β_m. β_m can also be expressed as an effective index of the guide or $N_{eff} = \beta_m/k$. The angle of the path of propagation is restricted by the critical angle requirements of the guide, $\theta c < \theta_i < \theta s$. Equally restricted are the effective indices of the modes, which are limited to values between the film index and the substrate index, i.e. $Ns < Neff < Nf$.

The ray optics model provides an explanation of the behavior of the guide, the conditions of propagation, and the existence of modes. To obtain a more detailed picture of the electric field distributions across the guide, electromagnetic theory and Maxwell's equations must be used.

In order to calculate the field distributions across the waveguide, the wave equation for the guide must be determined. The derivation of the wave equation for a linear, asymmetric slab waveguide, surrounded by a lossless, isotopic media, follows Swalens's[34] and Kogelnick's[35] treatment. The coordinate system chosen for the derivation will be that depicted in Figure 3.

Two of Maxwell's equations for source free, time dependent fields are

$$\text{curl } E = -\partial B/\partial t \qquad 3.7$$

$$\text{curl } H = -\partial D/\partial t \qquad 3.8$$

$$\text{curl} = \text{del } X = (\partial/\partial x + \partial/\partial y + \partial/\partial z)\ X$$

where curl is the cross product of the del operator with the indicated field, t is time, and E(t), H(t), D(t) and B(t) are the time dependent vectors of the electric field, magnetic field, displacement field, and magnetic induction, respectively. Equations 3.7 and 3.8 are the differential forms of Faraday's induction law and Ampere's circuital law, respectively. The time varying fields are assumed to travel in the positive z direction, and have the form

$$E = E_o \exp^{i(\omega t - \beta z)} \qquad 3.9$$

and $$H = H_o \exp^{i(\omega t - \beta z)} \qquad 3.10$$

where ω is the angular frequency and β is the propagation constant in the z direction. For lossless media, E is related to D, and B to H by the constitutive relations[36]

$$D = \epsilon E \qquad 3.11$$

$$B = \mu H \qquad 3.12$$

where ϵ and μ are the permittivity and permeability of the dielectric.

Applying 3.7-8 to 3.11-12

$$\text{Curl } E = -i\mu\omega H \qquad 3.13$$

$$\text{Curl } H = i\mu\epsilon E. \qquad 3.14$$

Since the beam is confined exclusively in the x direction, and the y direction is considered to be infinitely wide, (compared to the thickness of the guide), all derivatives with respect to y, may be set to zero. The field distributions are polarization dependent and the following derivation will be for transverse electric, or TE fields. For TE propagation, only the E_y, H_x, and H_z components need be considered[34]. Starting with 3.7

$$(\text{curl } E)_{x \text{ constant}} = -\partial E_y/\partial Z$$

and from 3.9

$$-\partial E_y/\partial Z = i\beta E_y \qquad 3.15$$

However, from the constitutive relation, 3.12,

curl $E = -i\mu\omega H$ therefore

$$i\beta E_y = -i\mu\omega H_x \qquad 3.16$$

Also,

$$(\text{curl } E)_{z \text{ constant}} = \partial E_y/\partial X$$

then from 3.13

$$\partial Ey/\partial X = -i\mu w H_z \qquad 3.17$$

Solving for the differential magnetic fields, equation. 3.8

$$(\text{curl } H)_{y \text{ constant}} = \partial H_x/\partial Z - \partial H_z/\partial X \qquad 3.18$$

but $\partial Hx/\partial Z = -i\beta H_x$ so

$$(\text{curl } H)_{y \text{ constant}} = -i\beta H_x - \partial H_z/\partial X. \qquad 3.19$$

Using 3.8, 3.18 finally becomes,

$$-i\beta H_x - \partial H_z/\partial X = i w \epsilon E_y \qquad 3.20$$

To derive the wave equation for TE polarization, the magnetic fields terms are eliminated and equations 3.16, 3.17, and 3.20 are combined.

From 3.16

$$H_x = -\beta E_y/(\mu w)$$

and from 3.17

$$-\partial Hz/\partial X = (i\mu w)^{-1} \partial^2 E_y/\partial X^2 \ .$$

Substituting these into 3.20 and combining terms,

$$\partial^2 E_y/\partial X^2 + E_y(\beta^2 - \epsilon\mu w^2) = 0. \qquad 3.21.$$

However, the index of refraction of a dielectric is

$$n^2 = \epsilon\mu/(\epsilon_0 \mu_0)$$

and $k = 2\pi/\lambda = w/c = w\sqrt{(\epsilon_0 \mu_0)}$.

Therefore, equation 3.21 can be rewritten as

$$\partial^2 E_y/\partial X^2 + E_y(\beta^2 - n^2 k^2) = 0 \qquad 3.22$$

which is the wave equation for a TE polarized wave confined

to a linear, asymmetric waveguide. The wave equation for the TM modes is derived[35] in a similar manner and is

$$\partial^2 H_y/\partial X^2 - H_y(\beta^2 - n^2k^2) = 0 \; . \qquad 3.23$$

Suppressing the time dependence, a plane wave (~laser beam) that propagates along z, with a finite width along x, can be represented as

$$E(x,z) = E*\exp^{-i K_x x} * \exp^{-i K_z z} \qquad 3.24$$

where the K_x and K_z are the x and z components of the wave vector K_0. The dispersion relation for this wave is

$$K_0^2 = w^2 * \epsilon u = K_x^2 + K_z^2 \qquad 3.25$$

which indicates that each dielectric of the asymmetric waveguide possesses a unique K_0. However, due to the boundary conditions requiring field continuity at the cladding-film and film-substrate interfaces, the parallel component (Z) of the wave vector must be equal for all three dielectrics, i.e. $K_{1z} = K_{2z} = K_{3z} = \beta$.[33] The transverse propagation constants are thus related, and are

$$\begin{aligned} K_{1x} &= (\beta^2 - n_1^2k^2)^{\frac{1}{2}} \\ K_{2x} &= (\beta^2 - n_2^2k^2)^{\frac{1}{2}} \qquad 3.26 \\ K_{3x} &= (\beta^2 - n_3^2k^2)^{\frac{1}{2}} . \end{aligned}$$

Assuming a decaying exponential field in the cladding and substrate and an oscillatory field in the film, the fields across the waveguide can then be represented as equations 3.27

$$E(x,z) = \begin{bmatrix} A_1 \mathrm{Exp}^{-K_{1x}(X - T)} \\ A_2 \mathrm{Cos}(K_{2x}X + \theta) \\ A_3 \mathrm{Exp}^{K_{3x}X} \end{bmatrix} \mathrm{Exp}^{-iK_z z} \quad \begin{matrix} X \geq T \\ 0 \leq X \leq T \\ X \leq 0. \end{matrix}$$

Applying Maxwell's relations and the boundary conditions to these electric fields yields the corresponding magnetic field equations. Specifically 3.13 yields 3.28

$$H_z(X,Z) = \begin{bmatrix} -iA_1K_{1x}/(w\mu)*\mathrm{Exp}^{-K_{1x}(X-T)} \\ -iA_2K_{2x}/(w\mu)*\mathrm{Sin}(K_{2x}X + \theta) \\ iA3K_{3x}/(w\mu)*\mathrm{Exp}^{K_{3x}X} \end{bmatrix} \mathrm{Exp}^{-iK_z z}$$

The boundary conditions require that the electric and magnetic fields be continuous at both interfaces. Applying this condition at the cladding-film interface yields

E_{field} $\quad A_1 = A_2 \mathrm{Cos}(K_{2x}T + \theta) \quad X = T$

and H_{field} $\quad -iA_1K_{1x}/(w\mu) = -iA_2K_{2x}/(w\mu)\mathrm{Sin}(K_{2x}T + \theta).$

Taking the ratio to eliminate A_1 and A_2 gives

$$\mathrm{Tan}(K_{2x}T + \theta) = K_{1x}/K_{2x}$$

or $$K_{2x}T + \theta = \mathrm{Tan}^{-1}(K_{1x}/K_{2x}) \qquad 3.29$$

Similarly, matching E and H fields at the film substrate boundary yields

$$\mathrm{Tan}\theta = -K_{3x}/K_{2x}$$

or $$\theta = -\mathrm{Tan}^{-1}(K_{3x}/K_{2x}). \qquad 3.30$$

Substituting 3.30 in 3.29 and using the identity TanX = Tan(X ± nπ) yields

$$K_{2x}T - \mathrm{Tan}^{-1}(K_{3x}/K_{2x}) - \mathrm{Tan}^{-1}(K_{1x}/K_{2x}) = m\pi. \qquad 3.31$$

which is the same characteristic equation derived using the ray optics approach (equation 3.7). In 3.30, the arctangent

terms correspond to the phase shifts at the two interfaces and are equivalent to those calculated using Fresnel's formulas. The coefficients A_1-A_3, may be algebraically rearranged and represented as a function of A_1. Determination of the transverse propagation constant for any of the layers and application of the boundary conditions is then sufficient to solve for these normalization constants.

Application of Maxwell's equations to the field distributions has yielded two important equations. The wave equation 3.22, is analogous to the more familiar wave equation

$$\partial^2\psi/\partial y^2 + \psi(E-V) = 0 \qquad 3.31$$

found in the quantum mechanics literature, where β^2 is equivalent to the energy term, and n^2k^2 is related to the potential energy term of equation 3.31. From the derivation of the characteristic equation for the asymmetric waveguide we find that the propagation constants, β^2, are quantized; and, it becomes clear that the propagation of light in a dielectric waveguide is completely analogous to the quantum mechanical solution of the particle confined to a two dimensional potential well. As the potential energy is related to the index of refraction, the potential well corresponds to the boundaries made by the cladding-film interface and the film-substrate interface, and whose width is equal to the film thickness. Figure 4 diagrams this analogy. The spacing of the energy, or effective index

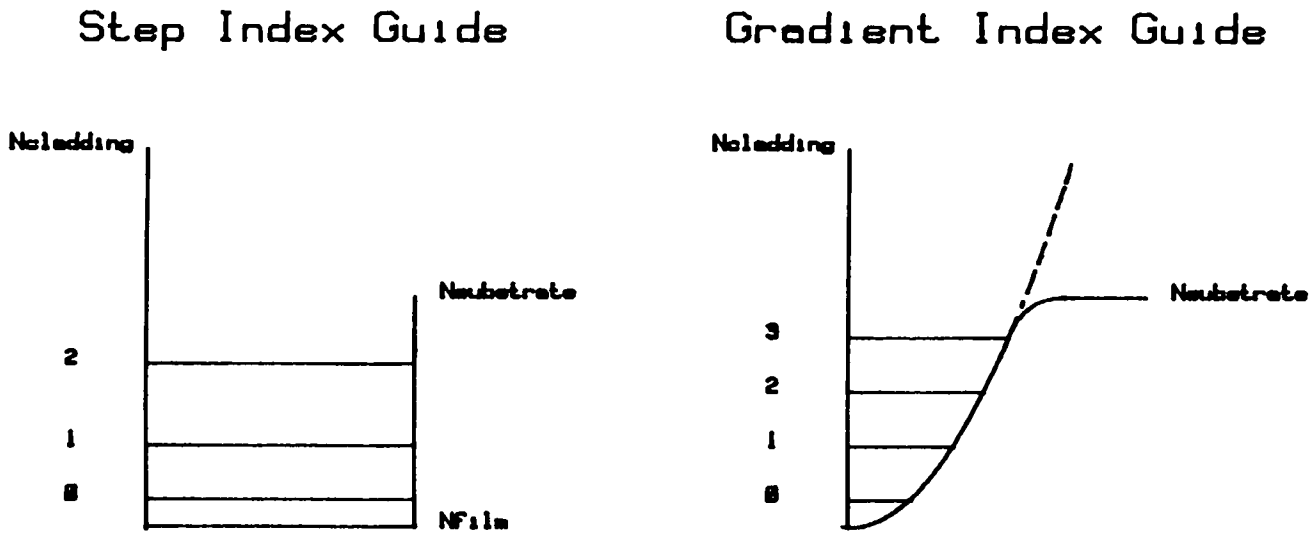

Figure 4. Effective Index Spacing for Two Index Profiles.

(β^2/k^2)levels, depends upon the relative height of the potential energy barrier. This spacing is proportional to the mode number squared for symmetric guides (or potential wells). As the form of the characteristic equation for an asymmetric waveguide is transcendental, β cannot be solved exclusively as a function of the mode number. However, and as will be shown experimentally, the spacing of the effective indices increases as a function of the mode number.

Figure 5 shows the electric field distributions for modes 0, 1 and 2 across a 1 micron thick polystyrene film supported on a glass microscope slide. For mode 0 the energy is largely confined to the center of the guide. For the higher mode numbers the energy distribution shifts toward the edges of the waveguide. The energy is not completely confined to the waveguide, but leaks into the substrate and cover regions. The depth of penetration increases as a function of the mode number and is proportionally larger into the dielectric with the lowest potential energy barrier (i.e. highest index of refraction). This "optical tunneling" is a consequence of the finite index differences between the waveguide and its surroundings, and is generally referred to as the evanescent wave.

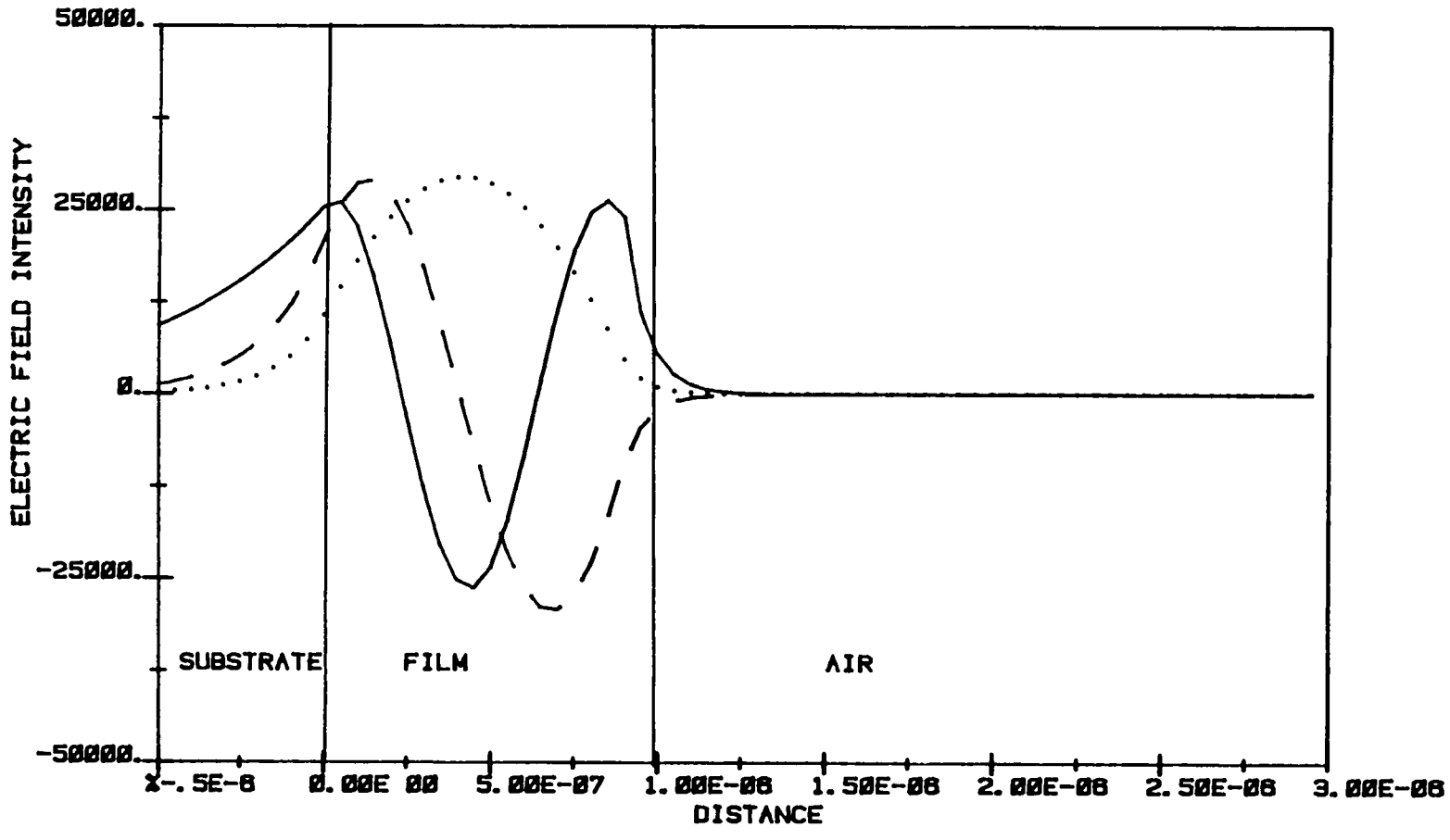

Figure 5. Electric Field Distribution Across a Polystyrene Waveguide.

A. Gradient Index Waveguides

If the waveguide is formed by a diffusion process, other potential profiles are possible. In this case the wave equation takes the form

$$\partial^2 E_y/\partial X^2 + Ey(\beta^2 - n(x)^2 k^2) = 0 \qquad 3.32$$

where the index of the guiding layer is now a function of the distance into the substrate. The dispersion equation, 3.25, is now altered to

$$K_x(X)^2 + K_z^2 = K^2(X) \qquad 3.33$$

where Kx(X), the propagation vector in the x direction, reflects the index dependence on distance. Equation 3.33 can be rearranged to

$$K_x(X) = k\,(n^2(X) - Neff^2)^{\frac{1}{2}} \qquad 3.34$$

where $$K_z = Neff = kn(X)Sin(\theta). \qquad 3.35$$

Using equation 3.34 , 3.33 finally becomes

$$\theta(X) = Cos^{-1}(1-Neff/n(x))$$

or if θ is measured with respect to the z axis

$$\theta(X) = Cos^{-1}(Neff/n(x)). \qquad 3.36$$

Equation 3.36 indicates the ray propagates at an angle that is dependent upon the x coordinate and the particular index distribution, n(x). Unlike the step index guide, where a discrete ray angle is determined by the solution of the characteristic equation, the ray angle for a gradient index guide varies continuously as the beam propagates down the waveguide.

To obtain a more accurate picture of the ray trajectory requires a knowledge of n(x), and the solutions of the wave equation, which now includes this index function. As a first approximation, the parabolic profile corresponding to the potential well of a harmonic oscillator can be used to model the actual index variation of a diffused waveguide. For the case of the harmonic oscillator potential profile, the index of refraction of the guide is represented as

$$n^2(x) = nmax^2\ (1 - (X/X_0)^2), \qquad 3.37$$

and the solutions of the wave equation take the form of

$$Ey = Hv(\sqrt{2}\ x/w)Exp(-x^2/w^2), \qquad 3.38$$

where Hv are the Hermite polynomials[35]. The characteristic equation for the symmetric parabolic profile is

$$\beta^2 = n_f{}^2k^2 - (2v+1)n_f(k/X_0). \qquad 3.39$$

This predicts that the energy levels (or propagation constants for the modes) are evenly spaced. This approximation is diagrammed in Figure 6. An important point concerning the behavior of a gradient index guide must be noted. Because there are no abrupt dielectric interfaces, the guided wave is reflected at a point in the waveguide where n(x) = Neff (the z component of the wave vector) of the propagating beam. The effective index of the guided wave decreases as the mode number increases. Therefore, the distance traveled across the film to reach this reflection point, n(x)=Neff, increases as a function of the mode

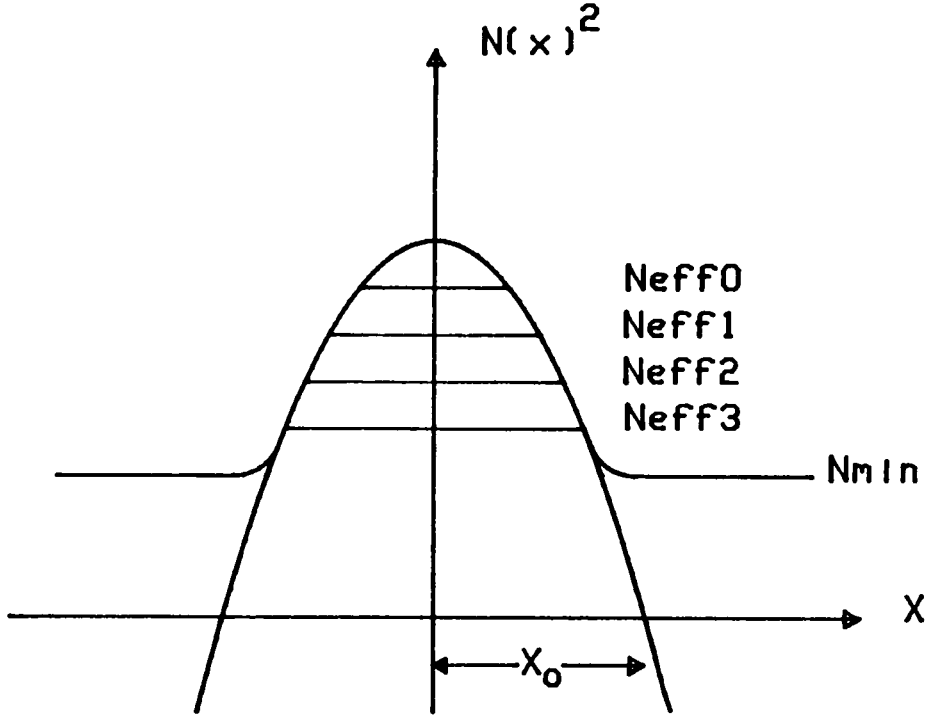

Figure 6. Gradient Index Profile Approximated by a Parabolic Well.

number. Thus, the effective width of the guide increases dramatically as the mode number increases. This is in complete contrast with the behavior of a step index guide in which the film thickness is essentially constant for all guided modes.

The ray trajectory for the parabolic profile can be determined from equations 3.36, 3.37 and 3.39[37]

$$x(z) = X0 \left[\frac{(2v+1)}{kn_{max} X0} \right]^{\frac{1}{2}} Sin(z/X0) \qquad 3.40$$

where z is the distance traveled along the guide path. This function is plotted in Figure 7. As a result, the parabolic index profile, x(z) increases as function of the mode number, i.e. the effective width of the guide increases. However, the periodicity, Sin(z/X0), or number of "bounces" per unit length, is the same for all mode numbers. This is again in sharp contrast to the step index guide where the guide width is fixed, but the periodicity of the ray is an increasing function of the mode number.

B. Evanescent Wave Absorption

The equations derived for wave propagation in an asymmetric dielectric waveguide, using either the ray optics model or Maxwell's equations, assumed that all layers were

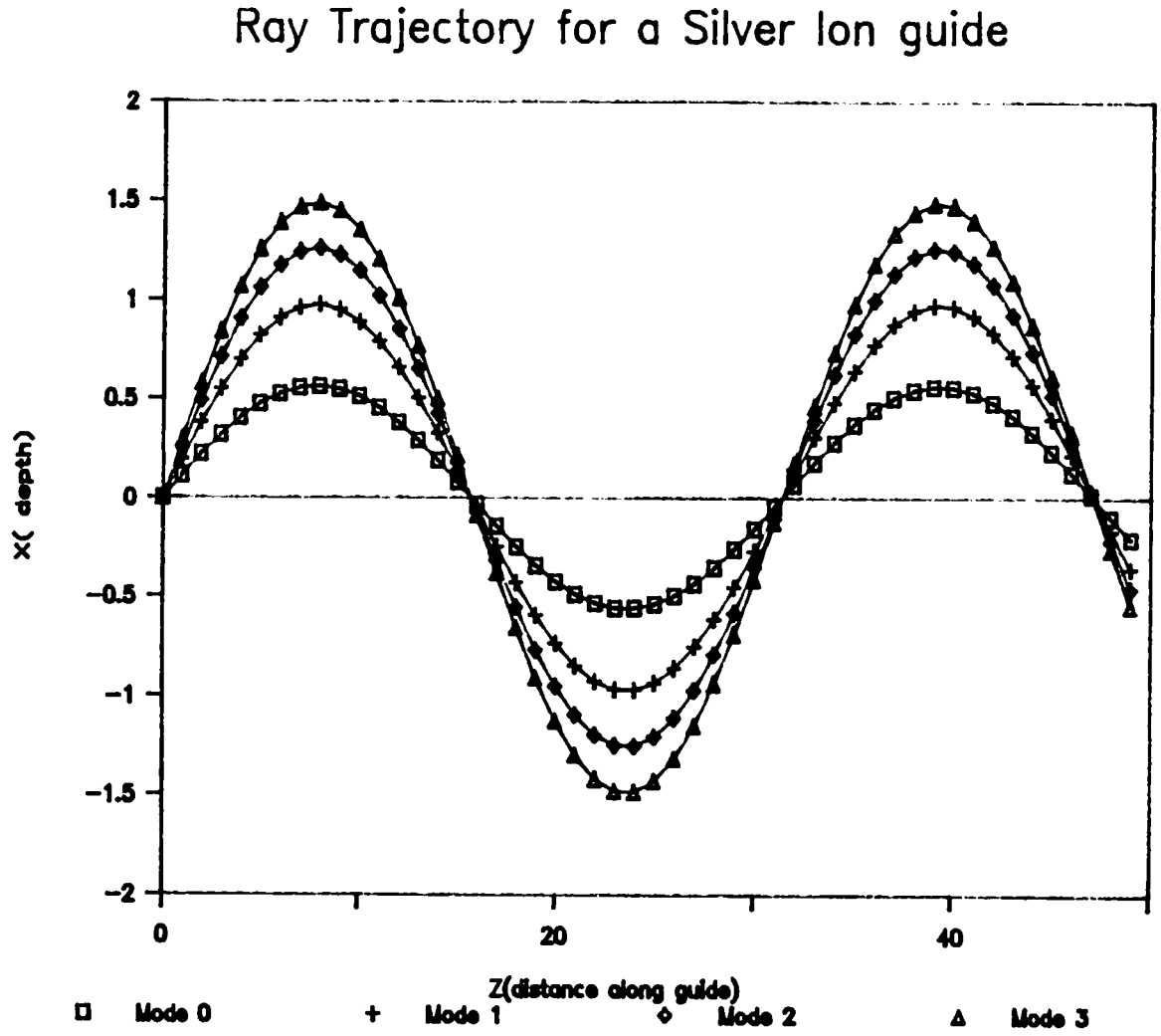

Figure 7. Ray Path for a Gradient Index Waveguide.

perfectly transparent. If one of the layers is absorbing, the refractive index of that layer becomes complex,[38]

$$\tilde{n} = n_r(1 - ik) \qquad 3.41$$

$$n_r k = \alpha/2k \qquad 3.42$$

where $\tilde{n}$ is the complex index, k the attenuation index, α the absorption coefficient, and k, as defined above, the free space propagation constant. As a result of the imaginary component of the absorbing layer, Fresnel's equations become complex. In the absorption free case, a precise critical angle exists between two dielectric layers, implying total internal reflection and a reflection coefficient of 1. However, in the presence of an absorbing, rarer medium the critical angle looses its distinction. The reflection coefficient at this interface is a function of k, and can only asymptotically approach unity. As a result, total internal reflection is never achieved, and the reflected beam is attenuated, hence the term attenuated total reflectance.

The attenuation for a single bounce of a totally reflected beam can be conveniently calculated using a series expansion of Fresnel's equations, originally derived by Hansen[39]. The equations are expressed in terms of an effective path length, where the absorbance,

$$A = \epsilon D_{eff} C,$$

and ϵ is the molar absorptivity, and C the concentration of the absorbing species. The effective path length is

dependent upon polarization and is determined using the first term of Hansen's expansion where

$$D_{TE} = \frac{(n_{12})^2 \mathrm{Cos}(\theta)}{2\pi(1 - n_{12}^2)(\beta)^{\frac{1}{2}}} \qquad 3.43$$

$$D_{TM} = \frac{n_{12}^4 \mathrm{Cos}(\theta)}{2\pi[(\beta)^{\frac{1}{2}}(n_{12}^4 \mathrm{Cos}^2(\theta) + \mathrm{Sin}^2(\theta))]}\left[1 + \frac{\beta 2}{n_{12}^2}\right]$$

$$\beta = \mathrm{Sin}^2(\theta) - n_{12}^2$$

provided $k \ll 1$. In equation 3.43 n_{12} is the ratio of the indices of the rarer media to the denser media, and the effective path lengths for both polarizations are normalized to the wavelength of the beam incident upon the interface.

This effective path length, or effective depth of penetration, is a measure of the strength of coupling of the evanescent wave to the absorbing rarer medium[38]. It is not only related to the depth of penetration of the evanescent wave, as calculated from the equations describing the Goos-Hänchen Shift (3.6), but is dependent upon several additional factors. The term n_{12} describes the degree of index matching between the two layers. Examination of equation 3.43 indicates that the effective path length increases as n_1 approaches n_2. This is intuitively understood by noting that if n_1 is equal to n_2, the interface vanishes and the depth of penetration is infinite (i.e. the beam propagates freely through the medium). The last factor is the sampling area[38] of the totally reflected

beam, which is related to $1/\mathrm{Cos}(\theta)$. This term is encountered in transmission measurements where the sample thickness increases as a factor of $1/\mathrm{Cos}(\theta)$ for oblique angles. Figure 8 is a plot of the normalized effective depth of penetration for an interface with a film index of 1.6, and a cladding index of 1.34. This figure demonstrates that the effective depth increases as the critical angle is approached, is always deeper for parallel (TM) polarization, than perpendicular polarization, (as a result of the polarization dependence of the Goos-Hänchen shift), and decreases to zero for grazing incidence.

The loss of power for a wave reflected at an absorbing interface can be expressed as

$$R^N = (1 - \alpha D_{eff})^N \qquad 3.44$$

where N is the number of bounces. If $\alpha D_{eff} << 1$ then the approximation

$$R^N \sim 1 - N\alpha D_{eff}$$

is valid and the absorption of the of the beam, as shown by Hansen, could be represented as

$$A = N\alpha D_{eff}. \qquad 3.45$$

Using the ray optics model and the treatment above, several observations can be made concerning the sensitivity of a thin planar waveguide. As each of the quantized paths of propagation travels at a unique angle, each can be expected to have a different effective path length. Also, since the incidence angle increases with the mode number, it should

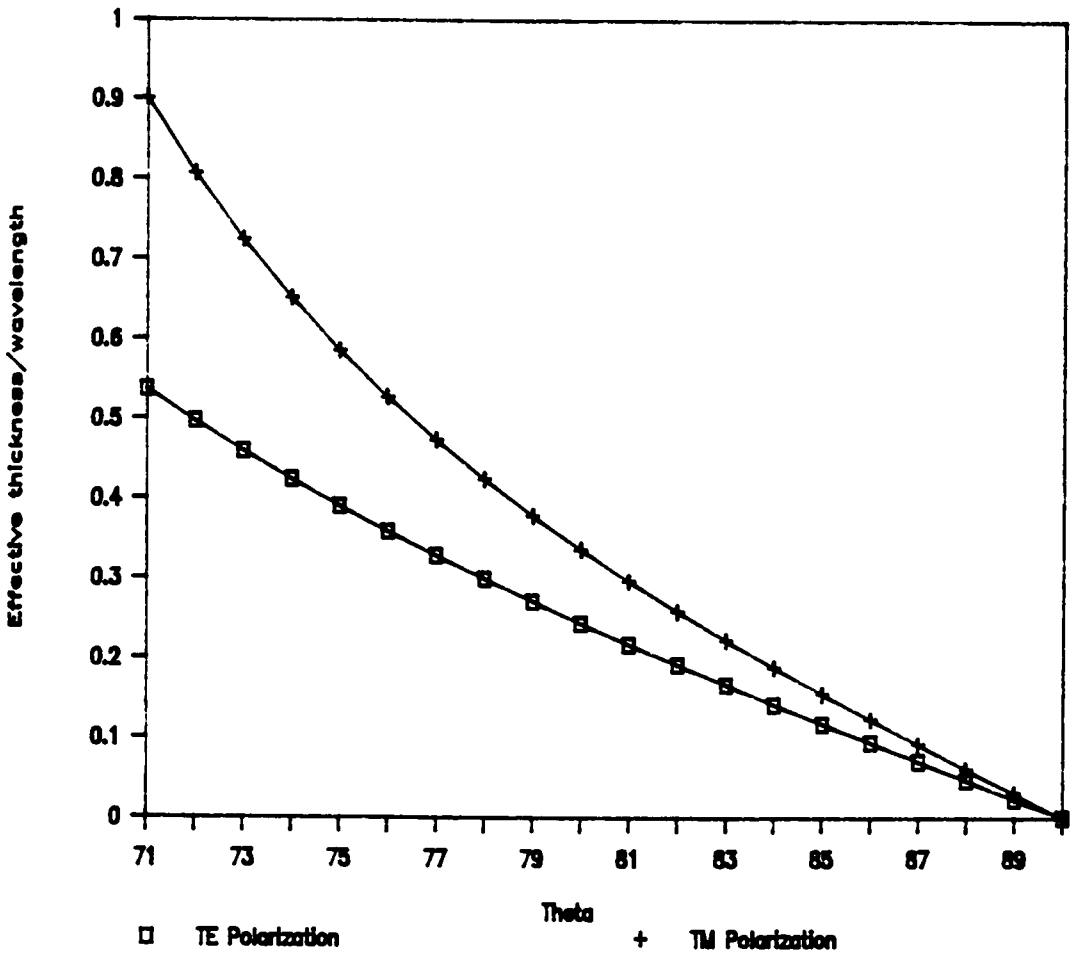

Figure 8. Effective Depth of Penetration for a Ag^{+} Waveguide.

not be surprising that the effective path length of the guide increases with the mode number. Furthermore, since the number of (hypothetical) bounces per unit length for each mode is, N = 1/(2*T*Tan(θ)), the total number of interactions is larger for increasing mode numbers. Additionally, it has been shown that parallel (TM) polarization has a greater effective penetration depth than perpendicular (TE), so it should be expected that TM polarization will exhibit a higher sensitivity than TE. Therefore, as a first approximation, the attenuation of the waveguide can, be calculated by

$$A = \alpha L D_{eff}/(2*T*\mathrm{Tan}(\theta)) \qquad 3.46$$

where L is the length of the guide exposed to the absorbing species.

However, by application of Maxwell's equations, the evanescent wave has been shown to exist continuously across the film cladding interface, rather than just interacting at discrete locations, as implied by the ray optics model. The attenuation of the guided beam calculated by equation 3.46, should therefore be too low. If the loss of energy in the guide is due solely to absorption, and scattering can be ignored, the power of the beam in the waveguide will decrease exponentially as

$$I = I_0 \exp(-\alpha_w x)$$

where α_w is the attenuation constant of the beam. This attenuation is attributable to the loss associated with the

absorbing rarer medium, with its associated attenuation constant α_{dye}. Unfortunately, due to the transcendental nature of the characteristic equation (3.31), it is impossible to solve directly for the attenuation of the waveguide as a function of the attenuation constant of the absorbing species. However, Polky and Harris[20], using a perturbation analysis of the absorption free case, derived an expression relating the attenuation constant of a dye, α_{dye}, to α_w. For TE modes

$$\frac{\alpha_w}{\alpha_{dye}} = \frac{n_3 [N_{eff} (K_3)^{\frac{1}{2}} (n_2^2 - n_3^2)]^{-1}}{\dfrac{K_1^{-\frac{1}{2}}}{(n_2^2 - n_1^2)} + \dfrac{K_3^{-\frac{1}{2}}}{(n_2^2 - n_3^2)} + (K_2)^{-1} \left[k_0 t + \dfrac{K_3^{\frac{1}{2}}}{(n_2^2 - n_3^2)} + \dfrac{K_1^{\frac{1}{2}}}{(n_2^2 - n_1^2)} \right]}$$

$$K_i = (N_{eff}^2 - n_i^2) \qquad 3.47$$

where n_3 is the cladding index, n_2 the film index and n_1, the substrate index.

They named the quotient, α_{dye}/α_w, the interaction ratio R, and interpreted R as the absorption rate of the guided wave relative to the absorption rate of an unguided wave propagating through the absorbing solution. It is a measure of the sensitivity of the waveguide to an absorbing species relative to a transmission experiment. Figure 9 is a plot of R versus the waveguide thickness normalized to the wavelength of light propagating in the waveguide. Each curve represents the interaction ratio of a specific mode, with the curve on the extreme left corresponding to mode

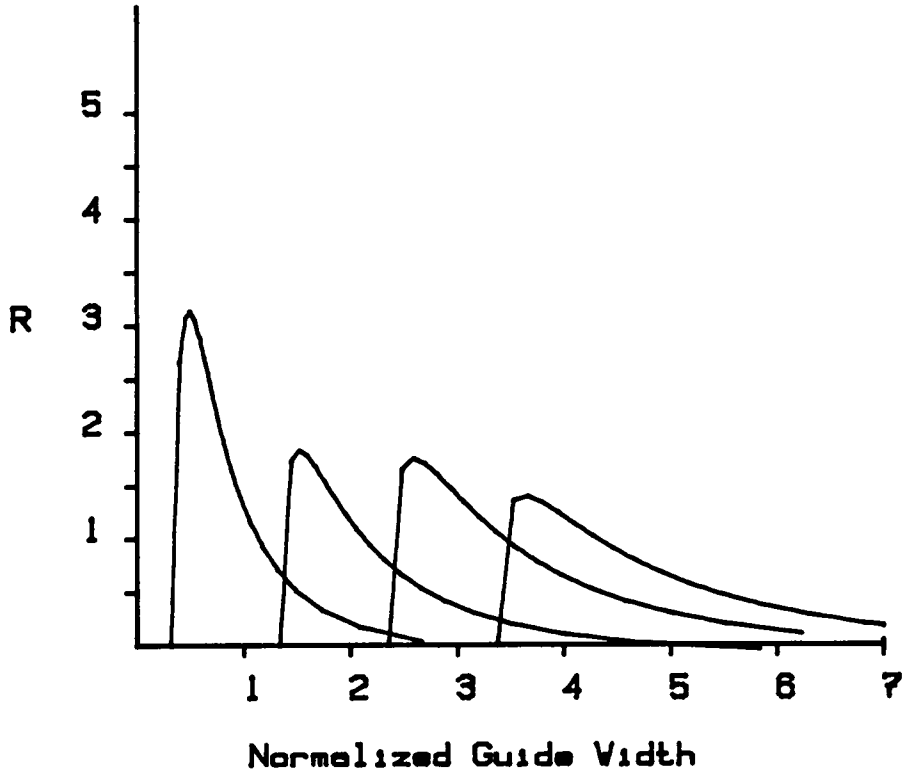

Figure 9. Interaction Ratio for a Waveguide with Nfilm = 1.59, Nsubstrate = 1.512, and NClad = 1.33. R is multiplied by 100.

zero. For a given guide width, the highest order mode supported is the most sensitive. However, this calculation also indicates that for given film, cladding and substrate indices, a film thickness that is large enough to support only one mode of propagation yields the highest sensitivity. Examination of equation 3.47 indicates that the sensitivity also increases as the film index increases. Although this seems to contradict the index matching argument, it can be seen that as the film index increases, the critical angle for either interface decreases. Thus, the waveguide can support paths of propagation closer to the plane of incidence. Resorting to the ray optics model, steeper propagation angles yield an increasing number of effective "bounces". As the film index increases, R approaches a limiting value of .5 (if the guide is symmetric). In the limiting case half of the evanescent wave would propagate in the substrate and the other half in the cladding. For guide indices typical of the spin coated polymers on glass microscope slides or metal ion diffused waveguides used in this study, R is on order of .01 to .05.

C. Prism Couplers

As the light propagating in a waveguide is subject to the conditions of total internal reflection, a device is needed to introduce light into the guide by some means,

other than transmission or reflection. Butt, or endfire coupling, is a means to introduce light into a fiber optic or planar waveguide. It entails illuminating the polished end of the guide with a light source. It is a relatively simple method of introducing light into a waveguide, but suffers from the disadvantage of exciting all available modes simultaneously. Holographically ruled grating couplers[40] , fabricated into a planar waveguide can also be used to couple light into a planar guide, but are tunable and will exclusively excite a single selected mode. Grating couplers are coplanar with the guide, and thus preserve the 2-D nature of the waveguide. This might be an important consideration for a sensor based on planar waveguides. Such gratings are, however, reasonably difficult to manufacture and were not considered for this study. The final option, and arguably the most efficacious means of coupling light into a planar waveguide, is through the use of a prism coupler, a device independently invented by Tien[41] and Harris[42] .

The method involves clamping a half prism to the planar waveguide and illuminating the rear portion of the prism through its face. Typically, a small air gap, on the order of 1/8 to 1/2 the wavelength of the laser, is present between the prism and waveguiding film. As the prism is necessarily (vide infra) made of a material with a higher index of refraction than the waveguide, the beam is totally

internally reflected at the prism air gap interface. This results, as previously discussed, in a decaying exponential evanescent field present in the air gap. This field can be represented[33] by the wave vector A_3 which equals k*Nprism, and is shown in Figure 10. If the air gap is made narrow enough, the evanescent field will penetrate the waveguide, and may excite a light wave in the film. As previously discussed, a guided ray has a propagation constant K_0, which is equal $k*n_{film}Sin(\theta)$, and is represented as A_1 in Figure 10. This vector can be resolved into its vertical and horizontal components, $kn_{film}Cos\theta$ and $kn_{film}Sin\theta$. If the horizontal component of the evanescent wave, kNprismSinø, or ß, can be made to match the horizontal component of a supported mode, light will, through frustration of the total internal reflectance at the prism-air gap, flow across the gap and into a guided mode. Each supported mode of the waveguide may then be exclusively excited by proper adjustment of the angle ø. The conditions for exciting a guided mode are then

$$kN_{prism}Sin\phi = kN_{film}Sin\theta = \beta. \qquad 3.48$$

As Sinø is generally less than 1, it is readily seen that the prism index needs to be at least as high as the film index in order to satisfy the phase match condition. Input coupling efficiencies are theoretically[43] as high as 80 %. Light propagating in a waveguide can, by a similar process,

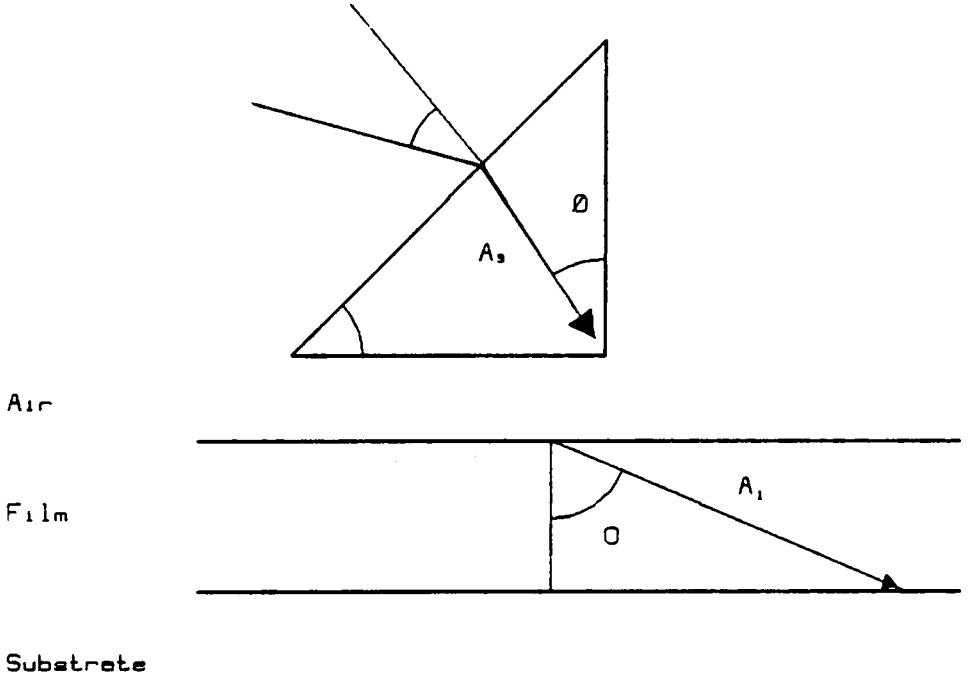

Figure 10. Prism Coupler.

be coupled out of the guide by using an identical output coupling prism.

Equation 3.48 suggests that by measuring the coupling angle, ø, for the guided mode that, the propagation constant ß, for that mode can be calculated. This is significant, since once the propagation constants for the guide are known, the characteristic equation, 3.31 can be solved iteratively for the film index and thickness. The input coupling angle of the laser beam with respect to the normal of the prism face, α, is related to ß by[44]

$$\beta = N_{prism}[\ \delta + \mathrm{Sin}^{-1}(\ \mathrm{Sin}(\delta+\alpha)/N_{prism})] \qquad 3.49$$

where δ is the acute angle of the coupling prism.

IV. INSTRUMENTATION

The complete system for the flow injection analysis of urea using a thin film optical waveguide absorbance detector is shown in Figure 11. This instrument is composed of three major components: the waveguide; the optical and detection elements; and the flow injection analysis manifold.

A. Waveguide Fabrication

Optical waveguides may be fabricated using many different technologies. Among the most common, are those techniques which are routinely used in the semiconductor industry, such as chemical vapor deposition, RF sputtering, or ion implantation. These methods however, require considerable expense and expertise in order to produce high quality optical waveguides. Fortunately, several other techniques exist for producing optical waveguides that are relatively inexpensive, require a minimum of capital equipment, and most importantly, are easily mastered. The two methods investigated were the application of thin polymer films and metal ion diffusion to fabricate, respectively, step and gradient index optical waveguides. Both techniques provide a means to fabricate waveguides quickly, and with a varied range of indices and physical properties.

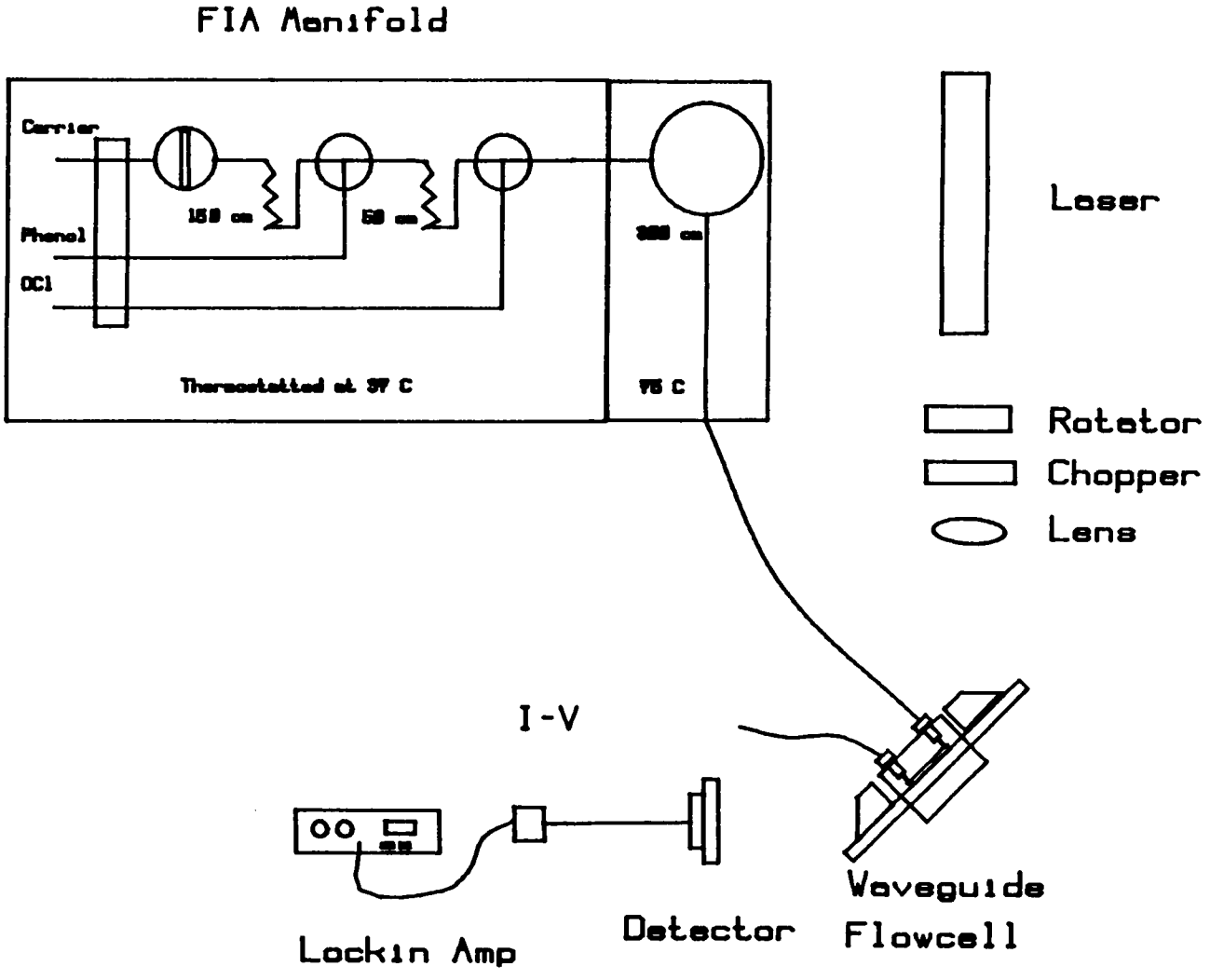

Figure 11. Experimental Apparatus for the FIA of Urea using a Planar Waveguide Absorbance Sensor.

1. Polymer Waveguides

Polymers were among some of the first materials to be studied as waveguides after the invention of the prism film coupler.[45] They have been extensively used as waveguides because they are easily and quickly made, and produce some of the lowest loss guides available.[46] Polymers must possess certain properties before they can be considered candidates as waveguide materials. First, the polymers' index of refraction must be greater than the substrate index. Second, the material must have a low absorption coefficient at the desired wavelength. Third, the material must be easily cast into smooth and well adhering thin films to prevent scattering loss. Additional desirable properties for a film that is to be used as a sensor are low solubility in aqueous environments and durability (i.e. resistance to abrasion). Based on these constraints, polystyrene and a positive photoresist (Shipley Microposit 1400-17) were studied as waveguide materials for the absorption sensor.

Polystyrene, obtained from Aldrich, has an index of refraction of 1.5916 at 589.2 nm.[47] This polymer has excellent optical properties as it forms water white films, is easily cast into thin films and adheres to silica substrates strongly enough to pass the "Scotch Tape" test.[48] Its index is sufficiently high to ensure waveguiding with the substrates available: microscope slides, N_d=1.51; Pyrex, N_d=1.47; Quartz, N_d = 1.45.

Since Microposit 1400-17 was developed as a photoresist, it, too, is easily cast into a thin film, and has excellent adhesion to silicon oxide substrates. Microposit has an index of refraction of 1.64 at 632.8 nm.[49]

Spin coating was the predominant method used to fabricate the thin polymer films. The technique is universally used in the semiconductor industry for the application of photoresists to semiconductor substrates. It is known to be one of the best techniques for producing films with minimal thickness variations. Spin coating involves flooding a substrate with a dilute polymer solution and subsequently spinning the substrate at speeds between 1500-3000 rpm. The spinning removes the majority of material from the substrate and accelerates the evaporation of the solvent from the remaining thin film. The film is then baked to completely remove remaining traces of solvent.

The spin coater was constructed in house, using a Cole-Parmer Instrument Co. GT 21 Motor controller and GT 21 Laboratory Mixer Motor[50]. The motor was mounted inside a metal box to protect it from the solvents used during spinning. Only its shaft extended through the top of the housing. A 3.5" diameter, .25" thick disk of aluminum was machined as the substrate carrier, and was fixed to the motor shaft by means of a socket head set screw. A large coffee can was then machined to cover the substrate carrier during the spinning operation.

The spin coater was calibrated using the circuitry show in Figure 12 . A 4" diameter cardboard disk was attached to the substrate carrier. A .25" rectangular slot was removed from this disk, to serve as an optical gate. A General Electric H13A1 matched emitter-detector interrupter was mounted such that when the disk was placed between the tabs of the chip, a logical one was sensed when the light beam was blocked and a logical zero sensed with the path open. This signal was inverted with a 7400 NAND gate and then input into an ORTEC 707 Buffer Scaler. The buffer scaler is a NIM BIN instrument designed to count a series of pulse events timed by an ORTEC 719 timer. The count duration is set on the 719 timer and the buffer scaler begins counting when the 719 timer is triggered either manually, or by computer control. A one minute integration period was chosen for these calibration tests. The motor controller rheostat was set to the desired setting and the spin coater allowed to operate for 1 minute before integration began. The results are tabulated in Table 1.

Before spinning, the substrates were cleaned using a method originally developed by the silicon semiconductor industry[45]. The substrates were first immersed in an ultrasonic bath and scrubbed for 15 minutes in Microclean detergent[51]. They were then removed and rinsed with copious amounts of distilled water. The slides were then subsequently boiled in a mixture of 7-2-1 parts by volume of

Table 1. SPIN COATER SPEED CALIBRATION

Rectifier Position	Counts(R.P.M.)
1.5	858
1.75	1523
2.0	2039
2.5	2787
3.0	3580
3.5	4454
4.0	6153

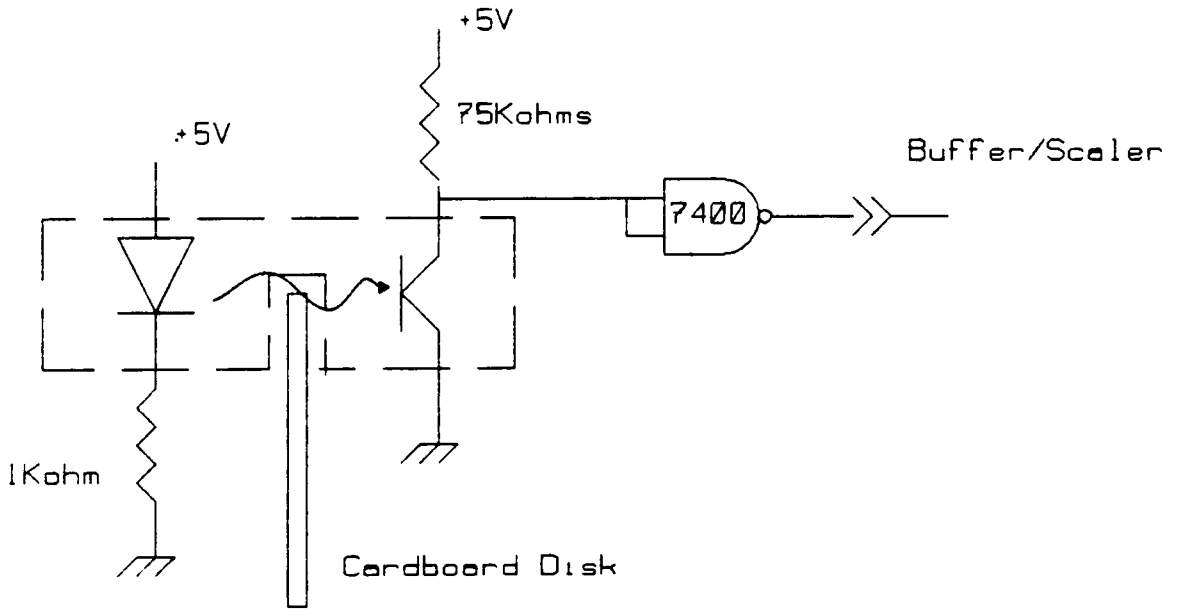

Figure 12. Spin Coater Calibration Circuitry.

deionized water, 30% hydrogen peroxide, and concentrated NH_4OH followed by boiling in a mixture of 7-2-1 parts by volume of deionized water, 30% hydrogen peroxide, and concentrated HCl. Finally the slides were rinsed with deionized water and dried at 150 °C for two hours. All slides were inspected during the final rinse step. A substrate was judged adequately clean if water wet the slide evenly and interference colors appeared across the slide upon draining. The substrates were then either used immediately or stored in a trichloroethane vapor degreaser.

Chlorobenzene, with a boiling point of 132 °C, was chosen as the solvent for polystyrene. The choice is important, as a solvent with too high a vapor pressure will cause the resulting films to have a mottled, or "orange peel" appearance, while a solvent with too low a vapor pressure will be difficult to remove from the film. Polystyrene dissolved in chlorobenzene made consistently better films than polystyrene dissolved in other solvents, such as dimethylformamide or acetone. The photoresist came as a liquid and was used without further dilution.

Thin films were prepared by flooding the substrates with a 10% polystyrene/chlorobenzene solution (by weight) that had been filtered with a 2 micron Gelman HPLC filter. The solutions were typically spun for 1 minute at 1500-2000 rpm. The substrates were removed and allowed to dry in their own vapor for 24 hours at room temperature. This

generally produced films that were approximately 1 micron thick, as determined by measuring the coupling angles and solving for the film index and thickness. Thicker films could be prepared by either making the solution more concentrated or by spinning at a lower rate. However, solutions greater than 15 % polystyrene by weight were too viscous to spin, and spinning at rates lower than 1000 rpm resulted in the formation of uneven films. Attempts to create thicker films by spinning multiple coats yielded poor results as the solvent from the top layer partially dissolved the bottom layer, completely destroying the film. Thicker films were then necessarily made with a different technique, such as dip coating.

2. Metal Ion Exchanged Waveguides

Although several species of metal ions may be successfully diffused into soda lime glass, the silver ion was chosen for the fabrication of the waveguides in this study. As silver ions have a relatively high diffusion coefficient in soda lime glass, low loss waveguides supporting several modes can be fabricated in minutes, as opposed to many hours for metals such as potassium.[52,53] The resulting refractive index change for silver ion diffusion, ~0.1, is also higher than that for other metal ions, which typically range from less than 0.001 to 0.013.[54] Finally,

silver salts are much less toxic than thallium salts, the only other metal ion which produces waveguides with similar properties as the silver ion guides.[11]

Silver ion diffusion into glass has been studied extensively by Doremus[55], and Stewart et al[56] who studied the process as applied to the formation of optical waveguides. The concentration and thus index profile of silver ions diffused into glass microscope slides was experimentally determined to follow a second order polynomial fit

$$n(x) = n_s - (n_s - n_{sub})\left[\frac{x}{d} + .64\frac{x^2}{d^2}\right] \qquad 4.1$$

where n_s is the surface index, n_{sub} is the substrate index, d the depth of the guide and x the distance into the substrate. The parameter d, is calculated, using the experimentally determined diffusion coefficients[56] as

$$d = 1.19*10^4 t^{\frac{1}{2}} * \exp(-1.02*10^4/2T) \text{ microns} \qquad 4.2$$

where t is the diffusion time in minutes, and T is the diffusion temperature in degrees Kelvin.

Two different substrates were used to fabricate the silver ion diffused guides. The soda lime glass substrates were either Fisher or Chance microscope slides, while the Pyrex substrates were Corning 7740 glass.[57] The Na_2O content of the microscope slides varies between 11-13 %[58],while that of the 7740 substrates is approximately 4%. As the

microscope slides possess a higher sodium concentration than the 7740 substrates, a larger refractive index change upon silver ion diffusion is predicted for the microscope slides. Experimentally, the surface index of the microscope slides changes from 1.51 to 1.59, while Pyrex substrates show a much lower change, from 1.47 to 1.50.[10] The interaction ratio for the Pyrex waveguides was much lower than that for the microscope slides, as determined by the index change. Therefore, subsequent experiments were based only on waveguides made with the microscope slide substrates. The microscope slides however, exhibit considerable fluorescence at wavelengths below 632.8 nm, and consequently waveguides made with these substrates appreciably attenuate a guided beam at these lower wavelengths. The silver ion exchanged regions on both types of substrates were also observed to fluoresce strongly below 514 nm, thus limiting use of these types of guides to operation between 632.8 nm and the Near Infrared.

As adhesion of a thin film to a substrate was not a consideration in metal ion exchange, the substrates were only cleaned ultrasonically. The substrates were dried, as previously discussed, and either used immediately or stored in a desiccator.

Initially, the substrates were ion exchanged in a silver nitrate bath, as this compound has the lowest melting point of the silver salts, 214°C. Chartier has shown

however, that mixtures of sodium and silver nitrate with greater than 10 mole % silver, produce waveguides with identical properties as those fabricated in a pure silver nitrate bath, at similar temperatures.[59] Therefore, in the interest of economy, a 10-15 % mole ratio silver to sodium nitrate solution was chosen as the standard ion exchange bath. Due to the higher melting point of sodium nitrate, the melting point of the mixture was approximately 300°C. Faster diffusion is achieved at higher temperatures, but nitrate salts are unstable and the practical temperature limit for silver nitrate baths is 400°C before decomposition of the nitrate ion occurs with evolution of NO_2.[11] Decomposition during the diffusion step usually yields poor results, and thus the temperature of the bath was maintained at 310°C.

The ion exchange was carried out in a convection heated Blue M oven, with a temperature stability of ±1°C. The substrates were allowed to come to thermal equilibrium in the oven for 10 minutes before immersion in the ion exchange bath. The glass substrates were then immersed in the melt for times ranging between 5 to 30 minutes, removed, drained, and cooled to room temperature. This produced waveguides that supported between 4 and 7 modes at 632.8 nm. Although several studies have shown that depletion of silver ion at the surface of the substrate may lead to waveguides with a buried index profile, and that stirring of the melt was

necessary to obtain a monotonically decreasing silver ion concentration in the substrate, this condition usually occurred only for diffusion times greater than 24 hours.[9] Because the goal was to produce waveguides with relatively few modes, the exchange time was brief, and this, coupled with a relatively high silver ion concentration in the melt, prevented surface depletion. Waveguides with a buried index profile are very difficult to excite with a prism coupler, and this difficulty was not observed in any of the ion exchanged guides fabricated in this study.[9]

Often, after silver ion exchange, the cleaned waveguides would appear slightly yellow. This yellowish tinge is due to the reduction of silver ions, and their subsequent aggregation and precipitation into submicroscopic crystals. Zsigmondy[60,11] determined that the reduction of silver ion in glass took place without the evolution of oxygen, and thus the formation of metallic silver could not be due the thermal dissociation of silver oxide

$$Ag_2O \dashrightarrow 2Ag + 1/2\ O_2 .$$

The reduction of silver ions was determined to be caused by reducing agents, such as FeO or As_2O_3, which are present as a result of processing in silicate glasses. The reduction processes were formulated as follows:

$$Ag_2O + 2FeO \dashrightarrow Fe_2O_3 + 2Ag$$

$$2Ag_2O + As_2O_3 \dashrightarrow As_2O_5 + 4Ag.$$

These reduced silver atoms then aggregate and form the submicroscopic crystals responsible for the yellowish tint and scattering observed in silver ion exchanged waveguides.[11] Substrates that were heavily tinted formed extremely lossy waveguides, and coupling light into these guides was very difficult. These waveguides were nevertheless easily cleaned by wiping the surface with dilute nitric acid, which removed the surface aggregations. Waveguides thus cleaned, were much easier to excite, presumably due to the much lower surface scattering. After several months it was observed that some of the more heavily exchanged guides began to yellow again. As a result, significant attenuation of the guided beam resulted. These guides could be restored to their original performance by repeating the cleaning procedure.

B. Optical System and Data Acquisition Hardware

The optical system for the absorbance sensor consisted of a source, beam splitter, polarization rotator, chopper, focusing optic, waveguide coupling optics, detection element, and data acquisition system. Although this is essentially a single beam instrument, source fluctuations, if present, were detected by a separate photodiode. This optical system is diagramed in Figure 13.

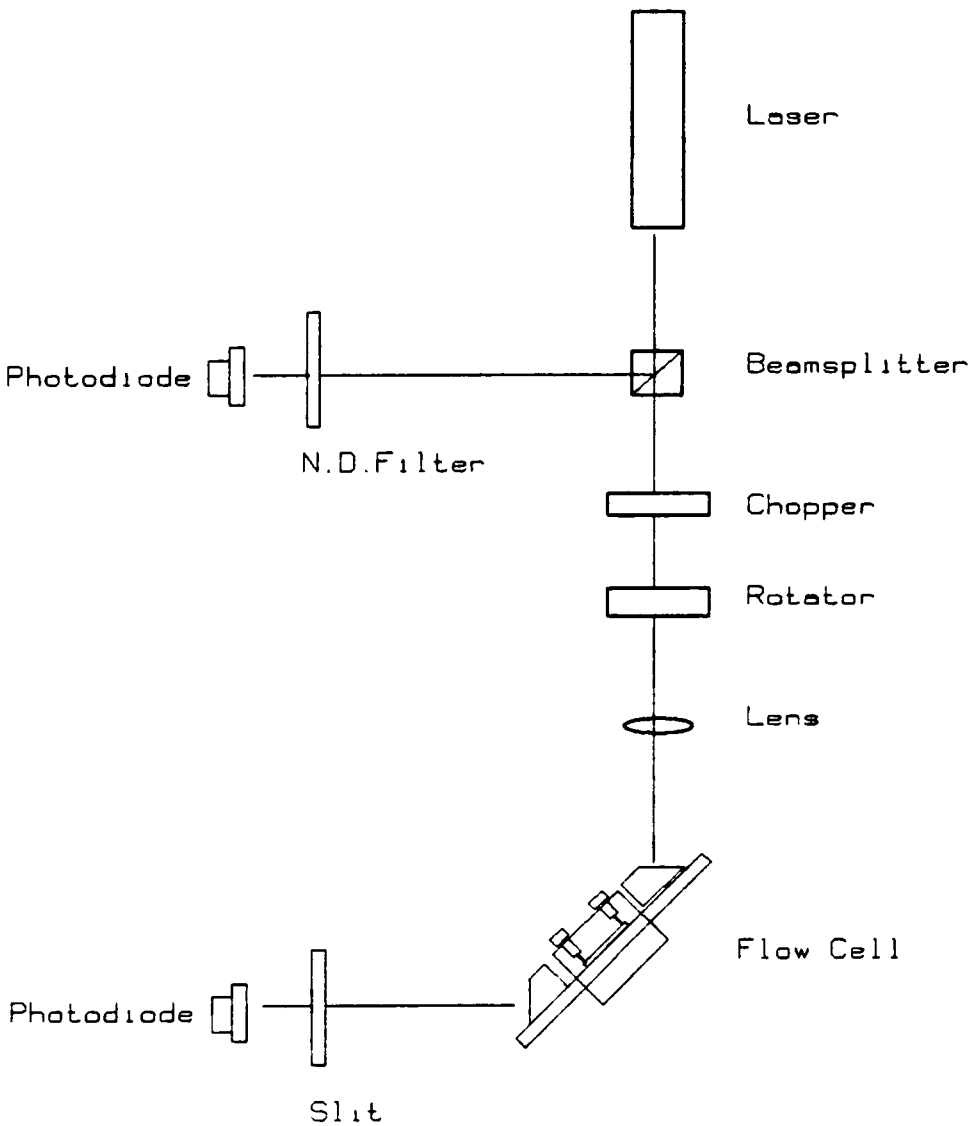

Figure 13. Optical System.

1. Source Optics

The source was either a Helium-Neon laser or an Argon ion laser. The HeNe was used for the absorbance experiments and waveguide evaluation, while the Argon ion was used exclusively for waveguide evaluation. The HeNe was a Hughes 3121H-P 1 milliwatt laser. The laser was linearly polarized to better than 500:1 and was mounted such that the polarization axis was normal to the optical bench. After warm up for 1 hour, the output power stability was determined to be consistently better than ±.5%. This laser operated exclusively at 632.8 nm in the TEM_{00} mode. The argon ion laser was a Spectra Physics model 165-05. The laser could be operated at 9 different wavelengths ranging from 454 nm to 514.5 nm. For waveguide evaluation (index and thickness), usually only the 488.0 nm and 514.5 nm lines were used. Operation in the TEM00 mode was ensured by proper adjustment of the mirrors, and focusing magnetic field, and was periodically checked by expanding the beam and observing its profile on a distant screen. The polarization was linear and oriented perpendicular to the bench, and the extinction coefficient for the vertical versus horizontal polarization was better than 500:1. The laser power was 5 watts maximum at all lines and nominally 2 watts at the 514.5 nm line. However, the beam power,

measured using a Spectra Physics laser power meter, was never allowed to exceed 100 mw at the input coupling prism.

The beam intensity was monitored using a cube beam splitter and photodiode detector. A prism cube beam splitter was used to prevent the ghost image and beam displacement problems inherent in using a plate beam splitter. The transmittance and reflectance for the beam was approximately 40%. The reflected beam was attenuated using neutral density filter and then detected with a UDT pin 10DP photodiode[61]. The diode was operated in the photovoltaic mode, and the resulting photocurrent was converted to a voltage and amplified by a current to voltage converter with a gain of 10000. The circuit diagram is shown in Figure 14. The resulting signal was then digitized by the data acquisition system (vide infra).

The polarization of the beam was manipulated with a half wave mica retarder[62]. The plane of polarization of a beam transmitted through a half wave plate is rotated by twice the angular rotation of the half wave plate with respect to its fast optical axis. Thus, a linearly polarized beam that was either parallel or perpendicular to the optical bench was produced by rotating the half wave plate ± 45°. A parallel (TE) or perpendicular (TM) polarized beam was preferentially excited in the waveguide by proper choice of this angle. The resulting angle of polarization was then confirmed using a linear polarizer.

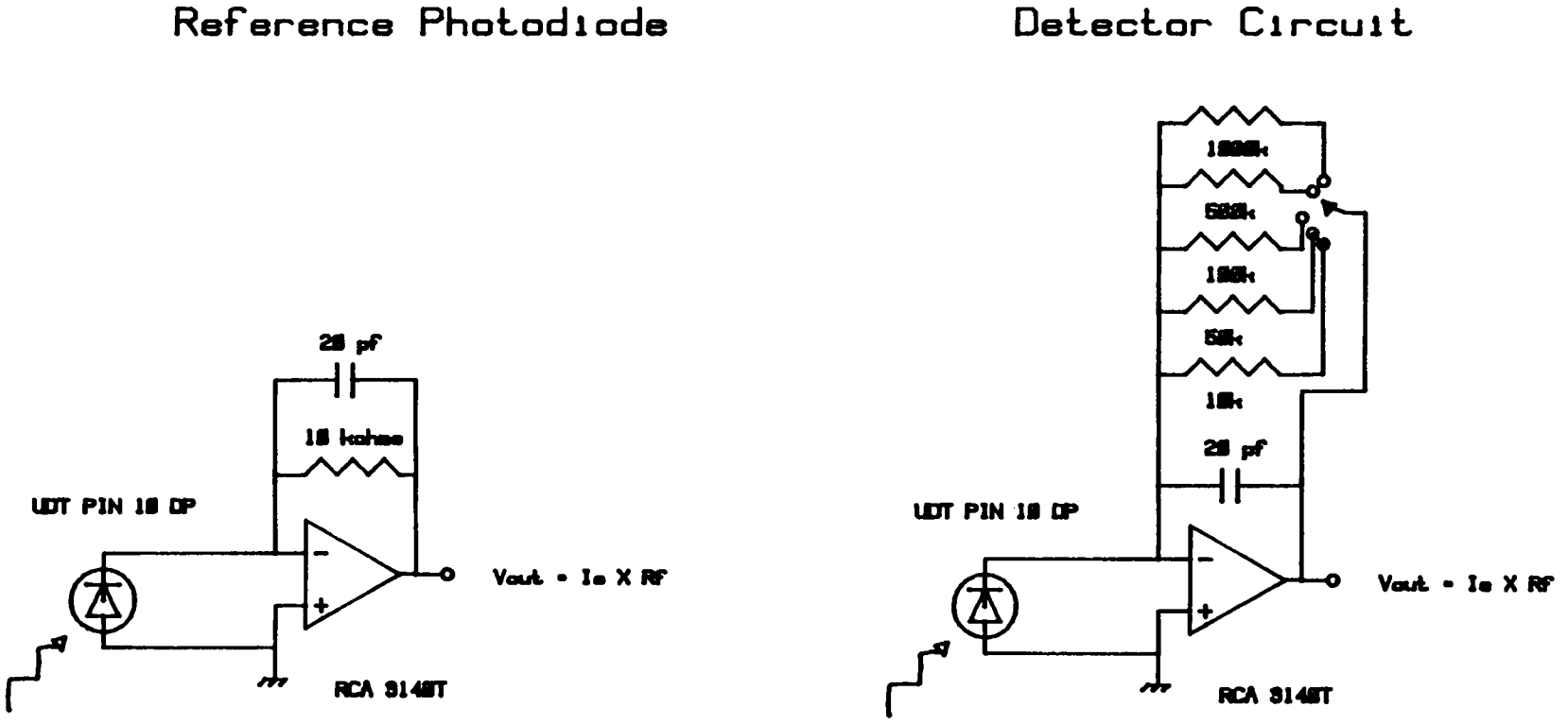

Figure 14. Current Amplifiers for the Photodiode Detectors.

The transmitted beam was then modulated at 500 hz with a model 7500 Rofin chopper. The chopping frequency was adjustable from 20 to 800 hz, with a stability of .05%, and a ±5 volt square wave signal was available on the chopper head for use as a reference input to a lock-in amplifier. The modulation of the beam was necessary to implement a phase sensitive detection technique. This modulated beam was then focused onto the input coupling prism with a f/3 75mm focal length achromatic lens.

2. Prism Coupler

Three different materials were fabricated into prisms to couple light into the planar optic waveguides : cubic zirconia; Schott glass LASF-5; and Schott glass SF-2. The cubic zirconia and the SF-2 glass were fabricated into 60° right angle prisms, while the LASF-5 was made into a 45° right angle prism. Each of these different prisms was designed to couple light into waveguides with different indices of refraction. The cubic zirconia prisms were used to excite waveguides with indices ranging from approximately 1.5 to 1.9; the LASF-5, waveguides with indices ranging from 1.5 to 1.8; the SF-2, waveguides with indices ranging from 1.4 to 1.6. These ranges were assigned based on approximations developed by Ulrich[65].

The cubic zirconia prisms were manufactured by Precomp, Inc.[66] The dimensions of the prisms are 12.5mm (base) x 11mm (height) x 10mm (wide). The top snipe (the flat surface on the top of the prism) was 6.15 mm and the acute angle is 60° ± 5 '. The index of refraction is 2.158 at 589.2 nm.

The LASF-5 prisms were manufactured by Precision Optical,Inc.[67] These prisms are .25" (wide) x .375" (base) * .25" (height) and the top snipe is .188". The acute angle is 45° ± 30'. The index of refraction is 1.8805 at 589.2 nm[5].

The SF-2 prisms were purchased from Edmund Scientific Co. as equilateral dispersing prisms for UV-VIS spectrometers[68]. The dimensions of these prisms were 1" x 1.0625 ". The angles were 60° ± 5 '. The index of SF-2 glass at 589.3 nm is 1.64769[69]. Before use as coupling prisms, the equilateral prisms were cut into smaller half prisms using a technique developed by Mitchell[70]. These equilateral prisms were cut using a .0625 " Carborundum cutoff wheel rotating at 1000 rpm. The dimensions of the resulting right angle prisms were 10mm(w)*12.5mm(l)*10mm(h) with a 6mm snipe. The base of the prism was then hand polished on billiard cloth with suspensions of 1.0 micron, 0.3 micron, and finally 0.05 micron alumina.[71] The final polish was continued until the surface was transparent with a slightly mottled or "orange peel" texture.

The prism index of refraction and acute angle are important experimental parameters in the determination of an optical waveguide's index and thickness. The acute angle of all the prisms purchased or fabricated was checked using a Mitutoyo Bevel protractor with an accuracy of ± 5 minutes of arc. All prisms were found to be within the reported specifications and the acute angle used in subsequent calculations was that reported by the manufacturer. The index of refraction of these prisms was also reported by the manufacturer and subsequently checked by the method of minimum deviations[72].

The prism coupler consists of an Oriel model 1641 precision rotational mount, a mounting plate, two jig clamps and two prism jigs. The 1641 mount has a rotational accuracy of 1 arc second. The mounting plate was machined from a piece of .25 " plexiglass stock. The dimensions of the rectangular plate were 3"x3.5", with 6-32 holes drilled in the center to allow mounting to the 1641 rotator (see Figure 15). Along the length and on both sides of the plate, spaced 2.5 inches apart, 6-32 holes were drilled and tapped at .5 inch intervals. The jig clamps could be fastened by any pair of these holes, thus separating the input and output coupling prisms by a variable path length. The prism jigs were fabricated from a single piece of .25 inch stock aluminum. The overall dimensions were 2.5" (w) by 3.5" (l).

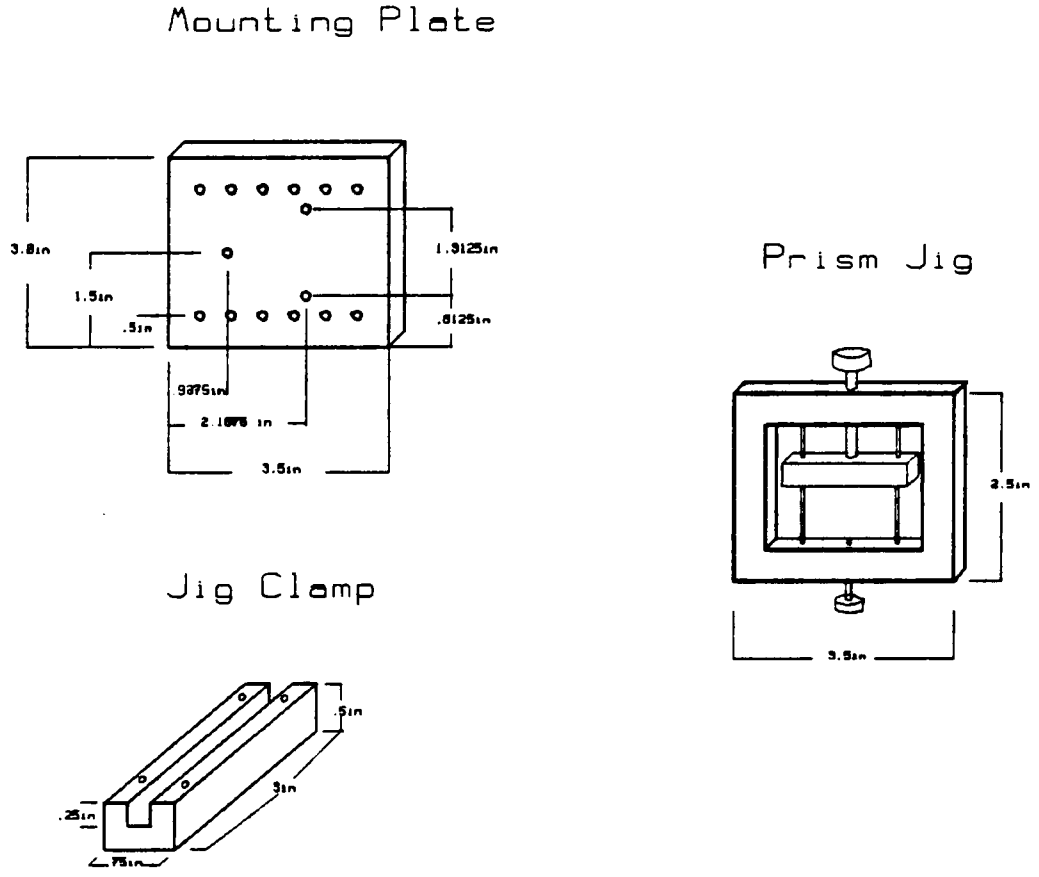

Figure 15. Prism Mount and Jig for the Waveguide Prism Coupler.

A rectangular hole 2" by 2.5" was removed from the plate to accommodate the prism and the waveguide.

The prism was pressed against the waveguide with a .5" (w) x .5" (h) x 1.75" (l) piece of plexiglass. Two holes were drilled through this piece of plexiglass to serve as guides. The press was then held in place by two heavy gauge wire guides that had been mounted in the jig frame. Pressure was applied on the frame and to the prism by a 6-32 clamping screw that was mounted in the prism jig frame. Finally, directly below the clamping screw in the jig frame, a 4-40 hole was tapped and drilled. The tip of a 4-40 socket head screw, that had been rounded, was then mounted into the 4-40 tapped hole and served as an adjustable anvil. After the prism waveguide combination was mounted in the jig and clamped into place with the clamping screw, small pressure adjustments could then be made with this anvil screw.

3. Acquisition

The experiments were controlled with a Digital Equipment Corporation LSI-11 microcomputer. This 16 bit computer was configured with 16 kilobytes of dynamic RAM, an Analog to Digital converter (ADC), two RS232-C asynchronous serial ports, a 16 bit parallel input/output port, and a real time clock[73]. As this system was diskless, the FORTH

operating system and any application programs were downloaded into memory from the central host computer using a serial network.

The data was acquired with an ADAC model 1050 ADC. This is a 12 bit, 50 khz successive approximation converter, that can multiplex up to 16 single ended inputs. The converter was configured to measure voltages between ±10 volts with a resolution of 4.88 millivolts. The A/D conversions were triggered either with an external clock or by a real time clock interrupt. The sense bits, REQ A and REQ B, associated with the parallel port, were largely used as hardware interrupts to signal the occurrence of an external event and coordinate the data acquisition software. The real time clock, is a programmable event timer, with frequencies varying in decades from .1 hz to 10khz.

4. Detection

Two detection schemes were used; the choice dependent upon the desired experiment. A photodiode array was used for survey scans of the mode spectra and for waveguide evaluation while a single photodiode was used for the absorption experiments. Either detector could be used with these experiments, but the single photodiode was chosen for the absorption experiment to facilitate phase sensitive detection, which would be difficult, if not impossible, with

photodiode arrays. On the other hand, the ability to image the complete mode spectra using the photodiode array aided mode assignment and the determination of the coupling angles.

A United Detector Technology PIN 10-DP silicon photodiode was used as the detector for the absorbance experiments. The large active area, 100 mm^2, increased sensitivity as a large portion of the excited mode could be imaged upon the detector. The photodiode was operated in the photovoltaic (unbiased) mode to reduce dark current noise to a minimum. The short circuit current, rather than the open circuit voltage of the diode, was measured to ensure linear operation. As a result of the large shunt resistance (2 Megaohms) of this element, the output current is linear over 10 decades of light intensity[74].

The current was measured using a current to voltage converter with variable gain. RCA CA3140T FET input operational amplifiers were chosen because of their high input impedance. The cathode of the photodiode was connected to the inverting input of the amplifier, while the anode and non-inverting input were connected to ground. The gain was variable between 10^4 and 10^6 by choosing the appropriate feedback resistor. The voltage produced at the output of the amplifier was related to the photocurrent by

$$V_{out} = i_s * R_f$$

where i_s the photocurrent and R_f is the value of the

feedback resistor. A 20 pf capacitor was placed in parallel with the feedback resistor to prevent oscillation. The circuit diagram is shown in Figure 14.

The output voltage from the current to voltage converter was further amplified by a PAR model 122 lock-in amplifier. Lock-in amplification is a phase sensitive technique that allows the rms value of a signal to be determined in the presence of noise.[75] Typically, in an absorbance experiment, the source is modulated before passing through the sample. The attenuated beam is detected, and then input into the lock-in, where only the signal that is in phase with the modulator is amplified. This effectively discriminates against stray light and 1/f noise, or drift. The practical consequence of using this technique is that an absorbance experiment can be run in the presence of room lights, eliminating the need to shield the detector from stray light.

The lock-in was tuned to the modulation frequency of 500 hz and adjusted to a quality factor of 10. The sensitivity was adjusted between 5 and 200 mv, depending on the signal strength, to provide an output voltage range of 0 to 10 volts full scale. The time constant was varied between 0.1 and 1 second and the data acquired at either 10 or 1 hz using the real time clock on the LSI-11 as the event timer. The software used to acquire data from the lock-in amplifier is listed in Appendix 1.

A Reticon 512 element S-series photodiode array was used to obtain the mode spectra for the various waveguides. The array is 12.8mm(l) X 2.5 mm(h) with the diodes spaced on 25 micron centers. Each pixel consists of a photodiode and a dummy diode, each with an associated capacitance. These diodes are connected to common video and recharge lines through a MOS switch. During a scan, the switches are sequentially closed for one clock period by the even and odd shift register scanning circuits, thereby charging the diode's capacitance with a preset charge. Between scans, light incident upon these elements creates a photocurrent which dissipates this charge. The amount of charge lost is measured and is proportional to the light intensity and integration time. The output signal is therefore a set of current pulses with a frequency equal to the scanning frequency of the array. The dummy diodes are used to compensate for dark current.

A Reticon RC-1024SA interface board was used to control the scan timing, acquire the video signal from the diode array, and convert the charge pulses into voltages. An interface board[76], Figure 16, was used to coordinate data acquisition between the 1024SA and the LSI-11 computer.

This board was modified to allow acquisition of all even numbered diodes. Three signals were needed to coordinate data acquisition; an ADC trigger, a start, and a clear pulse. The Clear pulse was obtained from the delayed

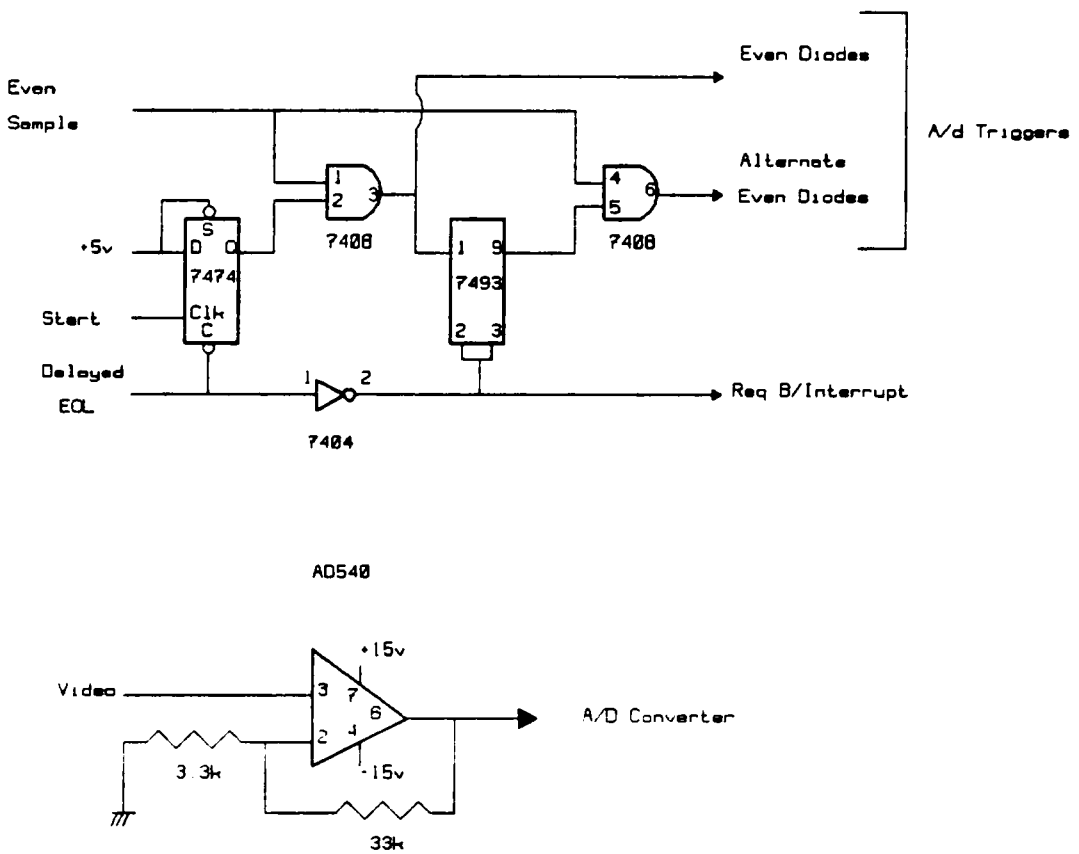

Figure 16. Modified Interrupt Circuitry for the Photodiode Array Board.

End of Line (EOL) signal on the Reticon RC-1024SA board. This signal is used on the 1024SA board to indicate the end of a scan. The EOL pulse was used to asynchronously clear a 7474 D flip flop which resets the interface circuit and disables the ADC trigger. This pulse is also inverted to provide an interrupt for REQ B on the LSI-11 parallel port to indicate the beginning of the next scan. The interrupt service routine enables the ADC for an external trigger which is provided by the START and EVEN SAMPLE signals. The START pulse is a 1024SA signal used to indicate the start of a scan and is used to toggle the output of the D flip flop to enable an AND gate. The EVEN SAMPLE pulse, used as a clock for the even diodes on the S series array, is then passed through the AND gate and used as the ADC trigger.

The integration, or scan frequency, is variable between 3hz and 300 khz for the S series array and was set to 142 khz. At this frequency one scan of the 512 elements required 14.4 milliseconds, or about 28 microseconds per diode. Digitizing only the even diodes allowed 56 microseconds per conversion, ample time for the acquisition hardware and software to acquire and store a data point. However, the refresh for the dynamic memory used in the LSI-11, disabled all interrupts for a period of 130 microseconds every 1.6 milliseconds. As a result, during this period no data was digitized. This fortunately was not a serious problem for obtaining qualitative mode spectral data, as it

meant that less than 10% of the data was lost due to these periodic refresh cycles. If the diode array was to be used for quantitative measurements on the other hand, switching to static memory would alleviate this problem. The software used to acquire the data from this array is listed in Appendix 1.

C. Flow System

The manifold for the flow injection analysis (FIA) of urea using Berthelot's reaction is diagramed in Figure 11.

1. Flow Injection Manifold

In this three line manifold, aqueous phenol and alkaline hypochlorite were subsequently added to a phosphate buffer carrier stream containing the sample of urea. Urea was first hydrolyzed with the immobilized enzyme, urease. The ammonia subsequently produced was oxidatively coupled to phenol to yield indophenol blue. The major components of this flow system were the sample injection system, tubing, and temperature control.

The sample was injected onto the manifold using a stainless steel Spectra Physics HPLC valve. The sample loops were made with 0.0305" i.d. stainless steel tubing and cut to 2.5", 5.0", 8.35", and 16.7" lengths. These lengths

equaled 30 µliter, 60 µliter, 100 µliter, and 200 µliter volumes, respectively. Standard male swage lock connectors were then added to the ends of the sample tubes. After fitting a sample loop to the HPLC valve (typically 60 µliter) the valve was attached inside the housing to maintain the contents of the sample loop at constant temperature.

The manifold was constructed using 0.5mm i.d., 1.588 mm O.D. (0.0625") Teflon tubing throughout, with 1/4"-28 Teflon Cheminert connectors[77]. The sole exception was a 150 cm length of 0.86 mm i.d. nylon tubing used for the immobilized enzyme column. This manifold was housed in an rectangular aluminum box which was lined with 0.25 inch foam core poster board as insulation. All tubing connections to the box were made through Teflon double ended, female bulkhead connectors which were sealed to the box with Dow Corning RTV Silicone. All reagents were brought into the housing through these connectors.

The reagents were pumped with a four channel Gilson Minipuls 2 peristaltic pump. The flow rate was controlled by choosing the appropriate diameter pump tubing while fine adjustments were made by controlling the pump speed. Typically, 0.76 mm i.d. Elkay Accurated™ peristaltic pump tubing was used for all three reagent channels. The overall and individual reagent flow rates were then calibrated by

determining the average weight loss from the reagent bottles as a function of time.

Two separate temperature controllers and heaters were used in this FIA manifold. The first was an air convection heater that was thermostated at 37°C to maintain maximum enzyme velocity[78]. The second was a reaction coil that accelerated indophenol color development. This coil was maintained at 75°C. Both used an RFL Industries model 72A zero voltage firing proportional temperature controller. The temperature range of these controllers is between -90°C to 450°C, with a stability of ± 0.1°C the setpoint temperature. Both controllers were configured similarly and the schematic is shown in Figure 17.

The air convection heater was an Eastern Air device heat gun which consists of a blower fan and a resistive heat element. The blower was wired to run continuously during operation, while the heat element was controlled by the temperature controller. Running the fan continuously reduced electrical noise and maintained an even temperature throughout the FIA housing. A model HB 27687-3 thermistor was used with this controller to allow temperature control between -35 to 70°C. Once the temperature set point had been fixed, the stability was determined to be better than ±0.5°C over an 8 hour period.

The reaction coil was a 300 cm length of Teflon tubing coiled around, and cemented to, a 2" diameter by 4" tall

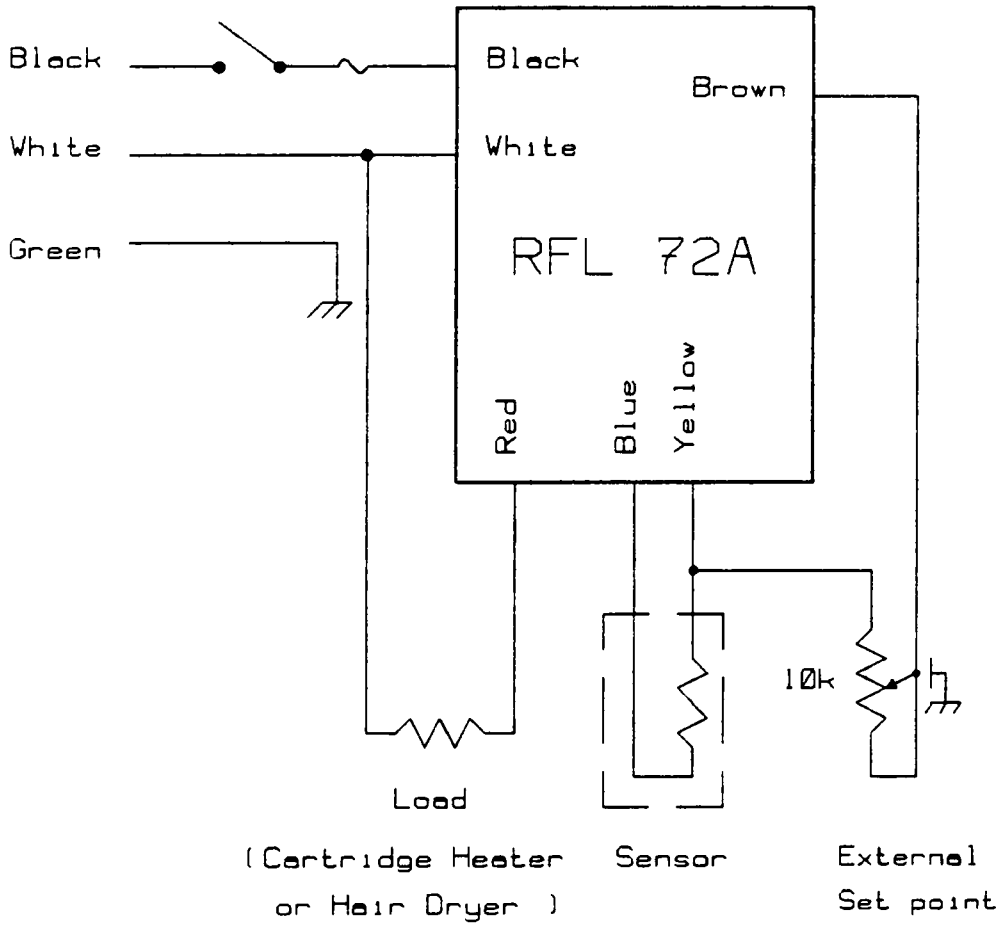

Figure 17. Temperature Controller Schematic.

aluminum rod. A 3/8" diameter by 2" deep hole was drilled into the center of the rod to accommodate a Vulcan 85 watt 120 volt cartridge heater. The temperature was monitored electrically with a HB-276787-5, 0-120 °C thermistor and verified using a thermometer.

2. Flow Cell Design

The planar waveguide was sandwiched between two pieces of Lucite, one of which contained a channel that served as the flow cell. Lucite is a transparent material that is relatively inert and one that can be polished to an optical finish. These were important qualities for several reasons. The flow cell was continuously exposed to a highly alkaline aqueous effluent (pH 12) and had to resist dissolution and deformation. Transparency was necessary to minimize absorption and scattering loss from the guided beam at the flow cell waveguide interface. The transparency of the material also allowed the guided beam to be viewed as it traversed the flow cell, an important consideration in optically aligning a 0.1mm wide beam confined to a 0.5-1 mm wide flow cell. The design and dimension of the flow cell are shown in Figure 18.

Several flow cells, with different volumes, were constructed. The channels were milled using ball end mills and subsequently polished with plastic scratch remover to

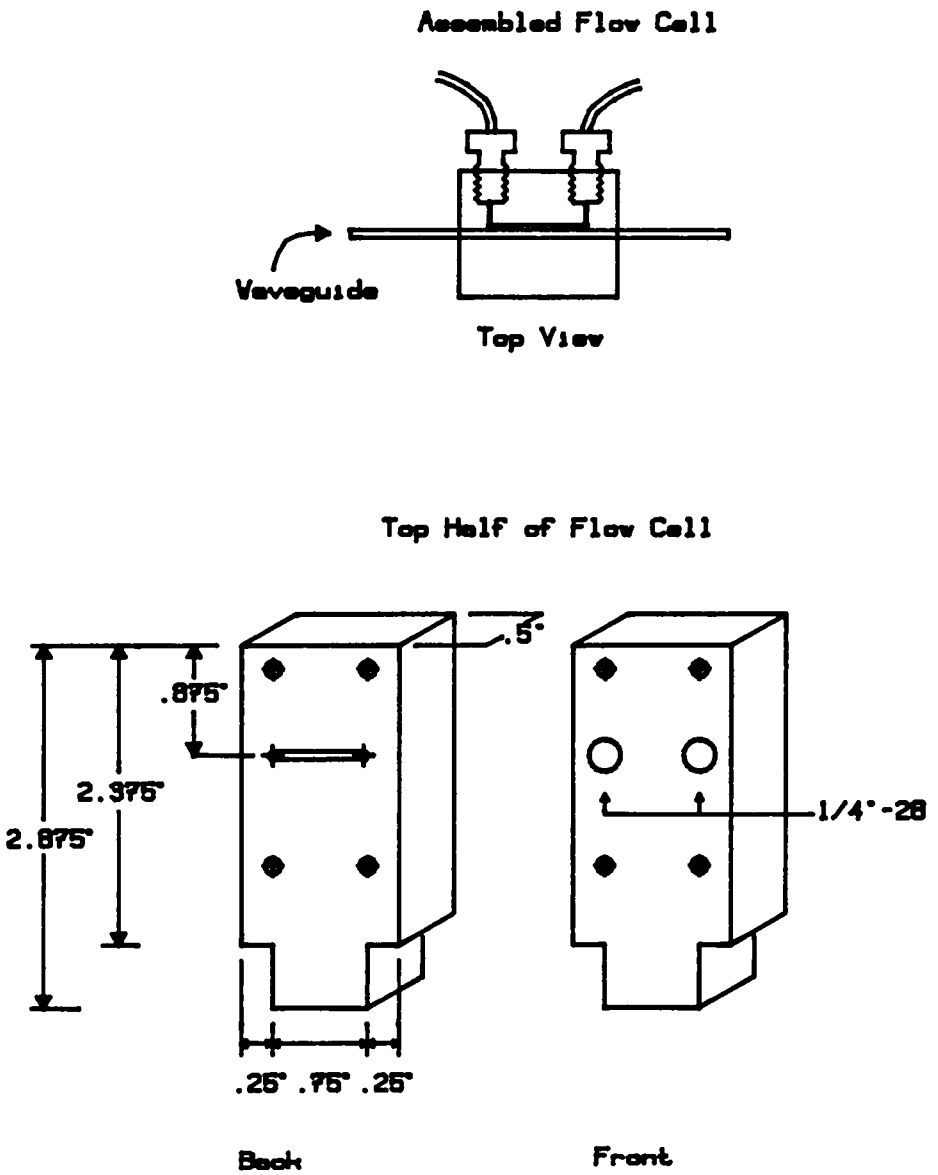

Figure 18. Flow Cell Design.

improve transparency through the cell, and reduce the number of sharp edges. The dimensions of the first cell were 0.125"(w)*0.035"(d)*0.75"(l). This resulting cell volume was 54 µliters. The next two cells were 0.015" deep and 0.75" long with widths of 0.025" and 0.050". The depth of the channel of these cells was kept consistent to match the i.d. of the Teflon tubing used in the FIA manifold and their resulting volumes were 4.6 and 9.2 µliters, respectively. At the end of each channel a 0.020" diameter hole was drilled to connect the channel to the 0.5 mm i.d. (0.019") FIA tubing. These holes were drilled out and tapped to receive a standard 1/4"-28 Cheminert male connector.

The dead volume, was the extra volume of these cells as compared to the 3.74 µliter volume of a 0.75" length of 0.5mm i.d. tubing. For the 54 µliter cell this dead volume was close to 50 µliters; whereas for the 4.6 and 9.2 µliter cells, the dead volume was approximately 1 and 6 µliters, respectively. As the latter two cells had dead volumes that were less than 10% of the injected sample volume (60µl), they were preferred over the 54 µliter cell. The compromises, however, encountered in choosing a cell volume involve problems caused by peak tailing in a large volume cell compared to the relative difficulty of optically aligning a small volume flow cell. For these reasons, the 9.2 µliter cell was preferentially used.

Initially the waveguides were sealed to the flow cells with a gasket fabricated from RTV silicone[79]. A thin film of RTV was wiped onto the Lucite block, covering the entire surface and filling the channel. This was then pressed against a Teflon block and allowed to cure. After curing, the block was easily removed from the Teflon block, leaving a thin, even coat of RTV on the surface of the flow cell. The RTV filling the channel was then removed with a single edge razor blade. The flow cell was then pressed against the waveguide using finger pressure and mounted into the prism coupler jig. The RTV gasket made an excellent seal and did not overly attenuate the beam in the waveguide. However, after period of a day, the beam was severely attenuated, and eventually was completely extinguished in the guide. Upon examination it was determined that the RTV had "creeped" and a thin film had covered the active portion of the waveguide thus, changing the coupling conditions for the waveguide. This is a common problem with silicon RTV and for this reason its use as a gasket material was discontinued[80].

Several other gasket materials were tried but the best results were obtained with Teflon tape. A slot that matched the dimensions of the flow channel was cut in a piece of Teflon tape 1.25" long and 0.75" wide. This was sandwiched between the flow cell and waveguide and the entire apparatus was held together with four bolts. With moderate pressure,

no leaks or attenuation of the guide was observed. With the 4.6 and 9.2 μliter flow cells, the pressure applied between the waveguide and the flowcell was sufficient to prevent leaks, and as a result, the Teflon gaskets were omitted. A diagram of the assembled waveguide flow cell combination is shown in Figure 19.

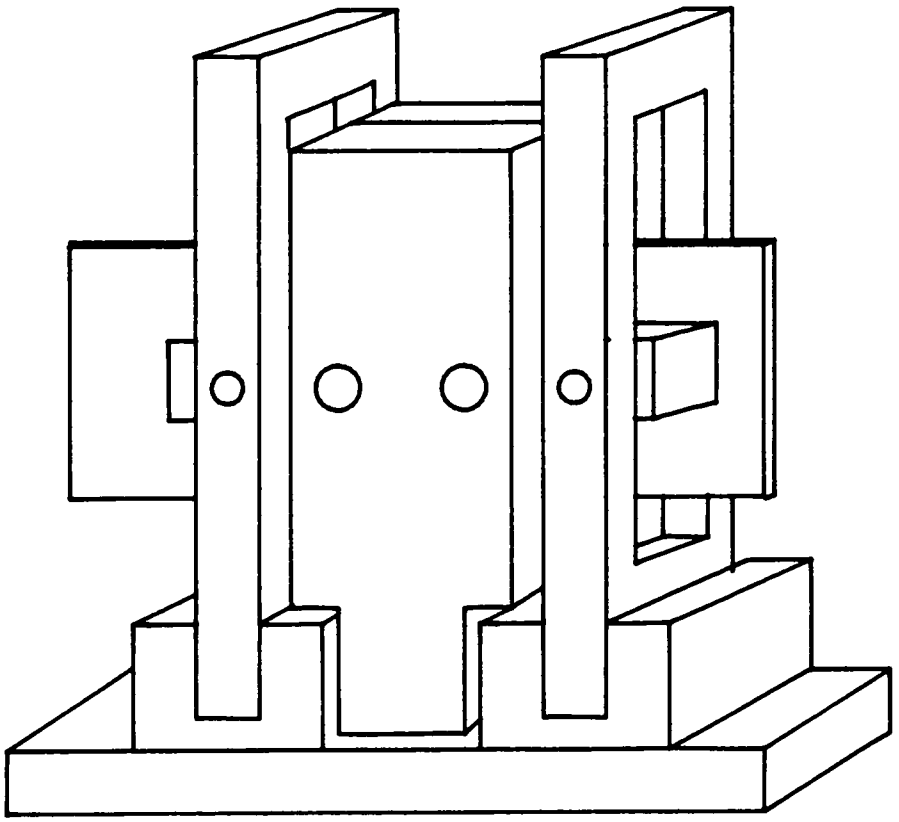

Figure 19. Assembled Waveguide Prism Coupler with Flow Cell.

V. EXPERIMENTAL

A. Waveguide Evaluation

The waveguides, after fabrication, were tested to determine three properties: film index, film thickness, and film index profile. The thickness and index of refraction of the waveguides were measured using the synchronous angle technique developed by Tien[42]. The refractive index profile of the waveguides was inferred from the fabrication process and corroborated by observing the mode structure. Determination of these physical properties was necessary to provide a measure of the sensitivity of the device as an absorption element.

All of these measurements relied upon accurately determining the coupling angle of each mode supported by the waveguide. Measuring the coupling angle for each mode is trivial; it is the discrete angle between the prism and laser beam which causes a streak of light to propagate in the waveguide. The real difficulty, as first pointed out by Zernike, is the determination of the reference angle from which the coupling angles are measured[45]. Normally the reference angle, 0°, is chosen where the prism face is normal to the input laser beam, thus reflecting the beam back onto itself. This reference point can be determined either rigorously, using an auto-collimator, or approximately, by "eyeballing" the angle at which the input and reflected beam overlap each other.

The auto-collimator and alignment procedure used, was very similar to Zernike's method (Figure 20)[2]. The laser beam was focused to a spot by a f/2, 50 mm focal length convex lens and recollimated by a 75 mm focal length f/1.5 lens. This beam was reflected from the front face of the coupling prism and imaged onto the detector through a 50 micron diameter pinhole, using a cube beam splitter. A Hewlett Packard 2-4207 photodiode, operated in the photoconductive mode, was mounted with the pinhole on an xy translation stage, and served as the detector.

The alignment of the pinhole is crucial to correctly autocollimate the transmitted beam (i.e. ensure that the prism face is normal to this beam). This initial alignment was accomplished with the aid of a plane mirror placed at the focal point of an additional focusing lens that was inserted into the system after the 75mm focal length lens. This mirror was rotated until the transmitted beam was reflected upon itself and the pinhole was then adjusted to give the maximum signal from the photodiode. The success of this method relied upon the fact that a focused beam cannot be auto-collimated. A beam that is focused onto a flat mirror and subsequently reflected back through the lens is recollimated by the focusing lens. As a result, the reflected beam is parallel to the incident beam, whether, or not the mirror is in the exact focal spot of the lens. Therefore, the position of the pinhole which maximizes the

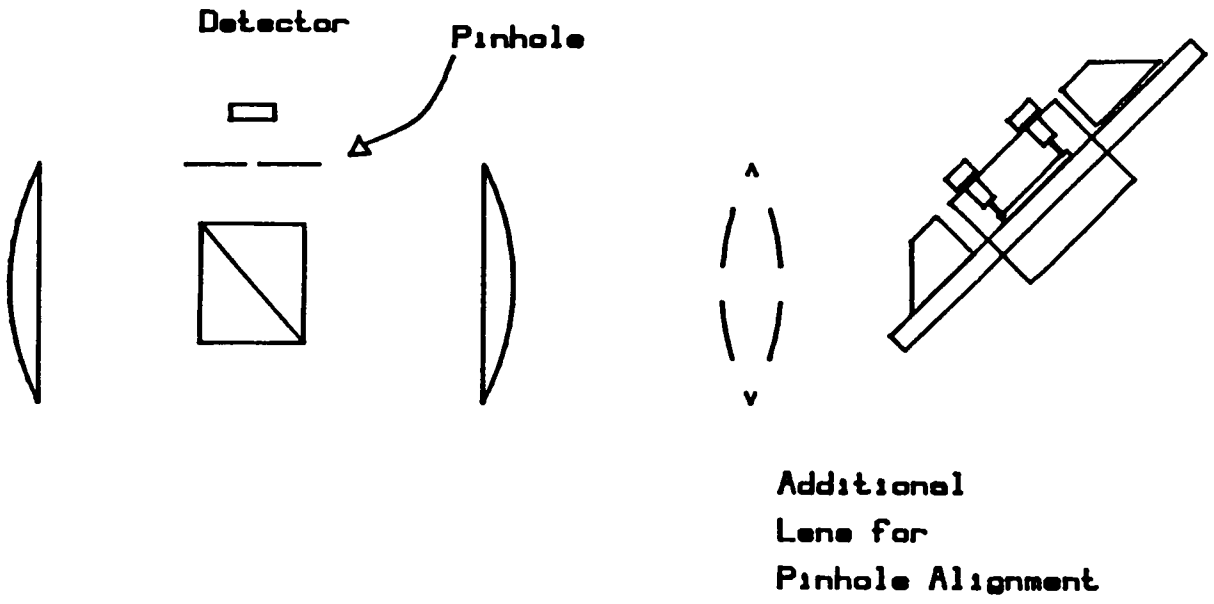

Figure 20. Autocollimator Optical Alignment.

signal from the photodiode will locate the angle where the two beams overlap. This angle was determined by removing the extra focusing lens and replacing the plane mirror with the prism jig coupler. The prism coupler was rotated until the beam reflected from the prism face overlapped the incident beam and the photodiode signal was maximized. The angle on the rotator compass was then recorded as the zero reference point.

The accuracy of this method was limited to the rotational accuracy of the rotator which was ± 1 arc minute. A much less time consuming method, and one that was not significantly less precise, relied upon observing the image of the beam reflected by the prism face back onto the focusing lens. In this case the beam was not expanded, but focused directly onto the coupling spot (the back edge of the prism). When the prism coupler was rotated such that the incident beam approached the normal to the prism face, the image of the reflected beam appeared on the focusing lens. Further rotation caused overlap between the image and the incident beam and when these two spots coincided, the angle on the rotator compass was recorded as the zero reference point. By repeated experiment it was determined that the zero reference point could be readily measured to within ± 0.1° using the vernier scale on the rotator. Conservatively, the error in determining this point was calculated to ± 0.2°, or 12 minutes of arc .

Once the zero reference angle was determined the coupling angles of each of the modes were then measured. The approximate angular positions were first determined by tightly clamping the prism to the waveguide, thus ensuring maximum coupling of the beam into the thin film. This however, slightly shifts the coupling angles due to the compression of the waveguide and air gap beneath the prism[67]. The correct angles were then determined after reducing the pressure on the prism coupler to finger tightness.

The index of refraction of the substrate was the final variable measured in order to calculate the three waveguide properties. This was determined, in a total internal reflection experiment, by measuring the coupling angles for both the critical and grazing incidence angles for a beam guided in the substrate. The substrate, which was either a glass microscope slide or a Pyrex 7740 slide, was mounted in the prism coupler and the reference point determined by the approximate method discussed above. At the reference angle the beam was usually coupled into the substrate at an angle greater than the critical angle and thus guided down its length by total internal reflection. Typically the beam was observed to bounce between the air substrate interface many times before exiting the end of the slide. Grazing incidence was determined by rotating the prism assembly until the number of bounces gradually diminished, and were

then eventually extinguished. The coupling angle for which the beam emanating from the end of the guide was just extinguished was used as the grazing incidence angle. The critical angle was determined by rotating the prism coupler in the opposite direction, and through the reference point. As the coupler was rotated to the angle where the guided beam traversed the substrate at the critical angle, the beam intensity was dramatically attenuated. This angle was recorded as the critical angle for the substrate air interface.

The coupling angles, i, for each of these measurements were related to the internal angle, ϕ_i, and thus, critical angle and grazing incidence by equation 5.1.

$$N_{sub} * \text{Sin}\ \phi_i = N_{prism} * \text{Sin}[A + \sin^{-1}(\sin(i)/N_{prism})] \quad 5.1$$

At the critical angle, the left hand side of equation 5.1 is equal to the refractive index of air, while at grazing incidence it becomes equal to the refractive index of the substrate. The measured indices for both substrates is presented in Table 2.

The effective indices and thickness of the waveguides were then calculated using the measured mode coupling angles and substrate indices by means of the three layer characteristic equation 3.21. The limiting source of error for these calculations was due to the uncertainty of the

Table 2. Refractive Index for glass and Pyrex substrates.

Substrate	Microscope Slide	Pyrex 7740
Wavelength	632.8 nm	632.8 nm
Grazing Incidence	11.6°	6.0°
Substrate Index (calc)	1.5127	1.4721
Substrate Index (reported)	1.5125	1.474
Critical Angle	-38.8°	N.A.
Index Air (calc)	1.0010	N.A.
Index Air (reported)	1.000297	1.000297

acute angle of the input coupling prism; this was usually not determined to better than 5 minutes of arc. In view of the considerable difficulty in aligning the auto-collimator, and its negligible contribution to increasing the accuracy of the measurements, the approximate method of determining the reference point was preferentially used.

The results of measuring the coupling angles and calculating the effective indices and guide thickness for a typical spin coated polystyrene film are listed in Table 3. The mode indices and width of a Ag^{+} diffused waveguide are also listed in this Table. As both the index and thickness of the thin film are unknown, the coupling angles for at least two modes must be measured in order to solve the characteristic equation. The form of the equation is transcendental and, as a result, can not be solved algebraically for the film index. Instead, a numerical approximation technique, based on a secant analysis[81], was used to solve iteratively for the best values of the film index and thickness, given the experimental mode measurements. As the characteristic equation was derived for step index planar waveguides, this method is not applicable to gradient index waveguides. However the approximate width of the silver ion diffused guides can be calculated using the diffusion coefficients determined by Stewart[57] and equation 4.2. The Fortran program, WAVSEC, is listed in the software appendix.

Table 3. Effective Indices for a Polystyrene Film.

	Mode 0	Mode 1	Mode 2
TE	22.97°	17.95°	12.66°
Effective Index	1.587	1.540	1.486
Substrate Index	1.4780 at 488.0		
Film Index	1.597 at 488.0 nm		
Thickness	.9864 microns		

10% polystyrene in chlorobenzene (w/w) spun at 1500 RPM

Effective Indices for a Silver Ion Diffused Waveguide

	Mode 0	Mode 1	Mode 2	Mode 3
Coupling angle TE	1.41	7.17	11.74	15.25
Neff	1.601	1.578	1.555	1.534
Substrate Index	1.5127 at 632.8 nm			
Diffusion Depth	4.55 microns			

Microscope slide immersed in $AgNO_3$ at 280 °C for 15 minutes.

The refractive index profiles of the waveguides were qualitatively determined by observing their mode spectra[54]. Waveguides fabricated by spinning or dip coating a polymer onto a glass substrate were assumed to have a step index profile, while those formed by a silver ion diffusion were assumed to have a gradient index profile. Mode spectra for both a polystyrene waveguide and a Ag^+ diffused guide are shown in Figures 21-22. The mode spacings for the polystyrene guide are closer together at the lower order modes and become progressively farther apart for the higher order modes. The mode spacings for the Ag^+ guide, on the other hand are evenly spaced, indicative of a gradient index waveguide. A plot of the effective index squared versus mode number squared for a polystyrene waveguide is approximately linear, in accordance with theory. However, a plot of the effective index squared versus the mode number, Figure 23, gives a much better fit to the experimental data. This is a result of the asymmetric index profile of the waveguide. The plot of effective index squared versus mode number for a Ag^+ ion diffused guide, Figure 24, shows excellent linearity. This agrees with the theoretical solution for a beam confined to a parabolic well[82].

The final evaluation of the waveguides was to test them under conditions similar to flow injection analysis. The guides were placed in a flow cell and mounted on the prism coupler. A helium neon laser beam was coupled into mode

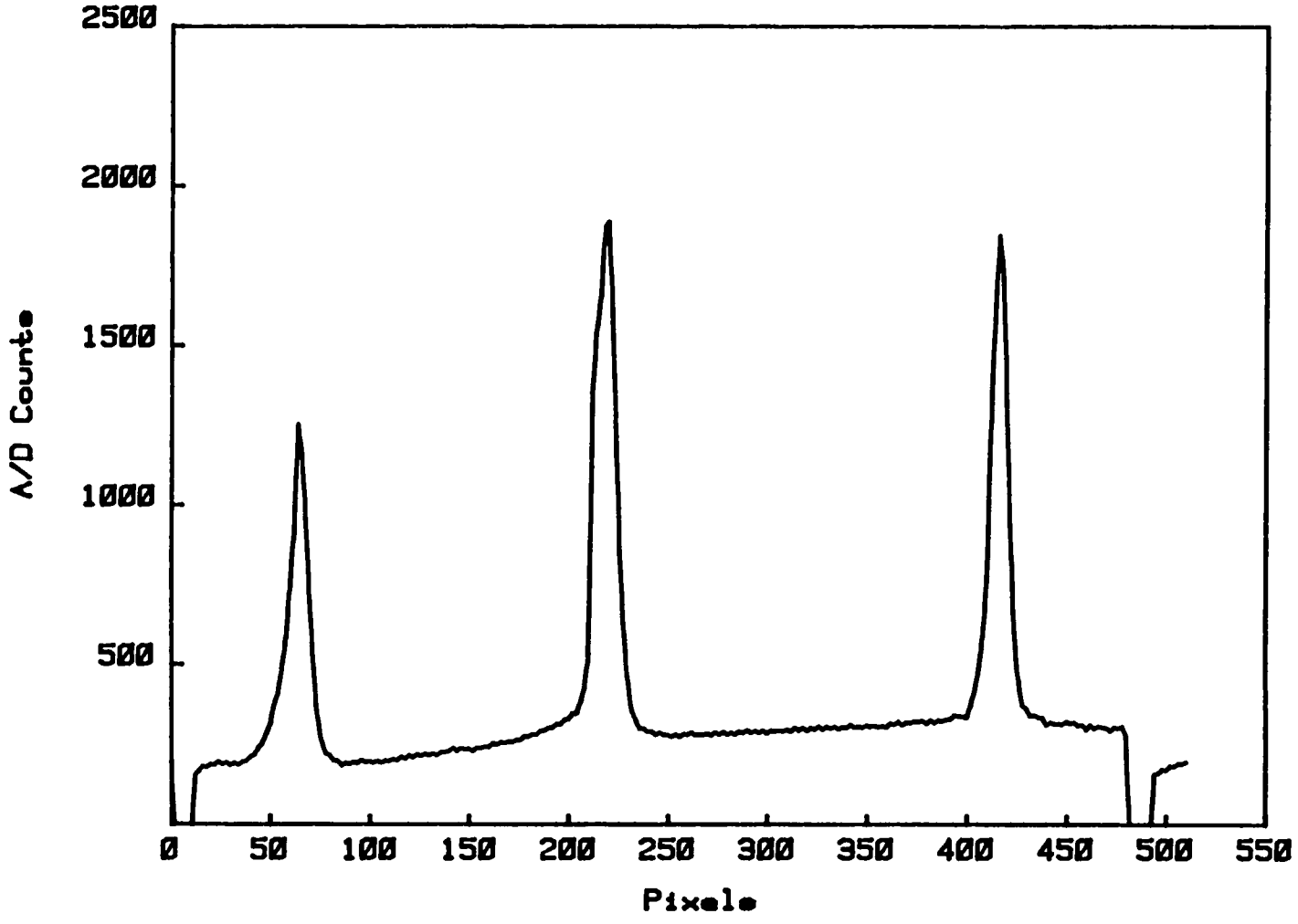

Figure 21. Polystyrene Mode Structure.

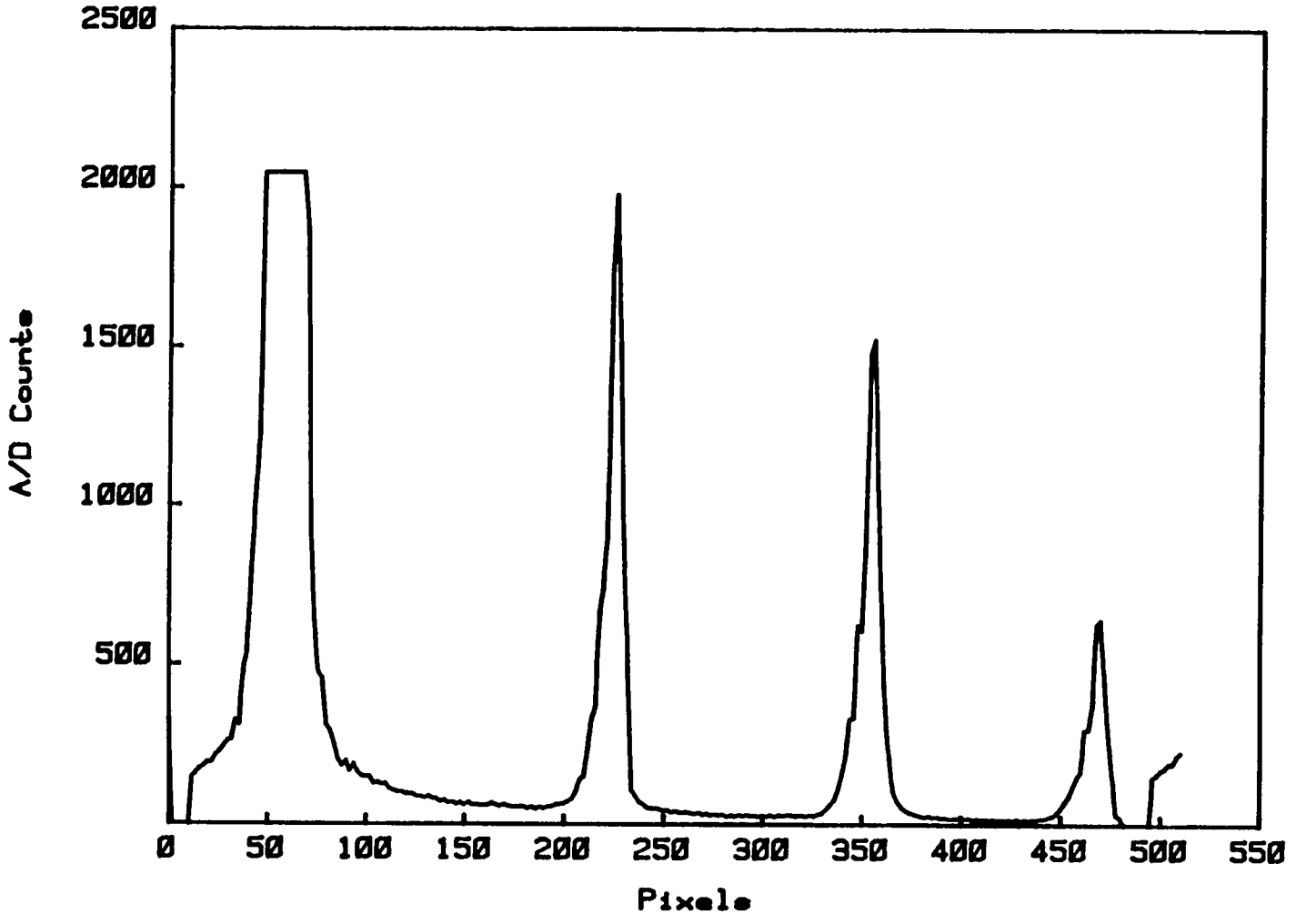

Figure 22. Silver Ion Diffused Waveguide Mode Structure.

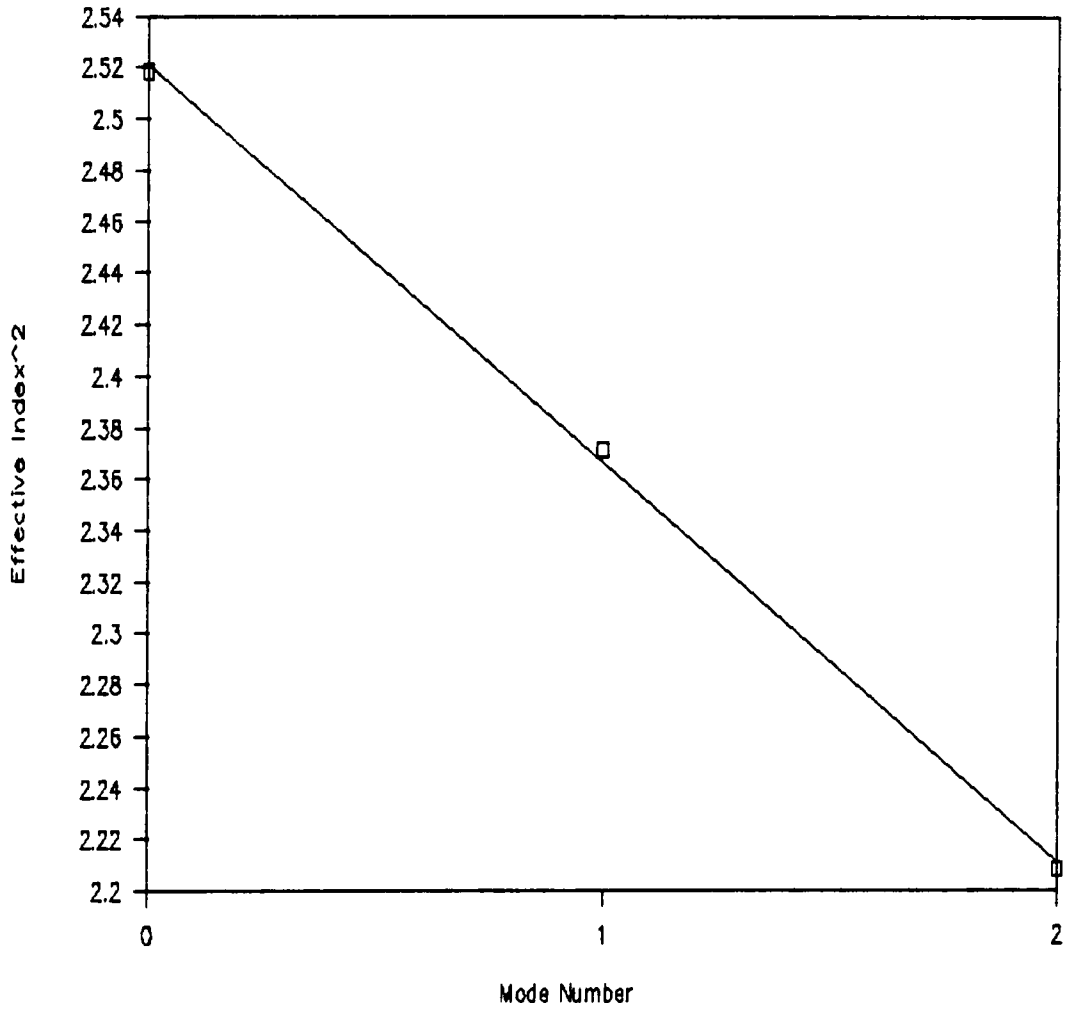

Figure 23. Effective Index Squared versus the Mode Number for a Polystyrene Thin Film Waveguide .

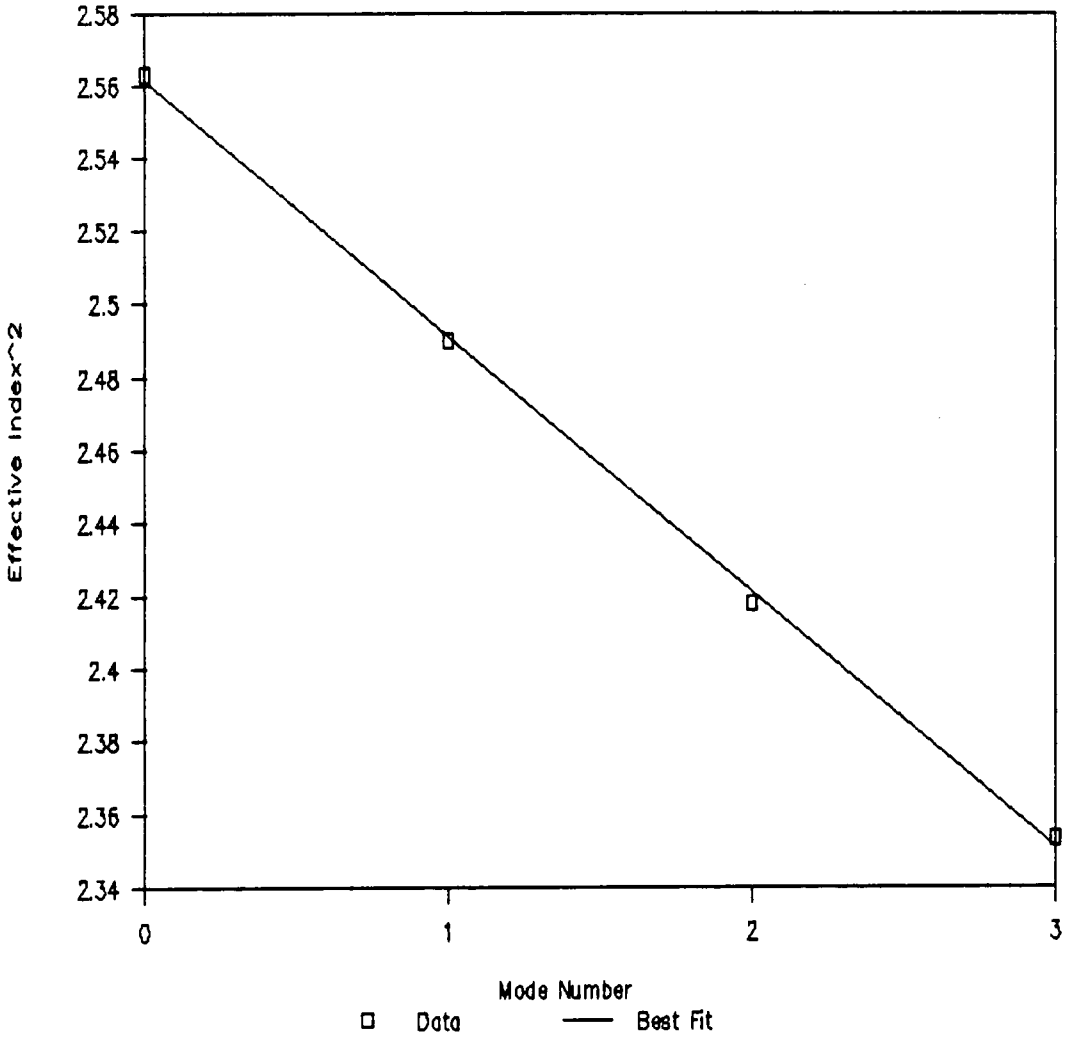

Figure 24. Effective Index Squared versus the Mode Number for a Silver Ion Diffused Waveguide .

zero for each of the guides, propagated down the length of the flow cell, and then coupled out and directed onto a photodiode power meter. The baseline was recorded for each guide under dry conditions for a period of 5 minutes. In all cases for the polystyrene, photoresist, and Ag^+ guides, these baselines were stable to within 0.5% of the total signal (i.e. the baseline fluctuation was no more than ± 0.025 volts on a 5 volt baseline). Next distilled water was pumped through the flow cell at rates varying from .1 to 3 ml/min, using a peristaltic pump. The polystyrene waveguides showed very erratic behavior and usually in less than 5 minutes the beam was completely attenuated in the film. It was determined that the thin film polystyrene waveguides were delaminated from the glass or Pyrex substrate, under all flow conditions. The photoresist guides were much more stable, and could be used for at least 1 hour in a flowing stream without any apparent signs of delamination. The Ag^+ guides were of course immune to delamination and physical abrasion, and were also very stable over a wide range of flow rates.

Next, the photoresist and Ag^+ guides were tested in an aqueous alkaline solution (pH=11) to determine their stability under conditions similar to the flow injection analysis of ammonia using Berthelot's reaction[83]. Under these conditions the photoresist guides were found to rapidly delaminate. Although a post bake appeared to

increase their resistance to delamination, the guides were eventually destroyed upon continued exposure to the alkaline solution. Although silane coupling reagents are often used to improve adhesion between a photoresist and substrate, they are unfortunately rapidly hydrolyzed in alkaline media, and therefore useless under these conditions. The Ag^+ ion guides maintained stable baselines at all flow rates for periods of several hours in the alkaline solution. As a consequence of their durability and stability, they were chosen as the type of waveguide to pursue as an absorbance sensor.

B. Berthelot Reaction

Indophenol blue or 2,5 cyclohexadiene-1-one-4-[4-hydroxyphenyl-imine] (CAS [500-85-6]), is the parent compound for a class of dyes that are normally produced by the oxidative coupling of p-aminophenol and its C-substituted derivatives with mono or polyhydric phenols. These compounds are decolorized on reduction to a diphenylamine derivative, the so called leuco-compound, and can be reversibly re-oxidized to the dye. The indophenol dyes are also acid-base indicators; the acid form of the dye is usually slightly yellow, while the base form is intensely blue. The color of the indophenolate ion is attributable to a single absorption band in the visible, centered at 630 nm,

whose intensity ($\epsilon_{max} \approx 10^4$) and response to substituents, is indicative of a π to π^* transition[84]. The visible spectra of indophenol blue is shown in Figure 25, while its structure and associated numbering system is depicted in Figure 26.

Indophenol blue can also be produced by the oxidative coupling of ammonia to phenol in an alkaline hypochlorite solution using Berthelot's[85] reaction. The reaction sequence for the formation of indophenol blue using Berthelot's conditions was first suggested by Bolleter, Bushman and Tidwell and is depicted in Figure 27.[86] It is a three step sequence in which hypochlorite first reacts with ammonia to form monochloramine at a solution pH greater than 7. This step is pH dependent, as dichloroamine is predominantly formed at solution pH between 5-7, while trichloramine is produced below pH 4.5.[87] Taking the rate of formation and pH dependent decomposition of the monochloramine into consideration, Patton and Crouch[88] determined that the optimal pH range for monochloramine formation was between 10.5 and 11.5.

The second, and postulated rate determining step is the oxidative coupling of monochloramine to phenol to form a quinone monochlorimine. The rate of the overall reaction, and ostensibly the rate of this coupling step, is greatly increased in the presence of a catalyst or coupling agent. Many different catalysts such as acetone[89], Mn(II)[90],

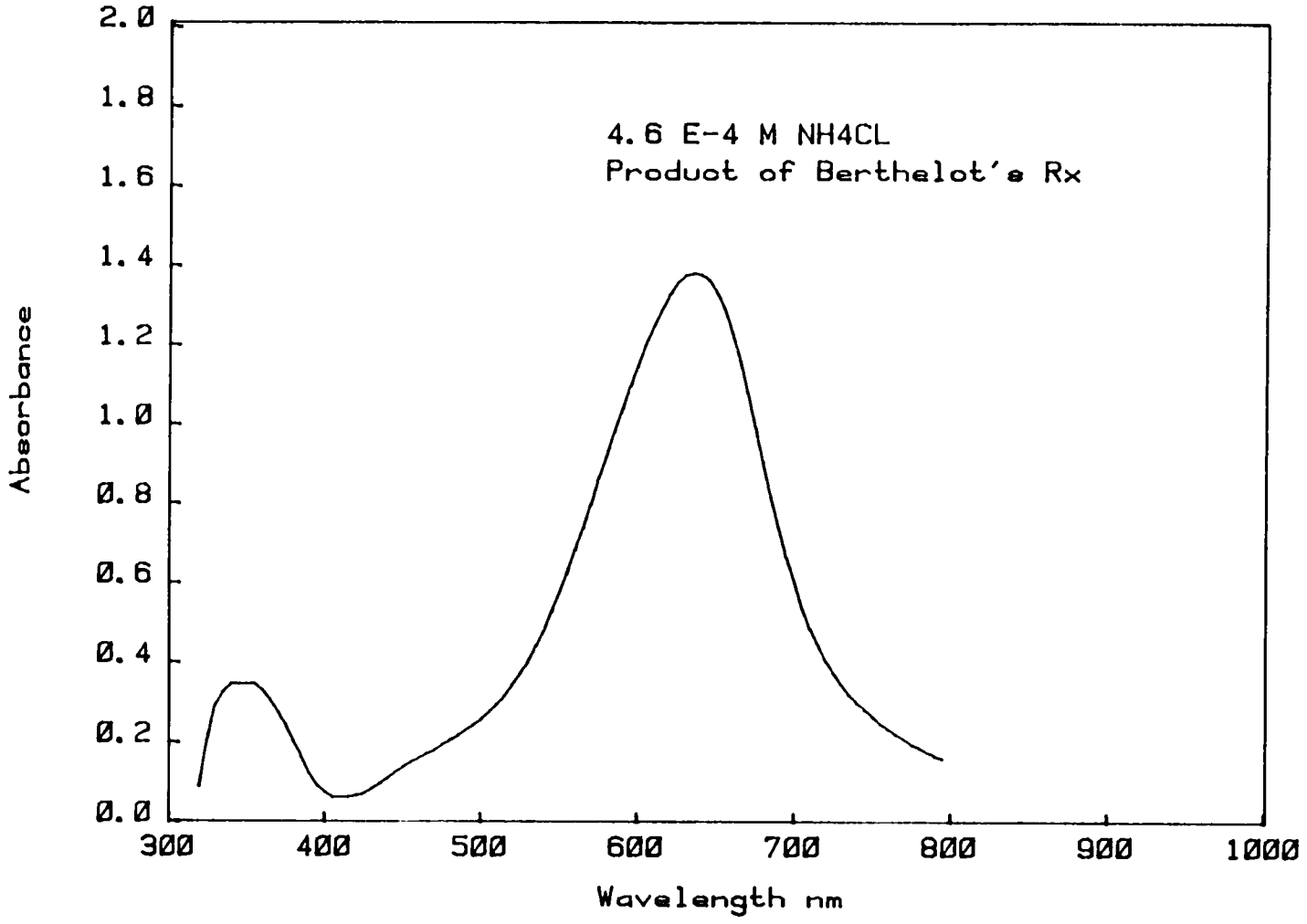

Figure 25. Visible Spectra of Indophenol Blue.

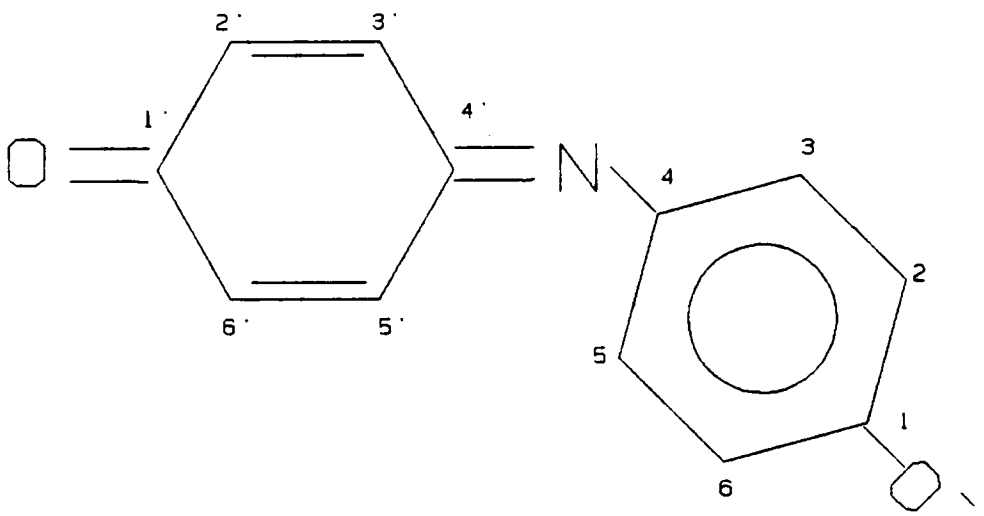

Figure 26. Indophenol Blue.

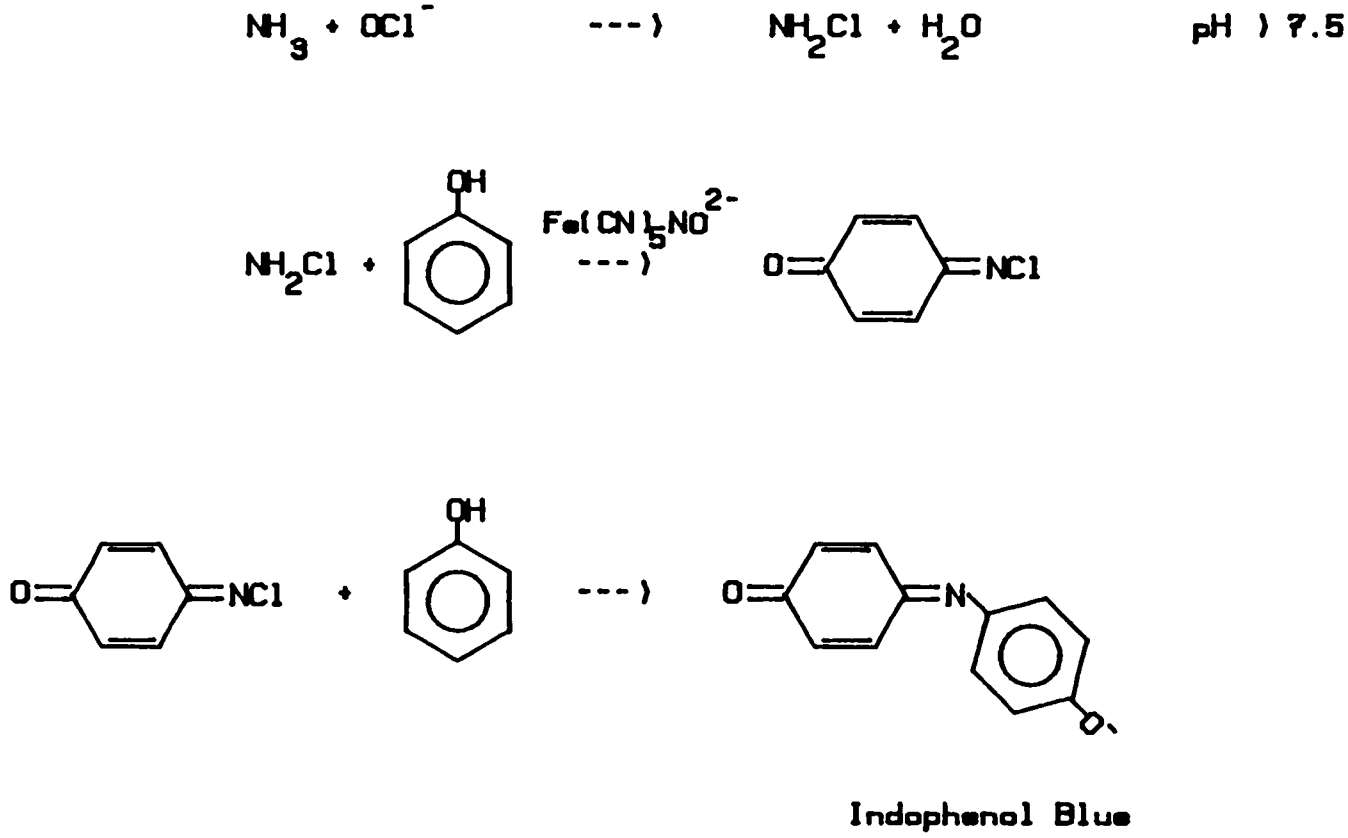

Figure 27. Berthelot's Reaction.

Fe(III)[87],Ag(I)[91] have been studied, but the most effective is sodium nitroprusside.[92] To this date, the role and mechanism of the "catalyst" is unknown, but several workers hypothesize that sodium aquopentacyano ferrate(II), a species in equilibrium with the nitroprusside ion, may form a complex with the monochloramine, which is then oxidatively coupled to phenol to form quinone chlorimine[89,93]

The quinone chlorimine produced is then rapidly coupled with an additional mole of phenol to form an indophenol dye. Corbett extensively studied the coupling reactions of benzoquinone imines with substituted phenols and determined that the reaction occurs in two steps[94]. The first is the rate determining electrophilic coupling of the monoimine with the para position of the phenol. The resulting leuco-compound, 4,4'-dihydroxydiphenylamine, is then rapidly oxidized by another mole of the monoimine (or suitable oxidizing agent), in the second step, to the indophenol. Soloway[92] studied the oxidative coupling of over 65 substituted phenols with ammonia and concluded that for adequate dye formation the para position of the phenol must be unsubstituted, lending credence to the final step of Bolleter's proposed sequence as an electrophilic addition of the quinone chlorimine to phenol.

Berthelot's reaction has been extensively studied and applied to the spectrophotometric determination of ammonia, phenols, and p-aminophenols[95]. The sensitivity of the

reaction is reported in the low ppb range for ammonia for both the standard[96] and for the automated[97] versions of the reaction. As a result, the method has been adopted by several government agencies including the American Public Health Association[97], the Environmental Protection Agency, the United States Geological Survey,and ASTM, as a standard method for the determination of ammonia in natural and waste waters. Unfortunately, due to the complexity of the reaction mechanism, optimization of this reaction is difficult, and poor precision has plagued the method in previous studies[89]. Application of the method by flow injection analysis, however, where tighter control of the reaction parameters is possible for a large number of samples, has improved the precision obtained[98]. In order to optimize the reaction conditions for the FIA manifold described in the Instrumental Section (Figure 11) a series of experiments was performed to determine the order of addition, optimal temperature, and flow rate of reagents.

1. Order of Addition

Normally, the spectrophotometric determination of ammonia using Berthelot's reaction involves the addition of two reagents to the solutions of ammonia, following Chaney and Marbach's procedure[99]. These reagents are typically a solution of phenol with sodium nitroprusside and an alkaline

hypochlorite solution. Bolleter's mechanism would suggest that the alkaline hypochlorite solution be added first, followed by the phenol/catalyst solution. However, it is frequently found that prior addition of the phenol to the ammonia solution yields much better color development and a higher sensitivity to ammonia, especially in automated versions of this reaction.[100] To determine the optimal order of addition of Chaney's reagents to ammonia solutions, both the standard UV-VIS method and an FIA method were studied using the manifold described in the Instrumental Section (Figure 11).

Standard ammonium chloride solutions were used to prepare the calibration curves for these experiments. Reagent grade NH_4Cl was dried to constant weight at 120 °C. A 1 mM stock solution was prepared by dissolving the weighed portion of NH_4Cl in a pH 7.0, 0.1 M phosphate buffer, which contained 5 mM EDTA and several milliliters of chloroform as a preservative. All working ammonia solutions were prepared by volumetric dilution of the stock solution, and refrigerated until used. The two Chaney and Marbach solutions were prepared as described in the original paper[103].

Solution A, a 0.5 M phenol/1mM $Na_2[Fe(CN)_5NO].2H_2O$ solution was prepared from reagent grade phenol and sodium nitroprusside dissolved in the 0.1 M phosphate buffer. Solution B, a 0.5 N NaOH/.03M OCl^- solution was prepared by

mixing 250 ml of reagent grade 1.0 N NaOH with 25.0 ml of commercial Chlorox bleach (5.25 w/v% OCL^-) and diluting to a final volume of 500 ml with 0.1 M phosphate buffer. Solution C, an alternative to the neutral phenol solution, was an alkaline 0.5N phenol/ 1 mM sodium nitroprusside solution prepared from reagent grade phenol and sodium nitroprusside and diluted with 0.5N NaOH stock solution (dilute 1.0 N NaOH with 0.1 M phosphate buffer). All solutions were stored refrigerated in dark glass containers until used.

Standard UV-VIS Experiments

Four experiments were performed to determine the sensitivity on the order of addition of the reagents to three standard ammonium chloride solutions. The orders tested were: neutral phenol followed by hypochlorite, hypochlorite followed by neutral phenol, alkaline phenol followed by hypochlorite, and hypochlorite followed by alkaline phenol. In a test tube, 1.0 ml of the first reagent was added to 400 microliters of the standard ammonium chloride solution and thoroughly mixed. Then 1.0 ml of the second reagent was added to this test tube, mixed, and then developed in a thermostatted water bath at 75 °C ± 1°C for 2 minutes. The absorbance of the solutions was measured after the solutions had cooled to room temperature and developed for a period of two hours. The absorbance

readings were taken on a Perkin-Elmer 330 UV-VIS spectrometer in 1 cm UV silica cuvettes. All absorbance readings were taken at 632.8 nm and for the blank absorbance by developing 400 microliters of .1 M phosphate buffer in a similar fashion as the ammonia samples. The results are tabulated in Table 4 and graphed in Figure 28-29.

FIA Experiments

Phenol, alkaline phenol, $NaOH/OCl^-$ and the phosphate buffer solutions were prepared as described above. Four ammonium chloride standards ranging in concentration from 4.6e-5 M to 4.6e-4 M NH_4Cl were prepared by volumetric dilution from a stock ammonium chloride solution. A 60 microliter sample of the ammonium chloride solution was injected onto the FIA manifold and the order of addition of the phenol and alkaline hypochlorite solutions varied to determine the sensitivity of the method under these conditions. The flow rates of all three reagent streams, the phosphate carrier, phenol, and alkaline hypochlorite were fixed at 0.7 ± .05 ml/min. The temperature of the FIA manifold was set to 37 °C ± 1 °C while the development coil was thermostatted to 75 °C. A Helium Neon laser focused through an 8 microliter, 1 centimeter path length, Kratos[101] 8 microliter, HPLC flow cell in combination with a UDT

Table 4. Absorbance of standard ammonia solutions as a function of the order of addition of the Berthelot reagents. Standard spectrophotometric method with neutral phenol.

Phenol followed by alkaline hypochlorite

[NH_4Cl]	Mean $A_{632.8}$ ± Std.dev (%RSD)
4.607e-4	1.349 ± .0173 (1.28)
9.213e-5	0.269 ± .0073 (2.70)
4.607e-5	0.133 ± .0079 (5.98)

Regression Results	
Y intercept	-0.0018
Standard error of Y Estimate	0.0134
Correlation Coefficient	0.9995
Number of observations	9.
Slope	2931.66
Standard error of Coefficients	24.00

Alkaline hypochlorite followed by Phenol

[NH_4Cl]	Mean $A_{632.8}$ ± Std.dev (%RSD)
4.607e-4	0.795 ± .049 (6.21)
9.213e-5	0.147 ± .0022 (1.47)
4.607e-5	0.111 ± .0082 (7.35)

Regression Results	
Y intercept	0.0135
Standard error of Y Estimate	0.0395
Correlation Coefficient	0.9878
Number of observations	9.
Slope	1691.75
Standard error of Coefficients	71.02

Table 4.(continued) Absorbance of standard ammonia solutions as a function of the order of addition of the Berthelot reagents. Standard spectrophotometric method with alkaline phenol.

Alkaline phenol followed by hypochlorite

[NH_4Cl]	Mean $A_{632.8}$ ± Std.dev (%RSD)
4.607e-4	1.109 ± .0070 (0.634)
9.213e-5	0.267 ± .0054 (2.04)
4.607e-5	0.149 ± .0053 (3.56)

Regression Results	
Y intercept	0.0486
Standard error of Y Estimate	0.0085
Correlation Coefficient	0.9997
Number of observations	9.
Slope	2303.87
Standard error of Coefficients	15.20

Hypochlorite followed by alkaline phenol

[NH_4Cl]	Mean $A_{632.8}$ ± Std.dev (%RSD)
4.607e-4	0.689 ± .0151 (2.19)
9.213e-5	0.162 ± .0029 (1.82)
4.607e-5	0.107 ± .0009 (0.88)

Regression Results	
Y intercept	0.0352
Standard error of Y Estimate	0.0110
Correlation Coefficient	0.9986
Number of observations	9.
Slope	1418.01
Standard error of Coefficients	20.22

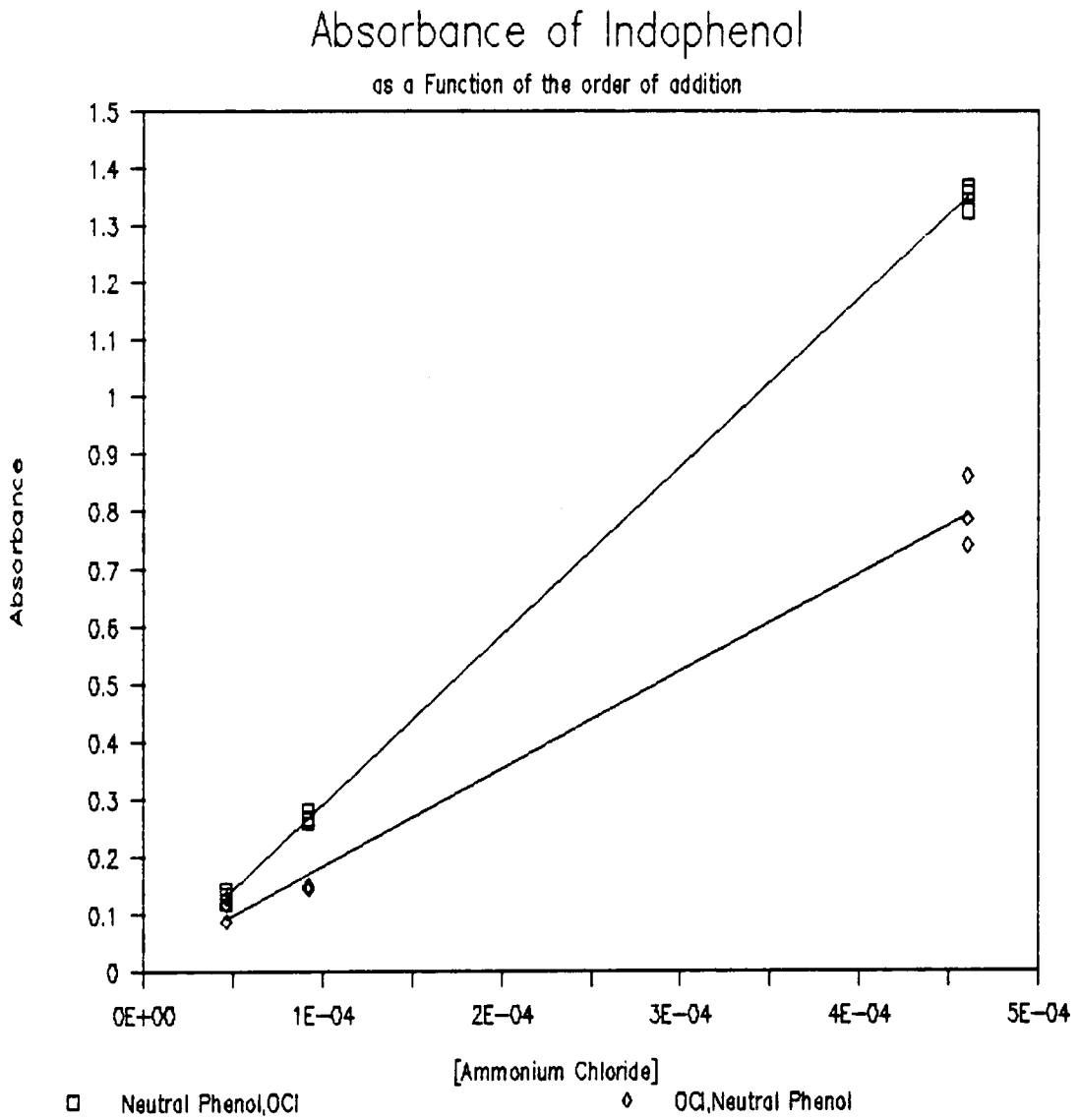

Figure 28. Results of the standard transmission experiment with phenol.

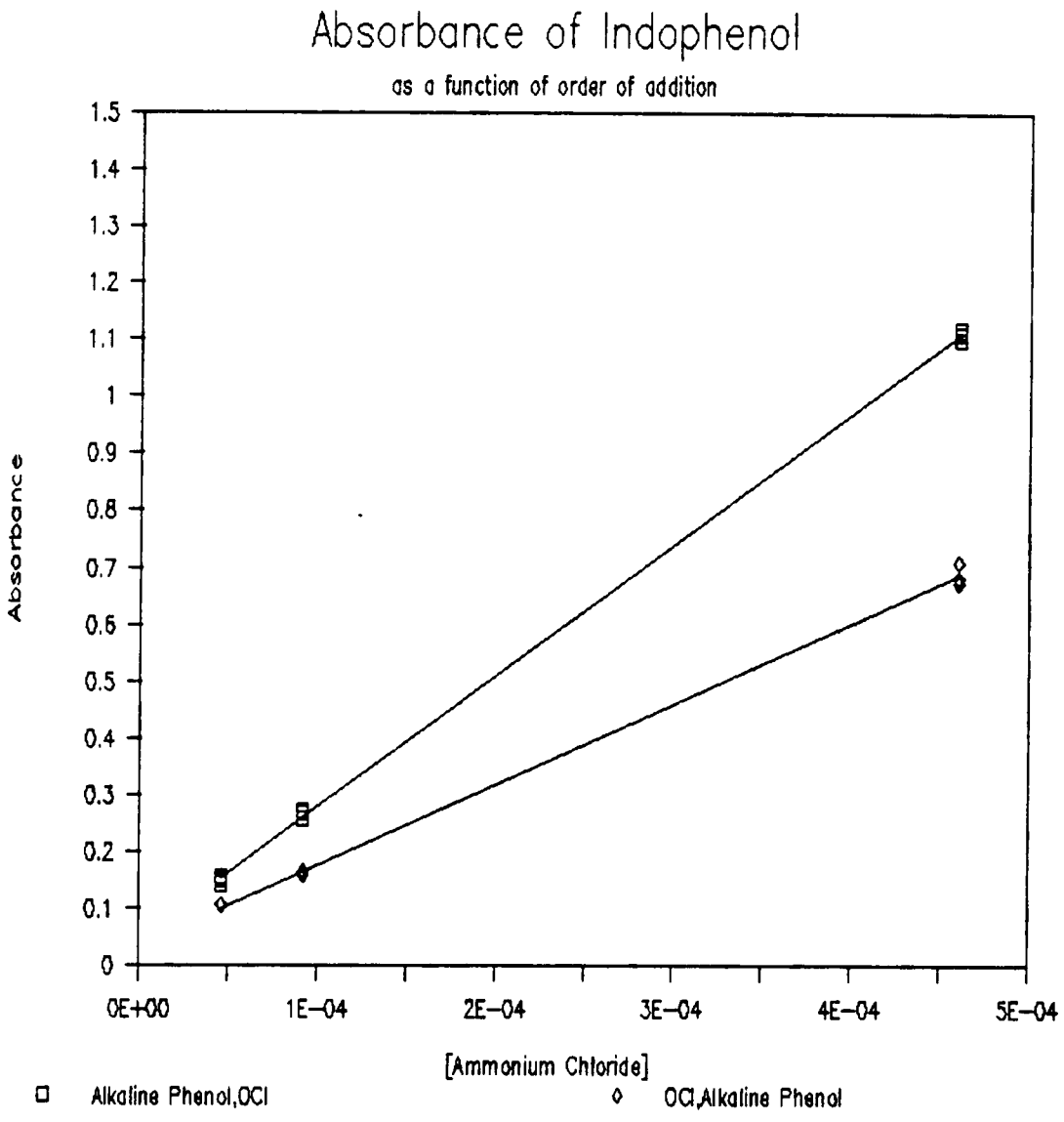

Figure 29. Results of the standard transmission experiment with alkaline phenol.

photodiode served as the absorbance detector. The results are tabulated in Table 5 and graphed in Figures 30-31.

Results of the Order of Addition Experiments

The order of addition of the reagents, as prepared by Chaney's method, was significant. Addition of the neutral phenol/sodium nitroprusside solution followed by the alkaline hypochlorite solution to an ammonia sample, in both the standard spectrophotometric and the FIA experiments, gave substantially higher sensitivities than any other combination of reagents. For the standard spectrophotometric method, addition of the sodium phenate followed by hypochlorite was approximately 15% less sensitive than adding the neutral phenol first. Addition of hypochlorite first followed by either phenol solution yielded approximately 50% the sensitivity of the neutral phenol. Similar results were reported by Mann[104] and Weatherburn[102].

The results obtained with the FIA experiments were similar, with addition of neutral phenol followed by hypochlorite giving the highest sensitivity. Unlike the standard spectrophotometric method however, hypochlorite followed by alkaline phenol yielded the next highest response in the FIA experiment. These experiments were repeated, under identical conditions, and the order and magnitude of the slopes of the calibration curves were repeatable to within ±5%. Harwood[99] obtained similar

Table 5. Absorbance of standard ammonia solutions as a function of the order of addition of the Berthelot reagents. Flow Injection Analysis method with neutral phenol.

Phenol followed by hypochlorite

$[NH_4Cl]$	Mean $A_{632.8}$	± Std.dev	(%RSD)
4.607e-4	0.854	± .010	( )
2.303e-4	0.421	± .0004	( )
9.213e-5	0.165	± .0035	( )
4.607e-5	0.100	± .0066	( )
0	0.0012	± .0004	( )

Regression Results	
Y intercept	0.0031
Standard error of Y Estimate	0.0097
Correlation Coefficient	0.9991
Number of observations	15.
Slope	1839.78
Standard error of Coefficients	15.02

Hypochlorite followed by phenol

$[NH_4Cl]$	Mean $A_{632.8}$	± Std.dev	(%RSD)
4.607e-4	0.355	± .0034	(0.96)
2.303e-4	0.189	± .0048	(2.53)
9.213e-5	0.147	± .0048	(0.61)
4.607e-5	0.111	± .0004	(4.20)
0	0.0021	± .0004	(18.14)

Regression Results	
Y intercept	0.0009
Standard error of Y Estimate	0.0058
Correlation Coefficient	0.9982
Number of observations	15.
Slope	776.62
Standard error of Coefficients	9.1

Table 5.(continued) Absorbance of standard ammonia solutions as a function of the order of addition of the Berthelot reagents. Flow injection analysis method with alkaline phenol.

Alkaline phenol followed by hypochlorite

[NH_4Cl]	Mean $A_{632.8}$ ± Std.dev (%RSD)
4.607e-4	0.273 ± .0018 (0.67)
2.303e-4	0.127 ± .0008 (0.60)
9.213e-5	0.043 ± .0011 (2.58)
4.607e-5	0.021 ± .0012 (5.72)
0	0.0023 ± .0050 (220.)

Regression Results	
Y intercept	-0.0056
Standard error of Y Estimate	0.0063
Correlation Coefficient	0.9965
Number of observations	15.
Slope	596.60
Standard error of Coefficients	9.75

Hypochlorite followed by alkaline phenol

[NH_4Cl]	Mean $A_{632.8}$ ± Std.dev (%RSD)
4.607e-4	0.531 ± .0026 (0.48)
2.303e-4	0.245 ± .0076 (3.11)
9.213e-5	0.090 ± .0034 (3.76)
4.607e-5	0.047 ± .0021 (4.37)
0	-0.0005 ± .0010 (192.)

Regression Results	
Y intercept	-0.0093
Standard error of Y Estimate	0.0098
Correlation Coefficient	0.9977
Number of observations	15.
Slope	1157.04
Standard error of Coefficients	15.28

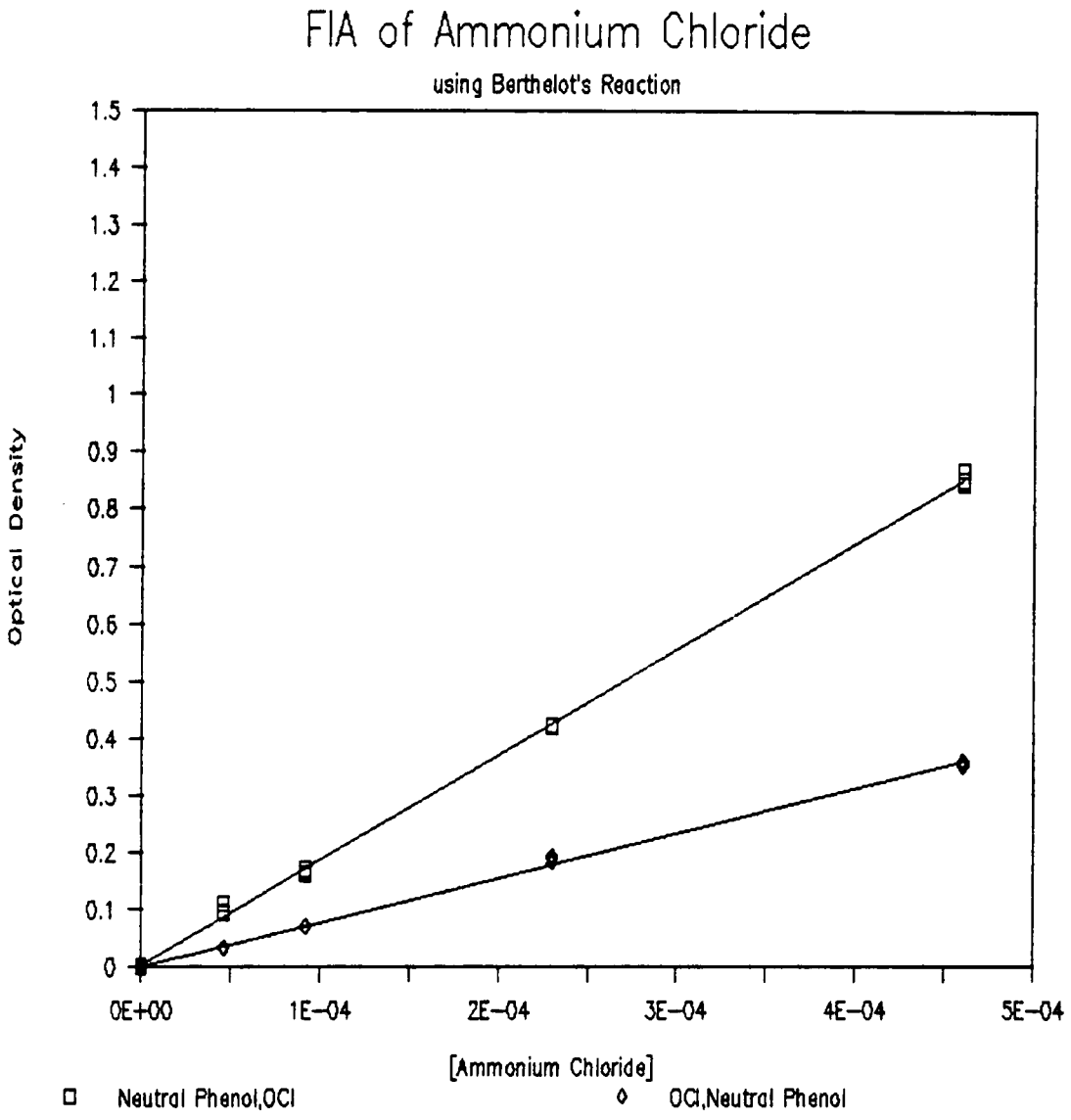

Figure 30. Results of the FIA transmission experiment with phenol.

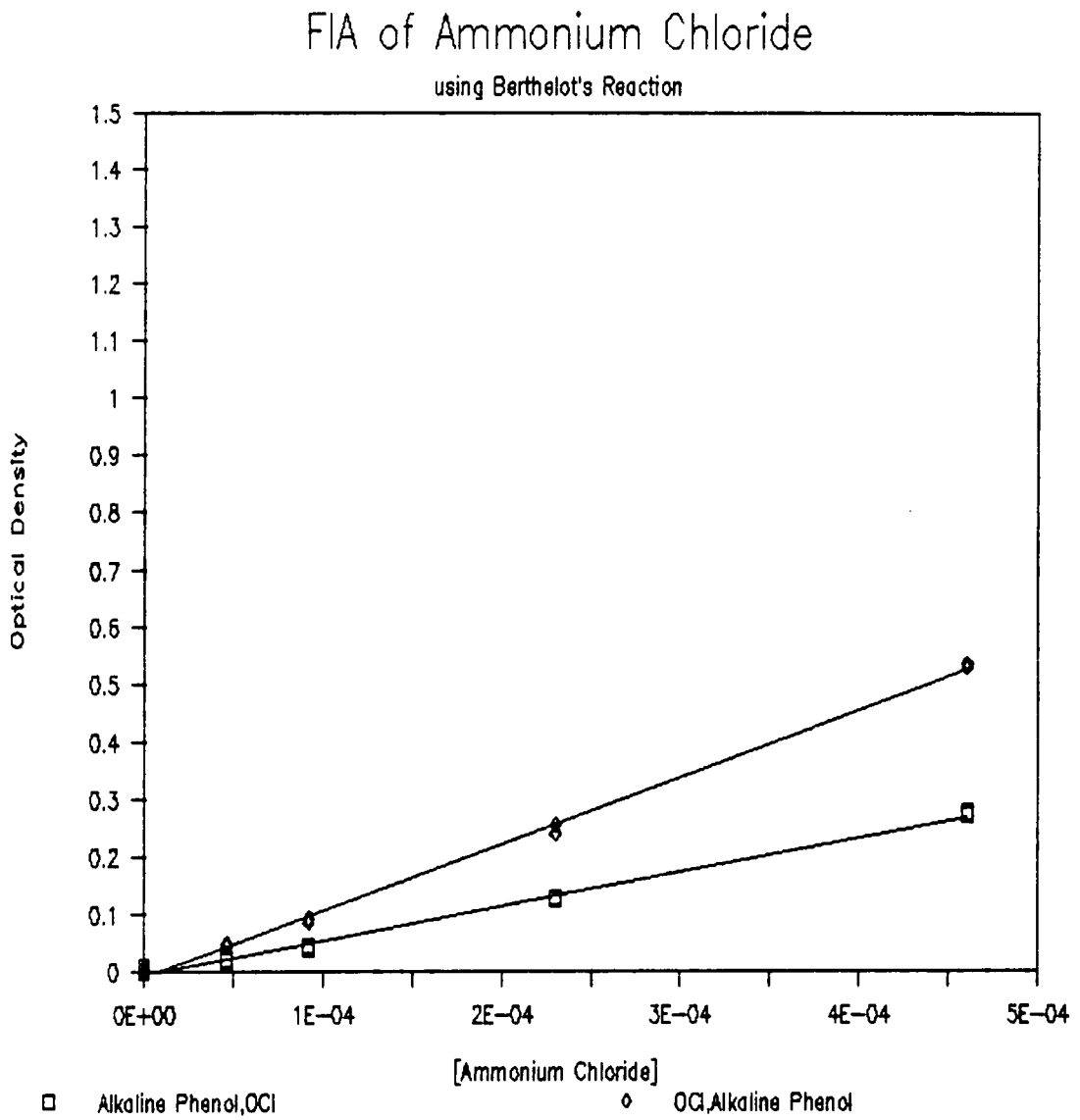

Figure 31. Results of the FIA transmission experiment with alkaline phenol.

results with a Technicon Autoanalyzer based determination of ammonia.

The results of this and previous investigations, where addition of phenol to ammonia followed by the addition of the hypochlorite solution gave maximum sensitivity, are difficult to rationalize given Bolleter's reaction scheme. This would require, for maximum sensitivity, initial addition of hypochlorite to the ammonia solutions. This has led several investigators to suggest that several reaction mechanisms might be involved[103,105,94]. However, it has been demonstrated that due to the acid-base characteristics of the dye, a final solution pH between 11 and 12.5 is necessary to optimize the sensitivity of this analysis. In a two reagent stream FIA method, this is typically ensured by using a sufficiently basic hypochlorite solution (ca. 0.5 molar in NaOH). The formation of chloramine, the compound responsible for oxidizing phenol to the quinone monochlorimine intermediate, is optimized at pH 8. Therefore, in an FIA manifold, if the first step in the experimental procedure is addition of neutral phenol followed by alkaline hypochlorite, dispersion in the flow stream will expose the ammonia sample to a gradually increasing pH. Conversion to chloramine will be more rapid than if the order of reagents were reversed. This observation explains the relative order of the standard UV-VIS results; the sensitivity of the analysis decreases as

the pH of the first added reagent, increases (neutral phenol pH=7, alk phenol pH=11, alkaline hypochlorite pH > 13). Thus Bolleter's reaction scheme seems to adequately describe Berthelot's reaction for either order of addition of the reagents, given the knowledge that solution pH affects both monochloramine formation and dye absorbance.

Another enigma is the structure of the catalyst. It is well known that sodium nitrosylpentacyanoferrate is converted to sodium nitropentacyanoferrate in alkaline solution,

$$[Fe(CN)_5NO]^{2-} + 2OH^- \rightarrow [Fe(CN)_5NO_2]^{4-} + H_2O$$
$$K_{eq} = 1.5 \times 10^6$$

$$[Fe(CN)_5NO_2]^{4-} + H_2O \rightarrow [Fe(CN)_5H_2O]^{3-} + NO_2^-$$
$$K_{eq} = 3.0 \times 10^{-4}$$

and that this nitro complex is also in equilibrium with the aquopentacyanoferrate ion[104]. The nitro complex has a strong absorbance band at 398 nm (Log ϵ= 2.92) while the nitrosyl compound has a much less intense absorbance band at the same wavelength (logϵ = 1.3). The nitro absorbance band has only been observed in the alkaline phenol solution, and more importantly, has never been observed in any indophenol spectra, regardless of the order of addition of reagents. Patton[89] reports an absorbance band at 392nm as the result of oxidation of the nitroprusside solution with either chloroamine or hypochlorite. Other workers[105] list 450 nm as the major absorption peak due to reduction of $Fe(CN)_5NO^{2-}$ in alkaline solution to $Fe(CN)_5NO^{3-}$. Neither the 450nm, nor

the 392 nm peak could be observed due to either low intensities or overlap with the intense indophenol absorption at 633 nm. While it is uncertain what form the "catalyst" takes during the coupling step of monochloramine with phenol, comparing the results of Patton and Crouch's method, who used the aquopentacyanoferrate complex, with those methods that use nitroprusside, suggests that the sensitivity of the reaction is not greatly affected by the initial structure of this ferricyanide complex.

2. Concentrations of reagents

The optimal concentration of the reagents for Berthelot's reaction has also been the focus of many studies[106,98,100,102]. The conclusion reached by these investigators was that above an empirically determined minimum concentration, the concentrations of the phenol/ nitroprusside and alkaline hypochlorite solutions could be varied over a wide range without affecting the sensitivity of the ammonia determination. Scheiner[105] found that the concentration of phenol could be varied between 2 and 7%(w/v overall) whereas Harwood[98] found that alkaline phenol could be varied between 2 and 5% with little affect on the final solution absorbance. Likewise, Weatherburn[102] determined that the concentration of the hypochlorite could be varied between 0.3 ml and 10 ml of commercial bleach solution

(5.25% hypochlorite) per 100 ml of alkaline hypochlorite solution with minimal affects upon the final solution absorbance. Scheiner's[105] results also indicated that the hypochlorite concentration could vary between 0.07 to 0.15%. Similarly, the optimum nitroprusside concentration was variable between 0.005 and 0.05% (w/w)[102]. Based on these studies, and the results from the initial FIA studies, the concentrations of the solutions used for the remaining experiments were 0.5M phenol/.025 %(w/w) nitroprusside in 0.1M pH 7 phosphate buffer and 0.5N NaOH/ .25 % OCl^- in pH 7.0, 0.1M phosphate buffer.

3. Temperature Dependence

Several investigators of the Berthelot reaction found that the temperature of the reaction had a significant effect upon the final color development. Weatherburn[102] was one of the first to study systematically the complex dependance of the reaction on temperature. In summary, he determined that the rate of color development between 20 °C and 50 °C was faster than at temperatures between 50 and 70 °C, but that higher temperatures produced a larger final solution absorbance. In contrast, Stewart[107] determined that heating the solution increased the rate of reaction significantly, but decreased its overall sensitivity. Furthermore, he found that the initial temperature of the

reaction controlled the overall sensitivity of the determination. Solutions initially at 5 °C yielded calibration curves with significantly higher sensitivities than those at higher temperatures (20-55°C), albeit determinations at 5 °C took over 17 hours before the color was fully developed. More importantly, he determined that the sensitivity of the method was preserved if the solutions were initially cooled; but then heated after an initial reaction period (5min) to increase the speed of development. Stewart's results have important consequences for an automated Berthelot analysis as they indicate that thermostatting the reaction initially at a lower temperature (37°C as will be necessary for an enzyme hydrolysis) followed by development at a higher temperature will maintain sensitivity yet speed color development. Several experiments were therefore performed to determine the temperature effects of a secondary development coil.

The phenol/nitroprusside and alkaline hypochlorite reagents were prepared as described previously. The ammonium chloride solutions were prepared fresh by volumetric dilution from a stock 1mM solution. All reagents were stored refrigerated until used. The FIA manifold used was described in Figure 11 with the exception of an additional 3 meter coil, attached immediately following the development coil. This additional coil was immersed in a 25 °C water bath, cooling the effluent to room

temperature before it reached the detector. A Kratos 8 microliter, 1 cm path length HPLC flow cell was used in conjunction with a UDT photodiode and Helium Neon laser as the detector.

During each experiment the overall temperature of the FIA manifold was maintained at 37 ± 1°C, while the temperature of the development coil was independently controlled between 37 °C and 75 °C. Four 60 microliter injections and a blank were measured for each concentration. The results are compiled in Table 6 and graphed in Figure 32.

Results of the Temperature Dependence Experiments

The sensitivity of the reaction was observed to increase monotonically with development coil temperatures between 37 and 61.5 °C and then to decrease slightly at higher temperatures. These results are in agreement with Stewart's findings for temperatures between 5 and 55°C, and also supported by Weatherburn, who noted that the color intensity rapidly faded at temperatures greater than 75 °C. Weatherburn concluded that at temperatures greater than 75°C, critical timing regarding the addition of the reagents and monitoring of the dye absorbance would be required in order to maximize the analytical sensitivity of the determination. Other investigators found that heating the

TABLE 6. FIA of NH_4Cl as a Function of Temperature.

Coil Temperature 37°C

[NH_4Cl]	Mean $A_{632.8}$ nm	± Std.dev. (%RSD)
9.213e-4	.2369	± .0069 (2.94)
4.607e-4	.0997	± .0032 (3.29)
2.303e-4	.0482	± .0009 (1.92)
9.213e-5	.0172	± .0017 (10.12)
Blank	-0.003	± .0017

O.D. = 261.05*[NH_4Cl] - .0095

Correlation Coefficient: .9924
Standard Error of Estimate: .0079

Coil Temperature 50°C

[NH_4Cl]	Mean $A_{632.8}$ nm	± Std.dev. (%RSD)
9.213e-4	1.2043	± .031 (2.58)
4.607e-4	.6378	± .022 (3.42)
2.303e-4	.3383	± .014 (4.06)
9.213e-5	.1341	± .0044 (3.27)
Blank	-0.0008	± .0035

O.D. = 1305.77*[NH_4Cl] + .017

Correlation Coefficient: .9969
Standard Error of Estimate: .0239

Table 6. FIA of NH_4Cl as a Function of Temperature (continued).

Coil Temperature 61.5°C

[NH_4Cl]	Mean $A_{632.8}$ nm	± Std.dev. (%RSD)
4.607e-4	.9566	± .0097 (1.02)
2.303e-4	.4847	± .0075 (1.55)
9.213e-5	.1894	± .0058 (3.07)
Blank	-0.0007	

O.D. = 2081.26*[NH_4Cl] - .0004

Correlation Coefficient: .9996
Standard Error of Estimate: .0079

Coil Temperature 73°C

[NH_4Cl]	Mean $A_{632.8}$ nm	± Std.dev. (%RSD)
4.607e-4	.8909	± .0042 (0.47)
2.303e-4	.4386	± .0112 (2.55)
9.213e-5	.1648	± .0022 (1.35)
Blank	-0.0036	

O.D. = 1963.67*[NH_4Cl] -.0139

Correlation Coefficient: .9995
Standard Error of Estimate: .0082

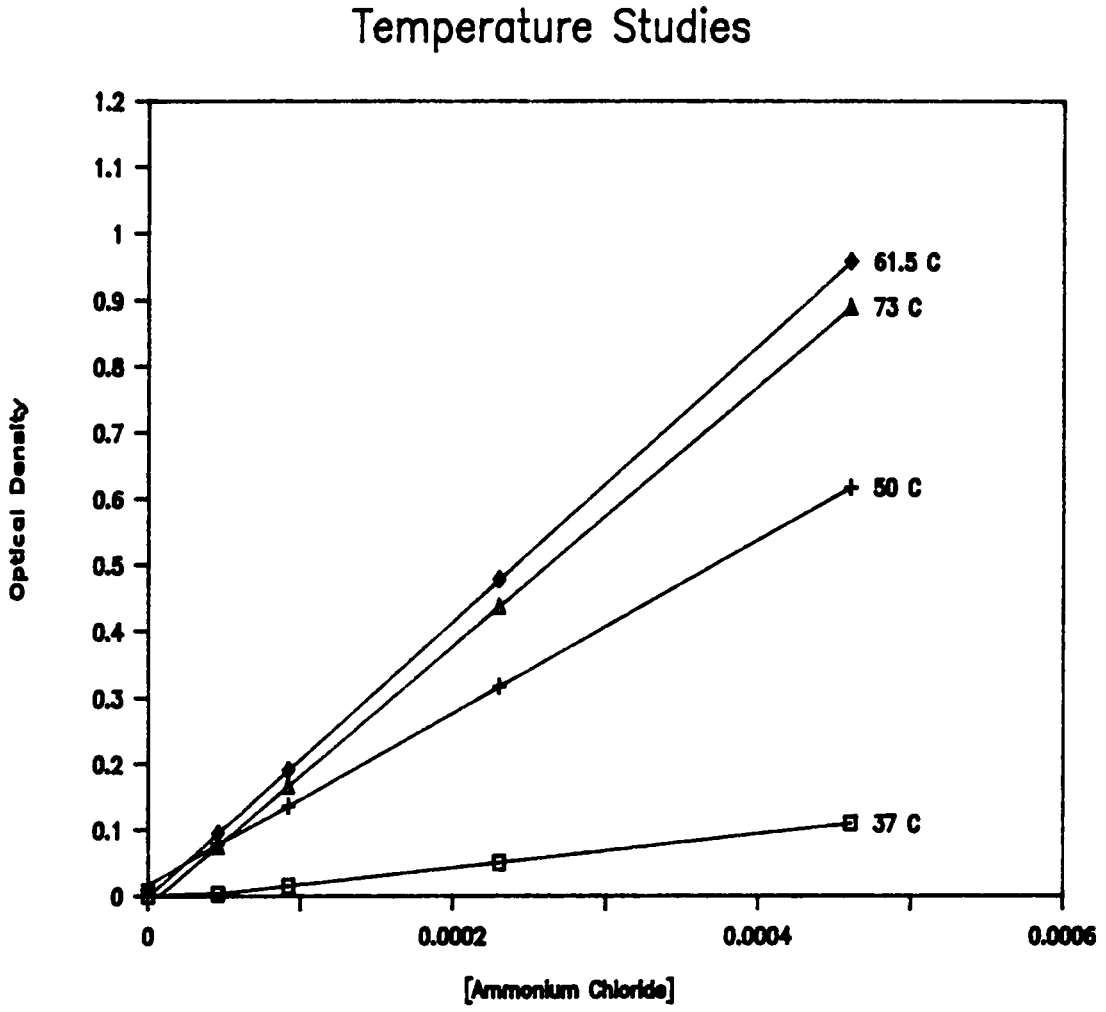

Figure 32. FIA of NH_4Cl as a Function of Temperature.

reaction past 70 °C, lead to color instability, decreased absorbance, and precision[91,102].

None of the investigators speculated upon the reason for this decrease in color stability, and it would be difficult to attribute the decrease in analytical sensitivity to any one of the proposed reaction steps. However, 1,4 benzoquinone monochlorimine, the product of the proposed rate limiting step, is known to be highly unstable, and will decompose in boiling water to 1,4 benzoquinone and ammonium chloride[108]. Thus, it is very likely that at elevated temperatures, the rate of formation of indophenol is impeded by the decomposition of the monochloroimine. The optimum temperature of the development coil for this FIA manifold is then between 60 and 75 °C, with the lower temperatures being favored to prevent solvent vaporization.

4. Dispersion

The dispersion, D, of an FIA system is a measure of the amount of mixing, or dilution, of the sample with the reagent stream. This parameter measures the effects of sample size, flow rate, and manifold length on the sensitivity of the method, and is commonly used as a reference for comparison to other FIA methods. It is the ratio of the initial, undiluted concentration of the sample to the diluted concentration of the sample and is

conveniently determined by measuring the absorbance of these two solutions.

$$D = C^0/C_{dil} = A^0/A_{dil}$$

The dispersion of the system was measured for the final configuration of the FIA manifold which was, as described in section 4 and Figure 11, a three line manifold with a 275 cm developing coil and a 300 cm cooling coil. The total length of the manifold was 695 cm. A_0, the initial absorbance of an indophenol dye, was determined by injecting a buffered sample of the dye into the Kratos transmission cell and measuring the absorbance directly. A_{dil}, was measured by injecting a 60 microliter sample of this dye onto the FIA manifold (all reagent streams were pH 9 borax buffer) and measuring the absorbance of the diluted sample. The dispersion of this system, with a 60 microliter sample loop, 695 cm manifold, and flow rate of 1.93 ml/min was 4.3. This is considered to be in the medium dispersion range for FIA experiments[109].

Although the dispersion of the system is reasonably independent of flow rates between 0.8 and 2.0 ml/min (see Figure 33), the sensitivity of the method is not. Lowering the flow rate increases the residence time of the sample in the manifold. For FIA methods where the sample is determined colorimetrically, this increases the sensitivity

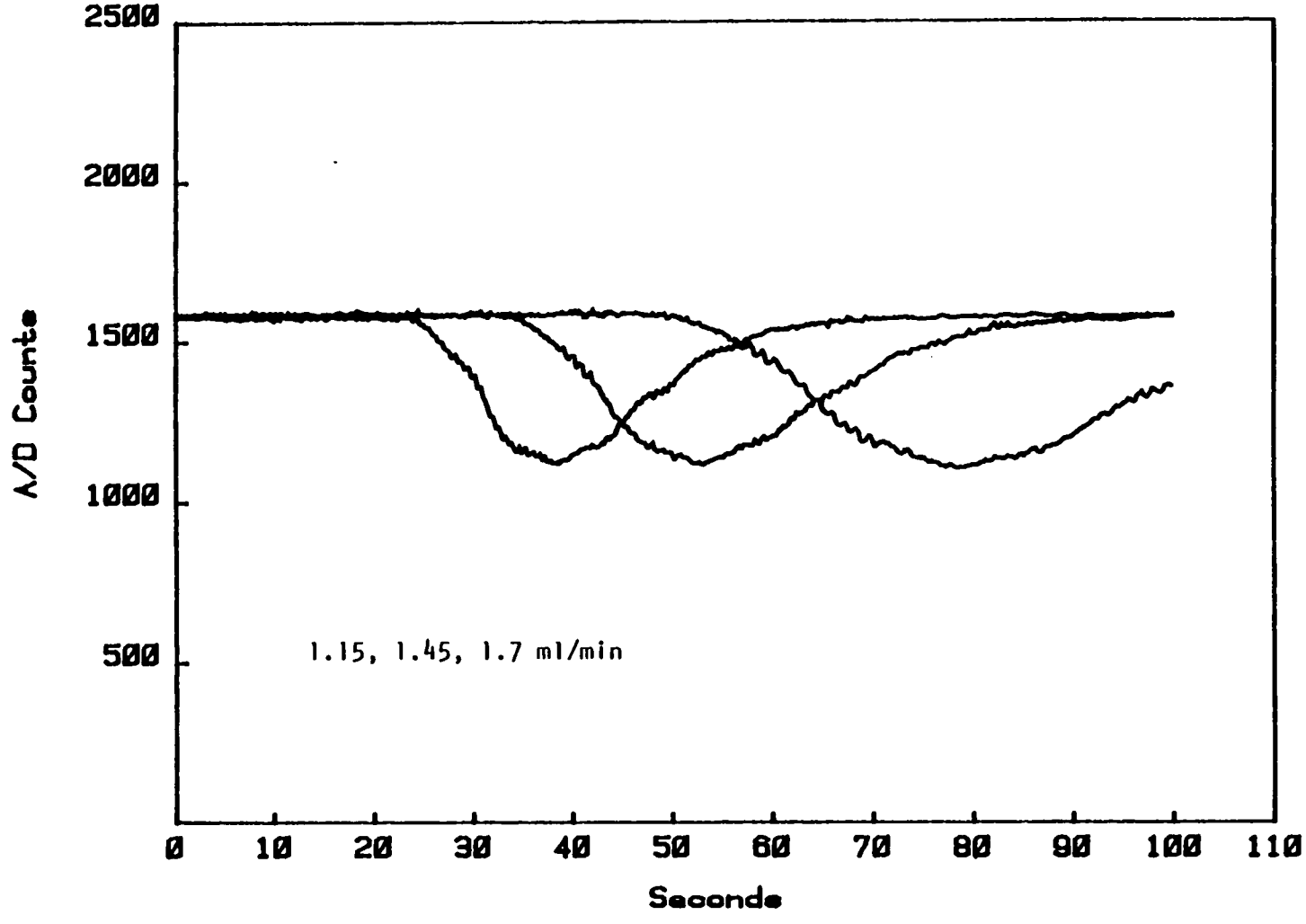

Figure 33. Dispersion of Indophenol dye as a function of flow rate.

of the method. Results for three 60 microliter injections of 0.7 mM ammonium chloride onto a 300 cm manifold, utilizing Berthelot's reaction, at different flow rates are shown in Figures 34-35. As the flow rate decreases, the sensitivity increases at the expense of analysis time. Determination of the optimum flow rate for a FIA method then becomes a compromise between the required sensitivity and the sample load. All subsequent analyses were measured with an approximate overall flow rate of 2.0 ml/min(~.65 ml/min for each reagent stream). This flow rate yielded adequate sensitivities for the comparison of a conventional transmission flow cell and the planar waveguide, and also provided a realistic sample throughput of 60 samples/hour.

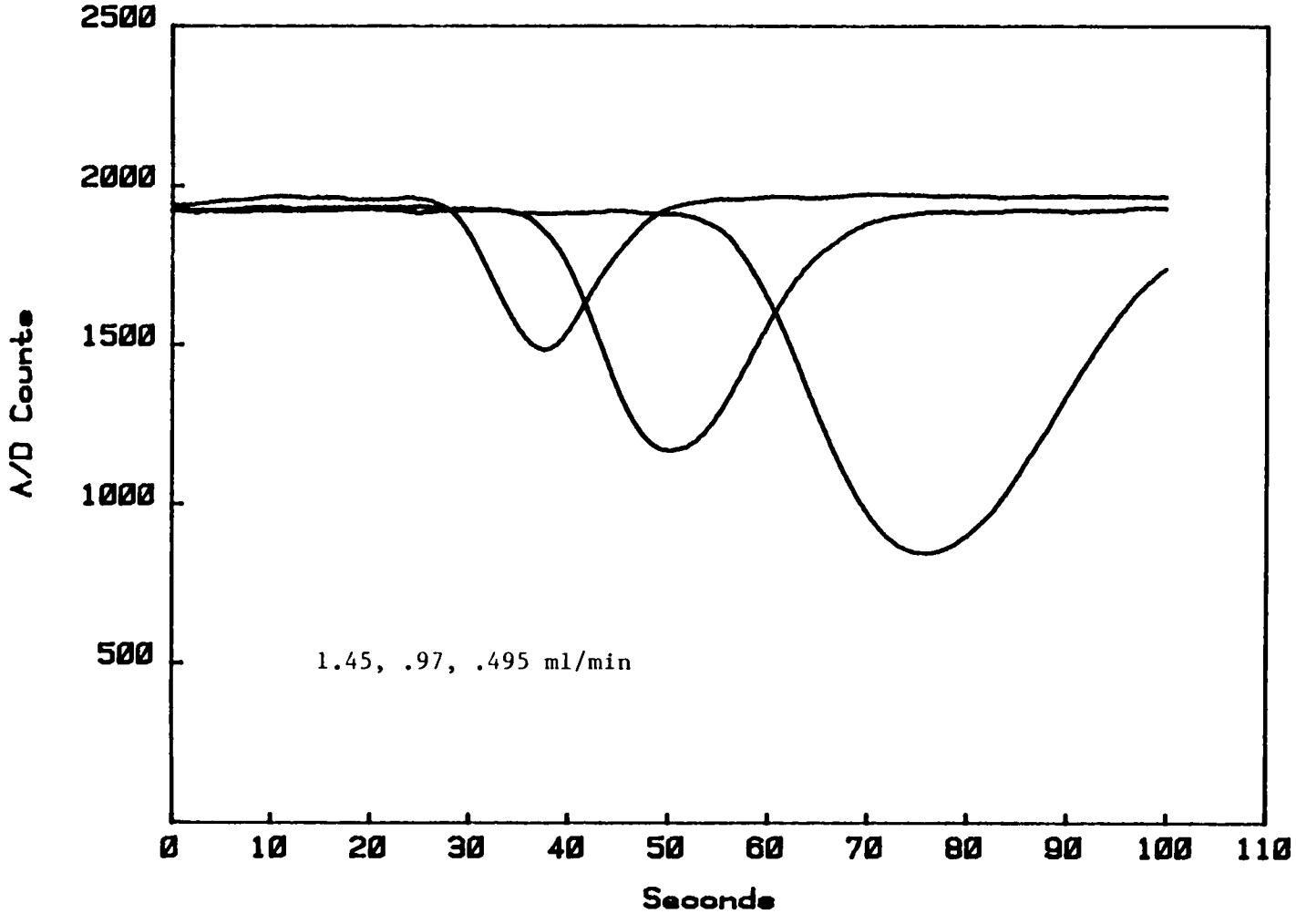

Figure 34. Response of Berthelot's reaction for constant [NH_4Cl] as a function of flow rate.

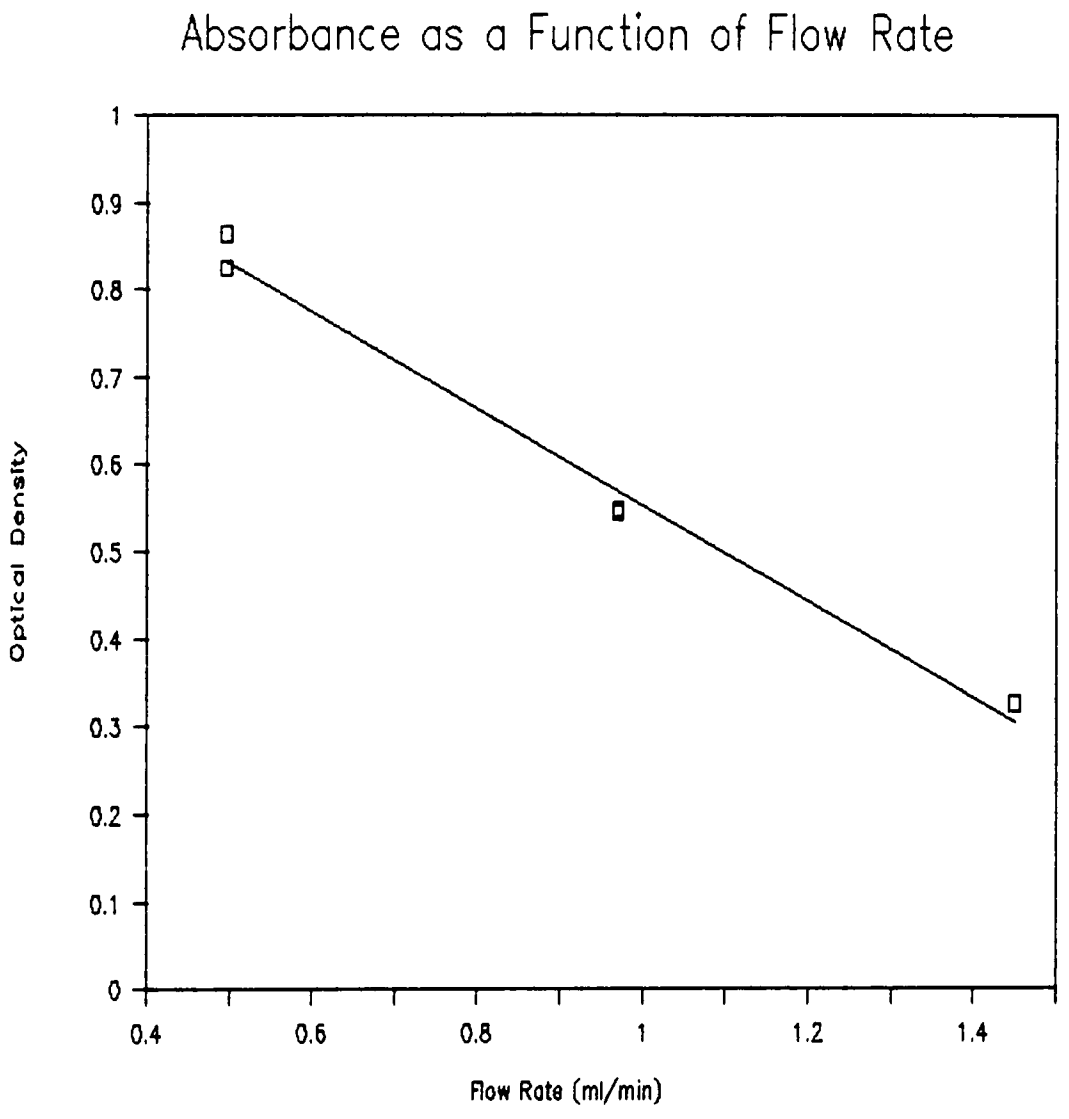

Figure 35. Absorbance of Indophenol Blue in the FIA of NH_4Cl as a function of flow rate.

C. Ammonium Chloride Standards

The FIA manifold used in the first experiments to determine the response of a Ag^+ diffused planar waveguide was a three line manifold, with a 100 cm mixing coil between the phenol and hypochlorite mixing tees, a 300 cm developing coil and an overall length of 515 cm. The overall flow rate was 1.8 ml/min with each of the reagent streams set to .6 ml/min. Five standard ammonium chloride solutions, ranging in concentration from 1.02 mM to 36.2 mM were prepared, as previously described, in .1M phosphate buffer. The manifold temperature was thermostatted to 37 °C while the development coil was thermostatted at 75 °C.

A silver ion guide that had been immersed in a 10 % mole ratio $AgNO_3/NaNO_3$ solution for ten minutes at 310 °C was used as the waveguide absorption element. This guide supported 4 modes at 632.8 nm, and the effective indices for each of these modes is listed in Table 7. For the initial experiments the 2 cm path length, 50 microliter flow cell was used with the planar waveguide as the combination flow cell detector.

The results for the analysis of ammonium chloride using the Ag^+ waveguide, tuned to mode zero, are shown in Table 8 and Figure 36. Beer's law was obeyed for concentrations less than 10 mM NH_4Cl. However, due to the high degree of scatter, the range is difficult to determine. Linear regression applied to the data between 1.02 mM and 10 mM

Table 7. **Effective Indices for a Planar Silver Ion Diffused Guide.;**

Mode #	0	1	2	3
Coupling Angle	23.0	18.5	15.0	12.1
Effective Index	1.578	1.556	1.535	1.519

Substrate Index = 1.512

Table 8. FIA of NH_4Cl with a Ag^+ planar waveguide and the 52 µl flow cell.

Mode 0,TE polarization

[NH_4Cl]	$A_{632.8}$ Std.Dev.	(%RSD)
.0102	.071 ± .0055	(7.72)
.00361	.029 ± .0036	(12.21)
.00102	.010 ± .0036	(35.85)
Blank	.002 ± .0039	(194)

O.D. = 6.58*[NH_4Cl] + .0042

Correlation Coefficient: .9708
Standard Error of Estimate: .0047

Mode 3,TE polarization

[NH_4Cl]	$A_{632.8}$ Std.Dev.	(%RSD)
.0102	.113 ± .0009	(0.84)
.00653	.086 ± .0014	(1.64)
.00361	.047 ± .0024	(5.20)
.00102	.014 ± .0020	(14.36)
Blank	-.002 ± .0025	(111)

O.D. = 11.32*[NH_4Cl] + .0055

Correlation Coefficient: .9785
Standard Error of Estimate: .0057

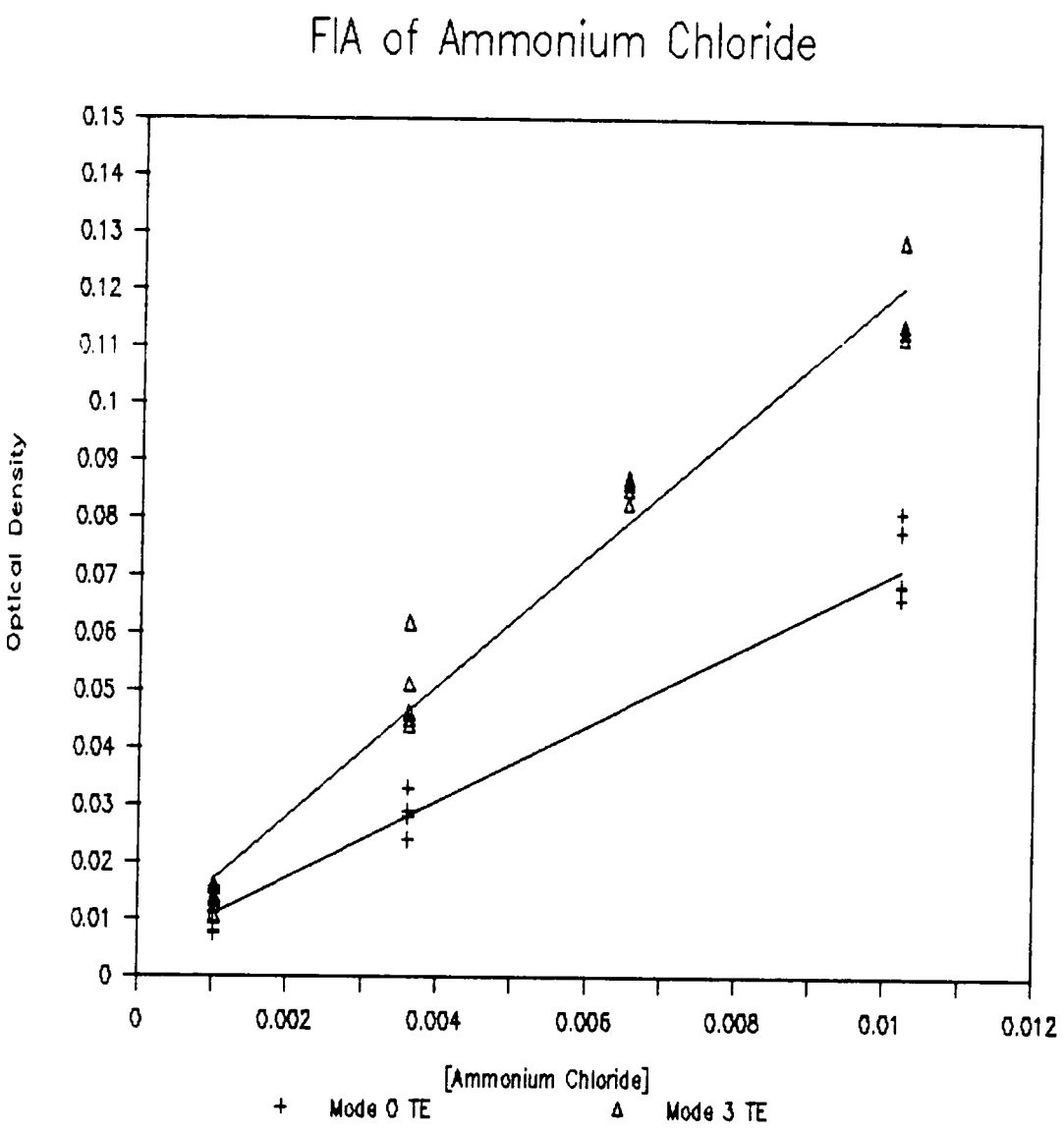

Figure 36. FIA of Ammonia using the 52 µl Flow Cell. The sensor was a Ag^+ diffused waveguide operated in modes 0 and 3 with TE polarization.

ammonia resulted in a correlation coefficient of 0.97, much lower than previous results obtained with the transmission flow cell. The reproducibility of the data was also poor. In general the precision was no better than ± 5% for a given concentration, and the standard estimated error of the data was 5 milliabsorbance units.

The calibration curve for the analysis of ammonium chloride, with the waveguide tuned to mode three is also shown in Figure 36 and Table 8. Again the curve deviated from Beer's law above 10 mM, and a high degree of scatter was observed in the data points. The precision of the data was equally poor, and the calculated correlation coefficient for concentrations between 1.02 mM and 10.2 mM was 0.978. The poor precision was observed to arise from two sources. As can be seen in Figure 37, subsequent injections of ammonia cause a significant reduction in the baseline. This was determined to be due to the absorption of indophenol blue on the surface of the waveguide. As this is a single beam instrument, any attenuation of the baseline causes a reduction in sensitivity for subsequent measurements. Secondly, as can be seen in Figure 38, significant peak tailing occurs, especially for the higher concentration samples. This is a result of the large dead volume of the 52 microliter flow cell. While the tailing problem was easily solved by using a smaller volume flow cell (9.2 microliter), reducing the adsorption of the indophenol

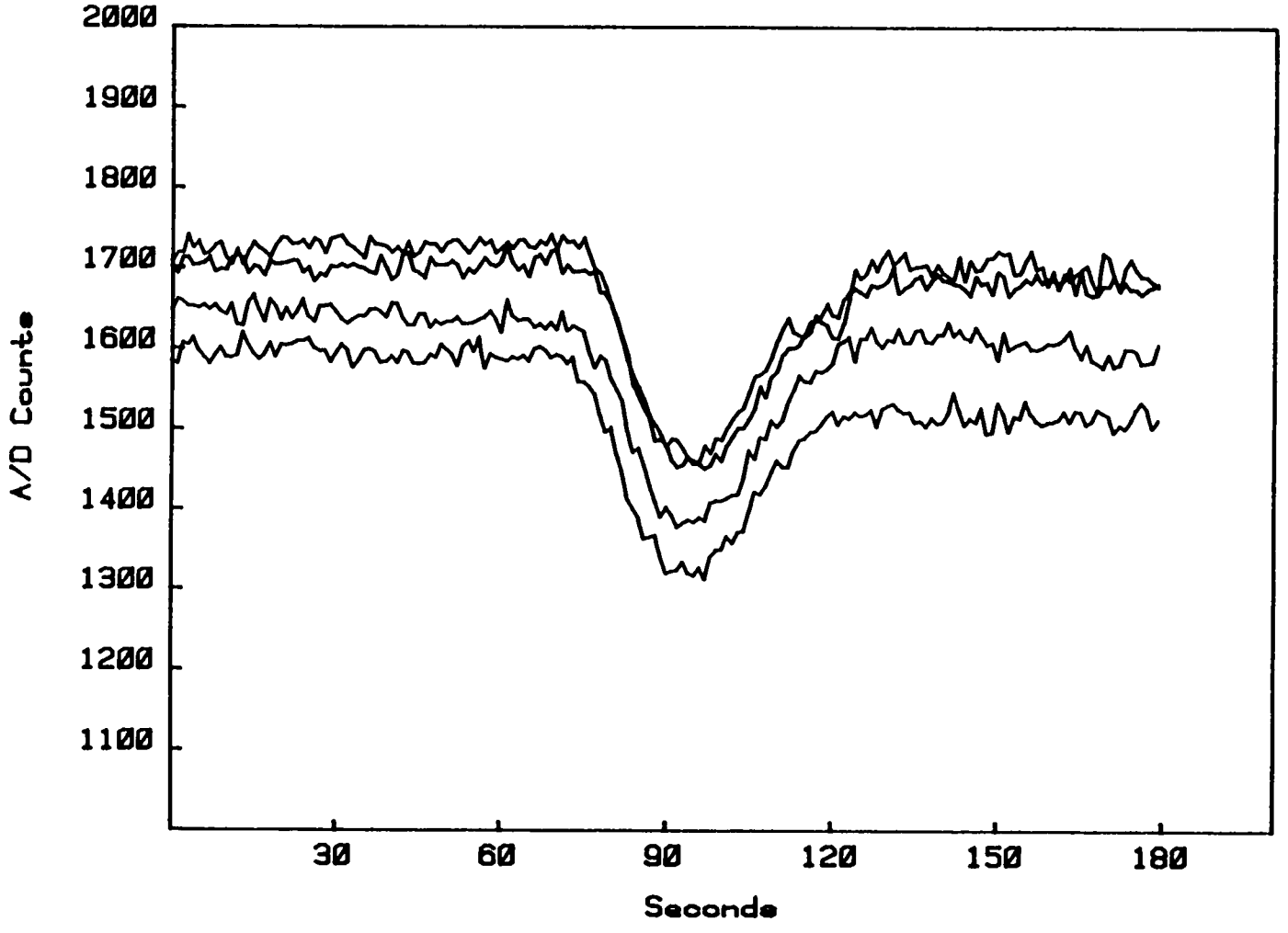

Figure 37. Four consecutive injections of NH_4Cl using the 52 µl flow cell.

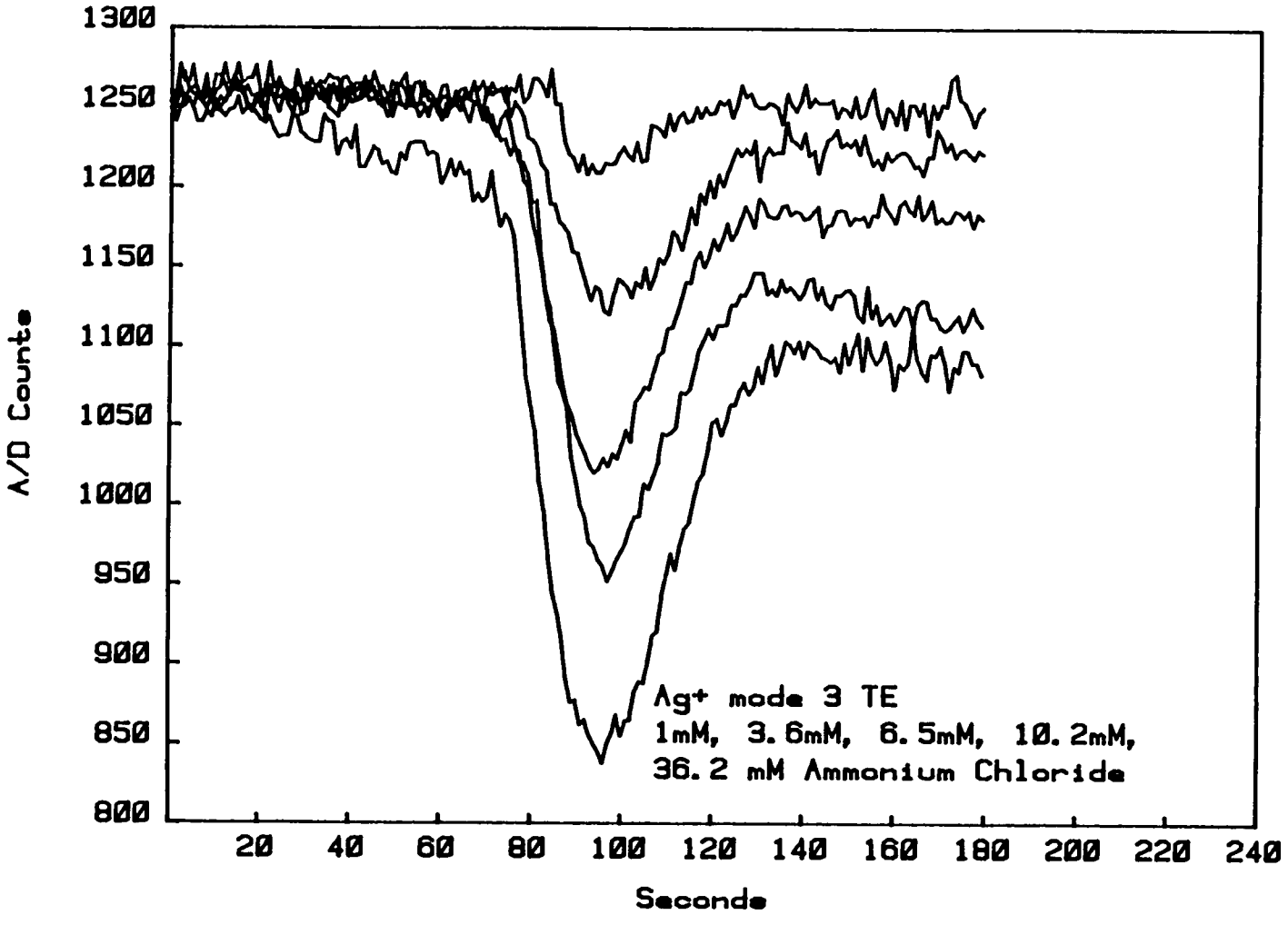

Figure 38. Superposition of peaks in the FIA of NH_4Cl illustrating peak tailing and adsorption effects.

proved to be more difficult.

Initially, attempts to passivate the surface by silanization with nonpolar groups such as trimethylchlorosilane (Petrarch Chemicals) were very successful in making the surface hydrophobic, as observed by contact angle measurements. These waveguides, when dipped in a solution of concentrated indophenol blue, did not stain, unlike the untreated waveguides. Unfortunately, due to the alkalinity of the effluent from the manifold (pH>12), the siloxyl groups were immediately hydrolyzed and the surface of the waveguide was exposed, allowing adsorption to occur. As a crude, yet seemingly effective step, the waveguides were preconditioned, before use, by exposing them to high concentrations of indophenol blue to saturate active sites that might be responsible for adsorption. Although this reduced the sensitivity of waveguide, the baselines were usually stable long enough to complete an analysis before cleaning was necessary (~200-300 samples). Silanization however, is likely to be the most effective method of passivating the surface, especially when the guide is exposed to solutions that are lower than pH 10[110]. Since the focus of this work was on showing the feasibility of using planar waveguides as sensors, rather than the pursuit of an enhanced ammonia detector, this problem was not pursued further.

During the next set of experiments the 52 microliter flow cell was replaced with the 9.2 microliter flow cell. This reduced the dead volume from approximately 49 microliters to 6 microliters. An additional 3 meters was added to the development coil in an attempt to improve sensitivity. Temperature, flow rate and the concentration of reagents were identical to those used in the initial silver ion experiment. The results are compiled in Table 9, and shown in Figure 39.

By using a smaller dead volume the flow cell peak tailing was eliminated. Pretreating the slides reduced adsorption and the sloping baseline was not observed, even after consecutive injections of concentrated ammonia samples. This is shown in Figure 40 which is the superposition of four consecutive 60 microliter injections of 6.62e-3 M ammonium chloride. The precision of the measurements, however, was as poor as the initial experiment. Although the baseline was observed to be stable for short periods of time, it would often wander randomly during the course of an analysis. This behavior is shown in Figure 41, which is a measure of the baseline stability from the absorbance sensor and laser over a period of 1000 seconds.

This random drift was never observed during experiments at room temperature, and ultimately the source of the baseline drift was determined to be a result of temperature

Table 9. FIA of NH_4Cl with a Ag^+ planar waveguide and the 9.2 µl flow cell.

Mode 0,TE

[NH_4Cl]	$A_{632.8}$	Std.Dev.	(%RSD)
.0102	.0498 ±	.0053	(10.62)
.0066	.0398 ±	.0039	(9.81)
.00363	.0273 ±	.0024	(8.92)
.00102	.0103 ±	.0032	(31.44)
Blank	1.4e-4 ±	5.5 e-5	(40.74)

O.D. = 5.73*[NH_4Cl] + .0052

Correlation Coefficient: .9421
Standard Error of Estimate: .0032

Mode 3,TE

[NH_4Cl]	$A_{632.8}$	Std.Dev.	(%RSD)
.0102	.0743 ±	.0011	(1.47)
.0066	.0616 ±	.0008	(1.30)
.00363	.0380 ±	.0037	(9.85)
.00102	.0185 ±	.0015	(8.11)
Blank	-.0009 ±	.00182	(200)

O.D. = 7.74*[NH_4Cl] + .0103

Correlation Coefficient: .9824
Standard Error of Estimate: .0025

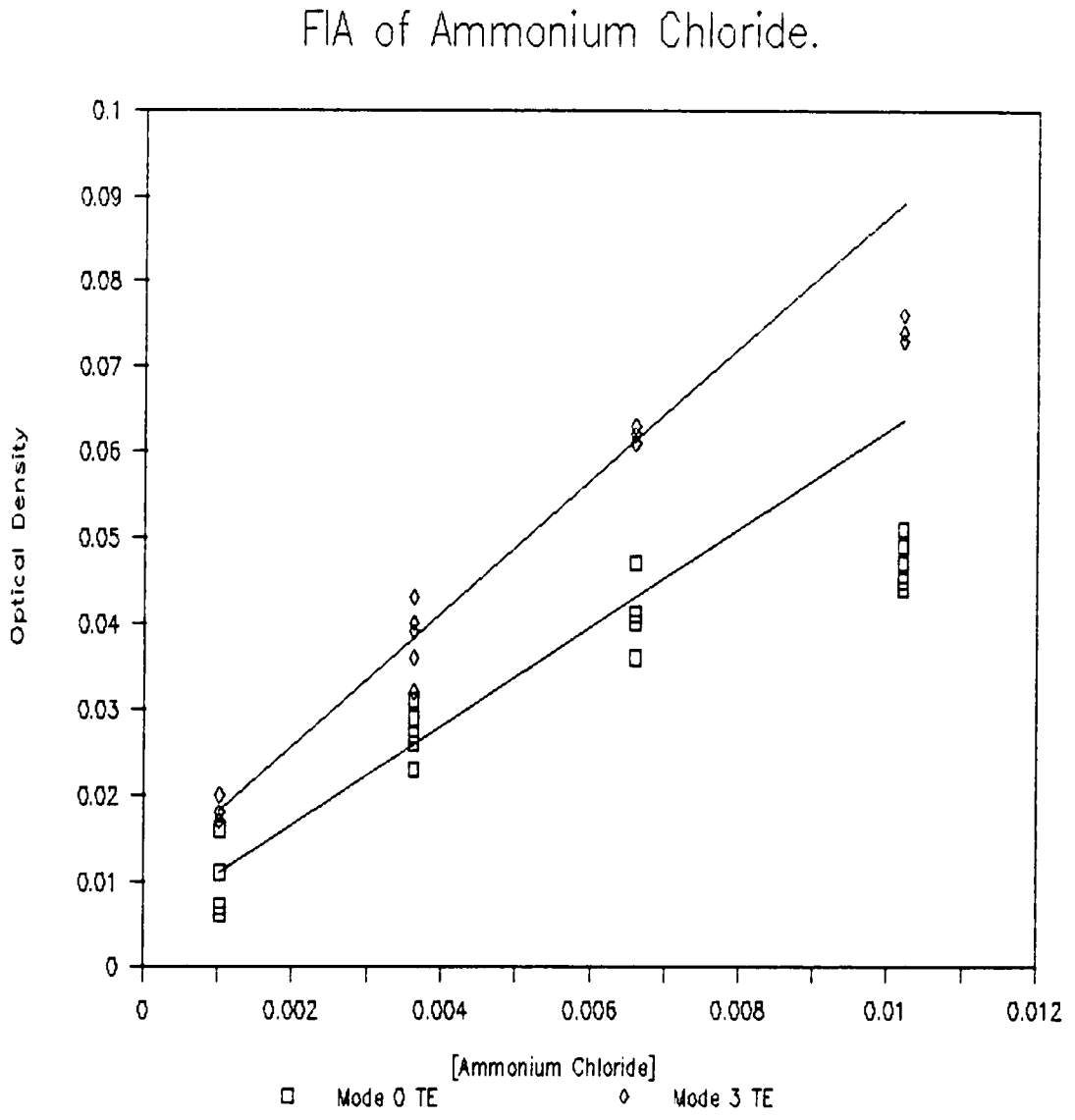

Figure 39. Calibration curve for the FIA of NH_4Cl using the 9.2 µl cell. The sensor was a Ag^+ diffused waveguide operated in modes 0 and 3 with TE polarization.

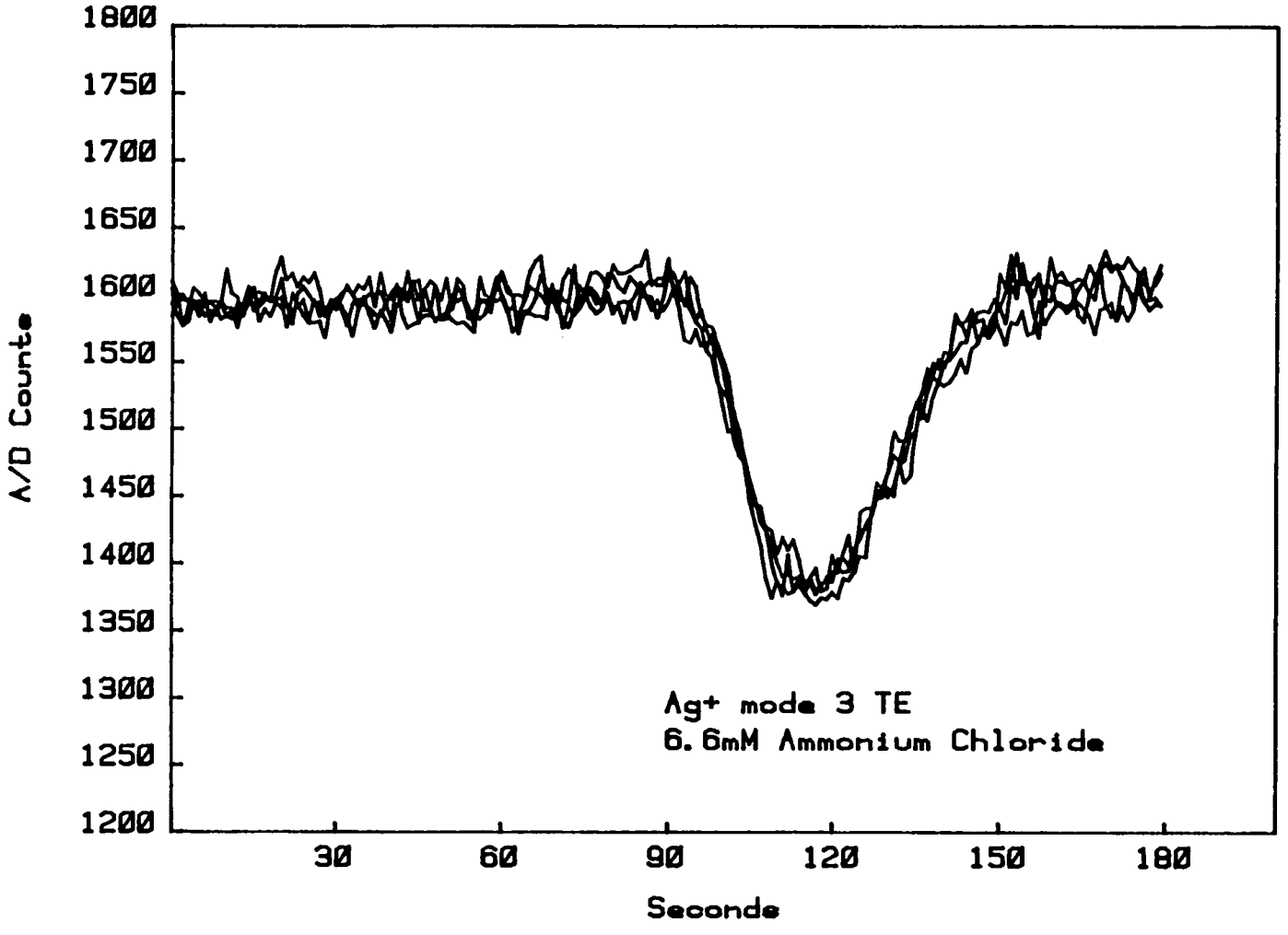

Figure 40. Four consecutive injection of NH_4Cl using the 9.2 µl flow cell.

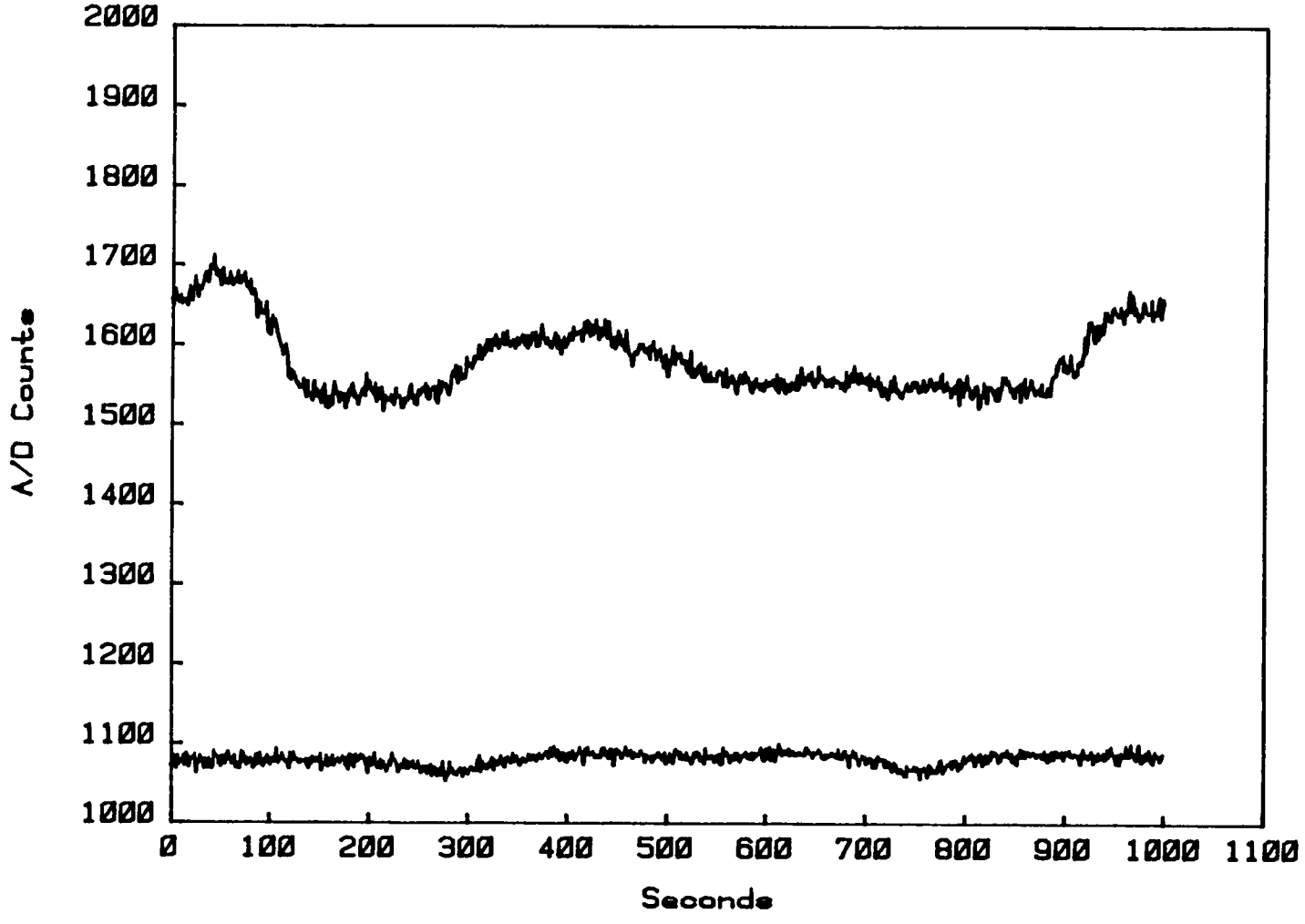

Figure 41. Baseline measurement without temperature isolation.

changes in the room and, more importantly, temperature changes in the waveguide due to the heated effluent from the FIA manifold. If the temperature changes significantly, the air gap between the prism and waveguide will change, thus affecting the coupling efficiency between the waveguide and laser. Because the heating and cooling of the waveguide is irregular, the coupling efficiency varied randomly, and thus the baseline drifted. To correct this problem, a 3 meter length of .5mm i.d. Teflon tubing was attached immediately following the development coil, and immersed in a water bath at room temperature. A .25 inch thick foam core housing was also constructed to completely enclose the planar waveguide absorbance cell, serving to isolate the sensor from random air currents. The effect of these changes is shown in Figure 42, which is a measure of the baseline for the sensor and laser over a 1 hour period with the reagents flowing through the manifold at 75 °C. As a result of the additions to the FIA manifold, the standard deviation of the baseline was improved by a factor of three (Table 10).

For the final set of ammonium chloride determinations with the Ag^+ waveguides, the FIA manifold was modified to include the modifications described above, and the development coil was shortened to the original 3 meter length. Overall, the length of the manifold was 675 cm. The final design is shown in Figure 11. The results for the

Table 10. Effect of Temperature Isolation on the Baseline for a Silver Ion Waveguide.

Baseline without temperature isolation:

Laser for 1000 Seconds: 1080.3 ± 8.01 (ADC units)

Sensor for 1000 Seconds: 1575.5 ± 41.5 (ADC units)

Baseline with temperature isolation:

Sensor for 3600 Seconds: 1552.1 ± 9.53 (ADC units)

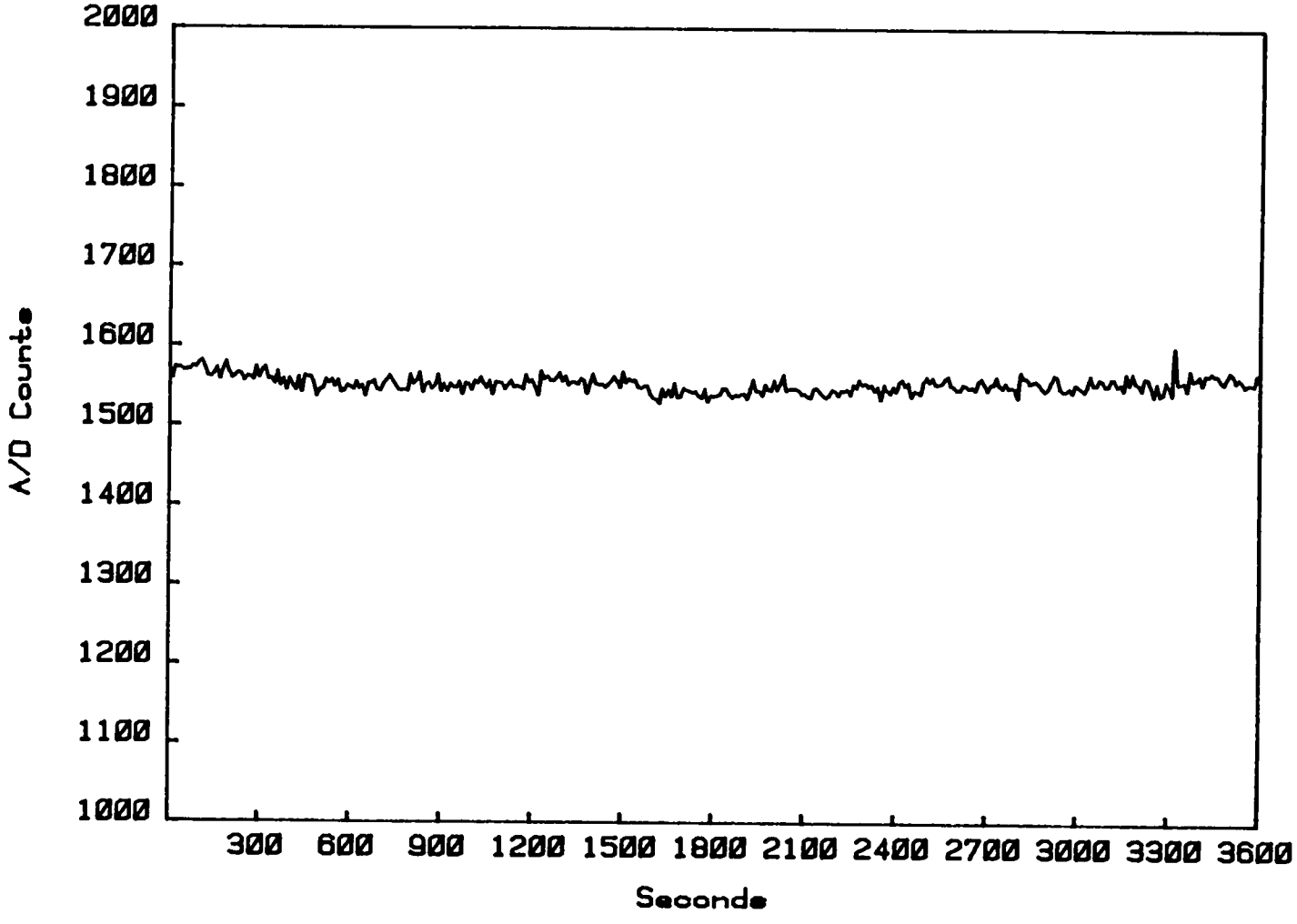

Figure 42. Baseline measurement with temperature isolation.

FIA determination of ammonium chloride for both mode 0 and mode 3 are shown in Figure 43 and Table 11.

As can be seen from the calibration curves for mode 0 and 3, the precision of the measurements has improved with these changes to the flow cell and the manifold. The standard error of estimate for either mode is lower than in previous experiments. Figure 44 shows four consecutive injections of 0.01 M NH_4Cl at 1 minute intervals. No appreciable temperature drift occurs and attenuation of the waveguide due to indophenol adsorption was minimized. The detection limit was approximately 1.0e-4 M ammonia, calculated as 3 standard deviations of the response to the blank measurements. The blanks were 60 µl injections of the 0.1 M phosphate buffer. The working range for this present method, is 3.0e-4 M (10 std deviation of the blank[111]) to 4.0e-3 M NH_4Cl, at 60 samples per hour. The higher limit stems from deviations from Beer's law at these concentrations.

D. FIA of NH_4CL using the Kratos Transmission Flow Cell

The planar waveguide sensor flow cell combination was replaced with the Kratos 8 microliter, HPLC flow cell and the analysis repeated using the same concentration reagents, temperatures, and flow rates. Fresh ammonium chloride solutions ranging in concentration from 4.6e-5 M to 4.6e-4

Table 11. FIA of NH_4Cl using a Ag^+ diffused planar waveguide with temperature isolation.

Mode 0,TE Polarization

[NH_4Cl]	$A_{632.8}$ Std.dev	(%RSD)
3.61e-3	.0517 ± .00123	(2.38)
1.02e-3	.0159 ± .00098	(6.18)
5.10e-4	.0058 ± .00059	(10.19)
Blank	.0023 ± .00071	(30.1)

O.D. = 14.28*[NH_4Cl] + .00031

Correlation Coefficient:	.9942
Standard Error of Estimate:	.0016
Minimum Detectable Quantity:	9.1 e-5 M NH_4Cl

Mode 3,TE polarization

[NH_4Cl]	$A_{632.8}$ Std.dev	(%RSD)
3.61e-3	.0771 ± .00137	(1.77)
1.02e-3	.0294 ± .00125	(4.25)
5.10e-4	.0142 ± .00098	(6.97)
Blank	.0009 ± .00071	(76.7)

O.D. = 20.10*[NH_4Cl] + .0055

Correlation Coefficient:	.9891
Standard Error of Estimate:	.0032
Minimum Detectable Quantity:	1.6 e-4 M NH_4Cl

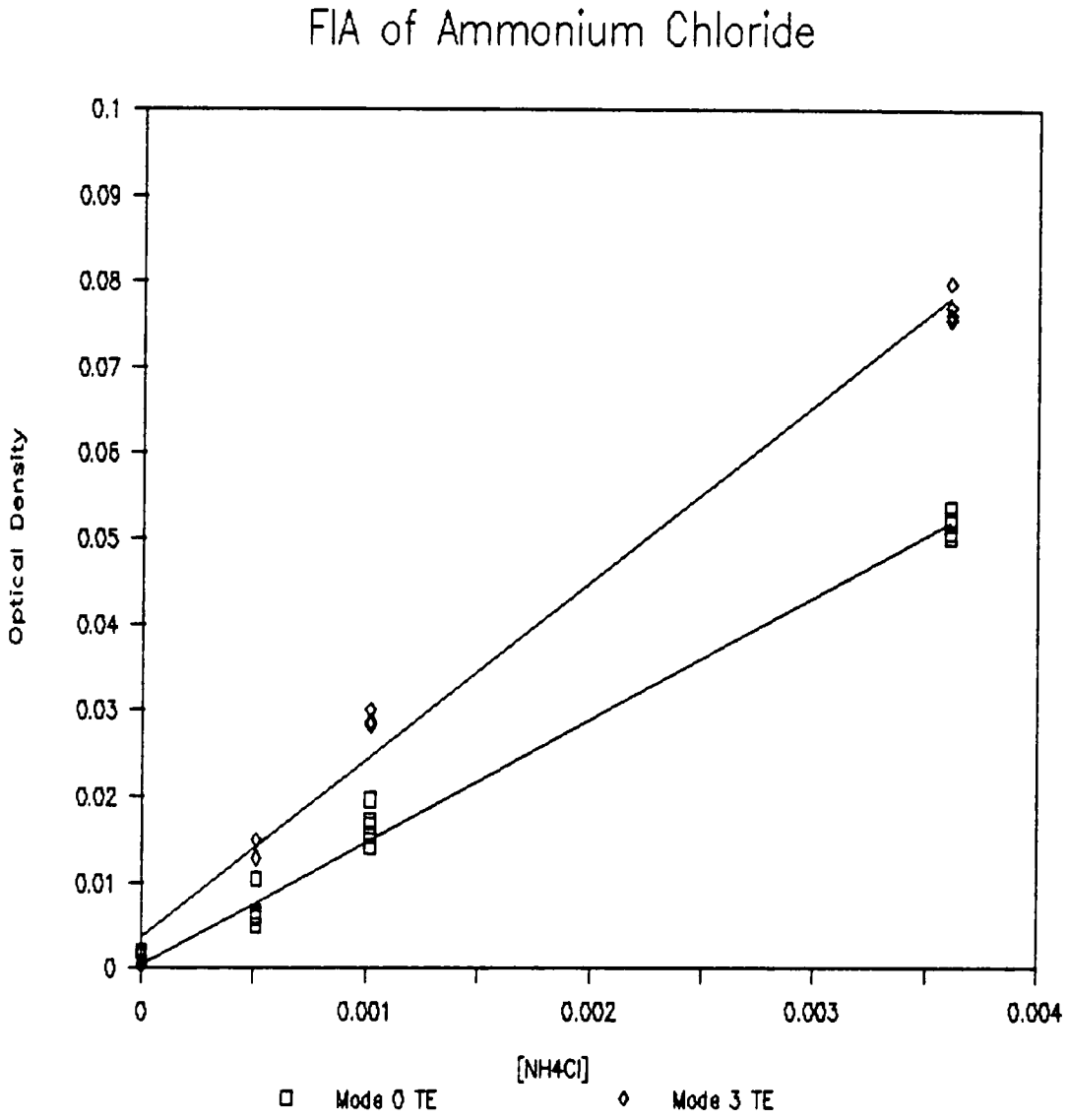

Figure 43. Calibration curve for the FIA of NH_4Cl using the 9.2 µl flow cell with temperature isolation. The sensor was a Ag^+ diffused waveguide operated in modes 0 and 3 with TE polarization.

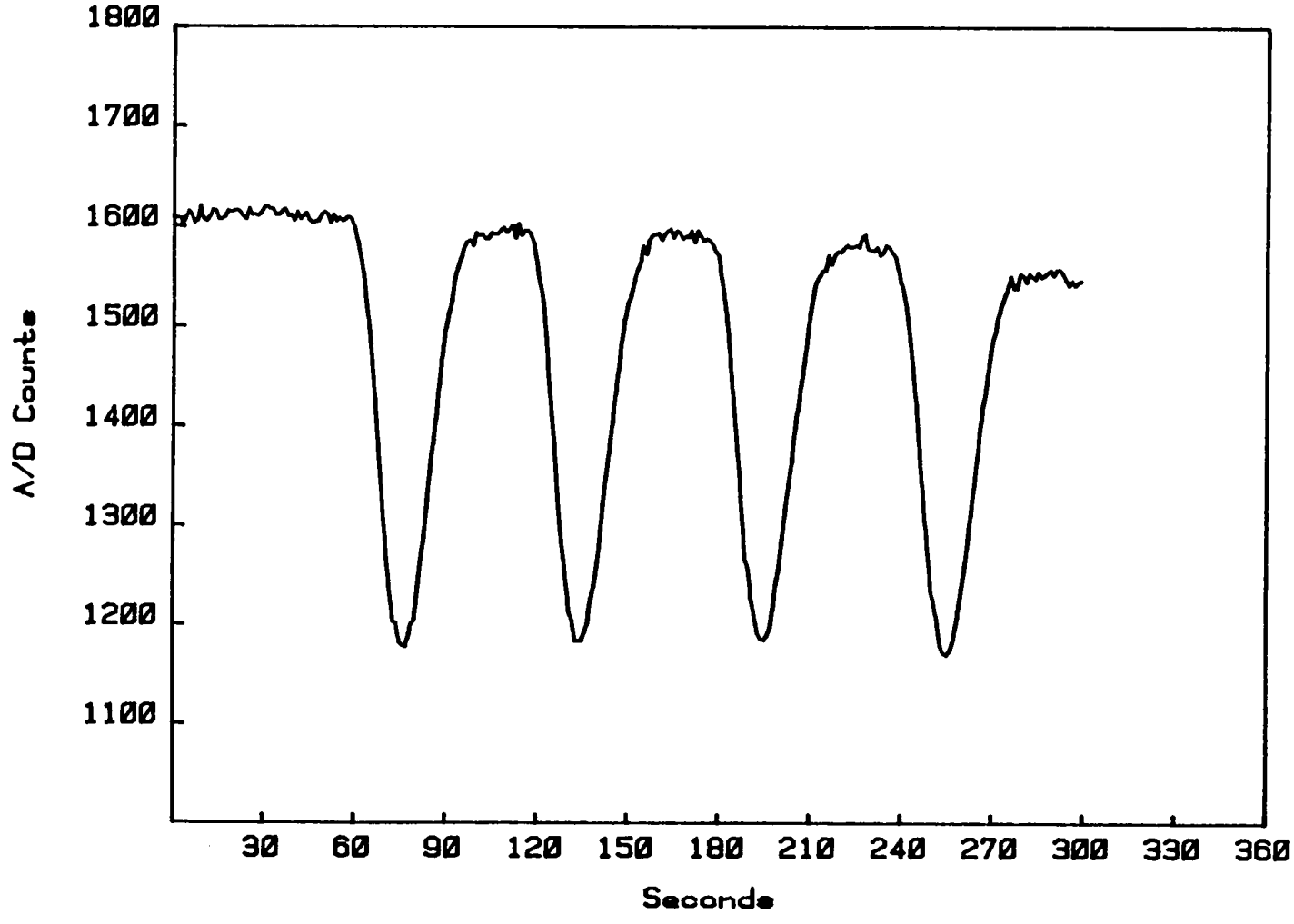

Figure 44. Four consecutive injections of NH_4Cl using the temperature isolated 9.2 µl flow cell.

M, were prepared from a stock solution by volumetric dilution, as previously described. The source was the Helium Neon laser focused through the flow cell and upon a UDT photodiode as previously discussed. The results for the analysis are shown in Figure 45 and compiled in Table 12. The minimum detectable quantity calculated, using the conventional 1 cm path length transmission flow cell, was approximately 5 micromolar ammonia. Based on the standard deviation of the blank, a working range of 2.0e-5 M (10 standard deviations) to 4.0e-4 M ammonia, is possible using the current conditions. This compares favorably with the results of other workers who found an detection limit of approximately .3 micromolar ammonia using a 5 centimeter transmission cell with a solution development period of 2 hours89. A precision of approximately ±3% is also typical of the results found in previous studies99. Figure 46 shows three subsequent injections of 2.303e-4 M NH4Cl, at one minute intervals. The locations of the peak maximums are reproducible and well separated, indicating that for the present conditions, the method will easily support a rate of 60 samples per hour.

E. Minimum Detectable Quantity of Indophenol

To determine the sensitivity of the planar waveguide, independent of the variables introduced by the FIA

Table 12. FIA of Ammonium Chloride using a HPLC Flow Cell.

[NH_4Cl]	$A_{632.8nm}$ Std.dev (%RSD)
4.607e-4	.777 ± .0131 (1.69)
2.303e-4	.389 ± .0030 (0.78)
9.213e-5	.155 ± .0050 (3.23)
4.607e-5	.068 ± .0013 (1.60)
Blank	-.002 ± .0013 (62.23)

O.D. = 1699.6*[NH_4Cl] - 0.00439

Correlation Coefficient: .9994
Standard Error of Estimate: .0077
Minimum Detectable Qty.: 4.85 e-6 M NH_4Cl

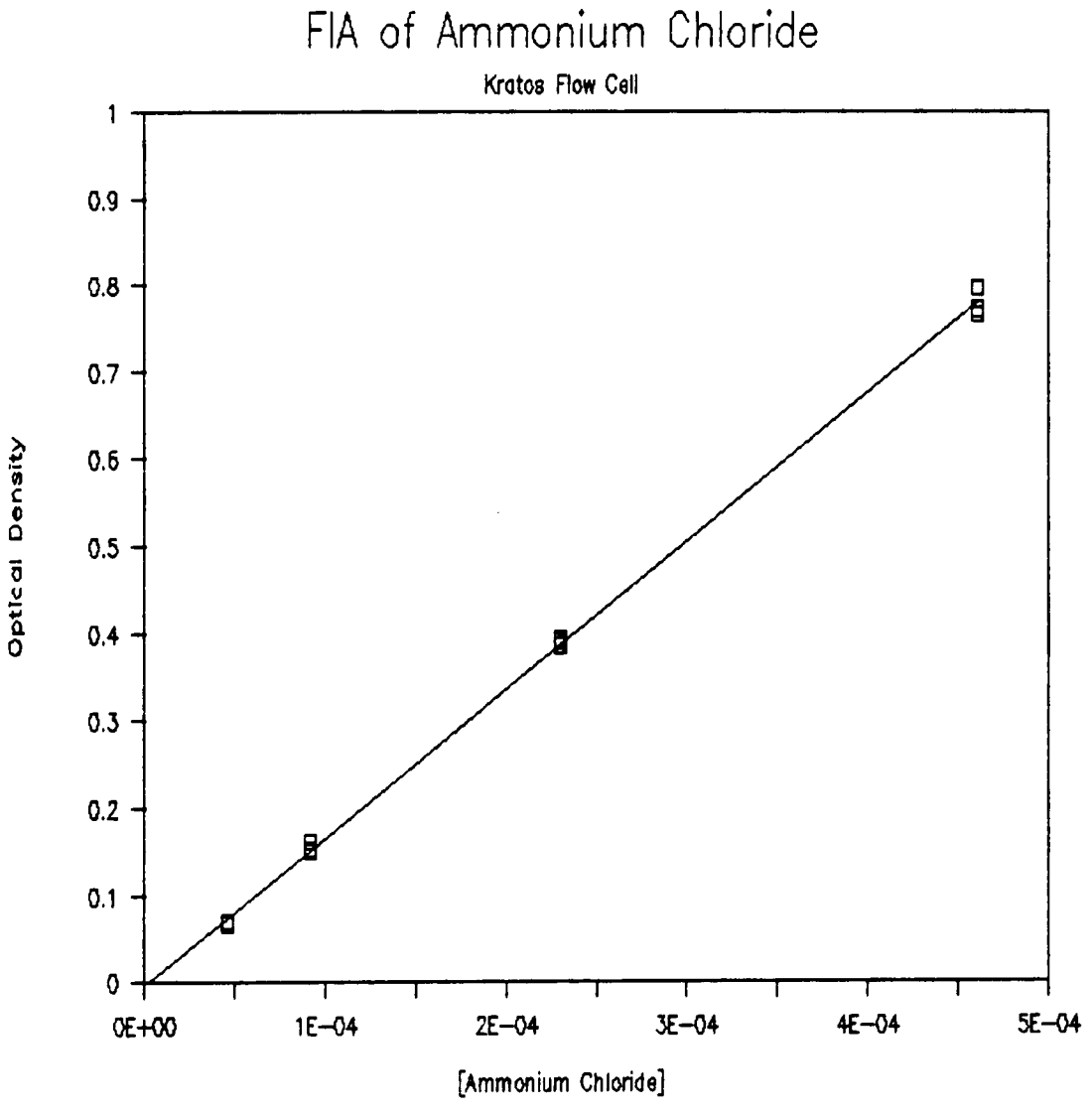

Figure 45. Calibration curve for the FIA of ammonia using the Kratos 8 µl HPLC flow cell.

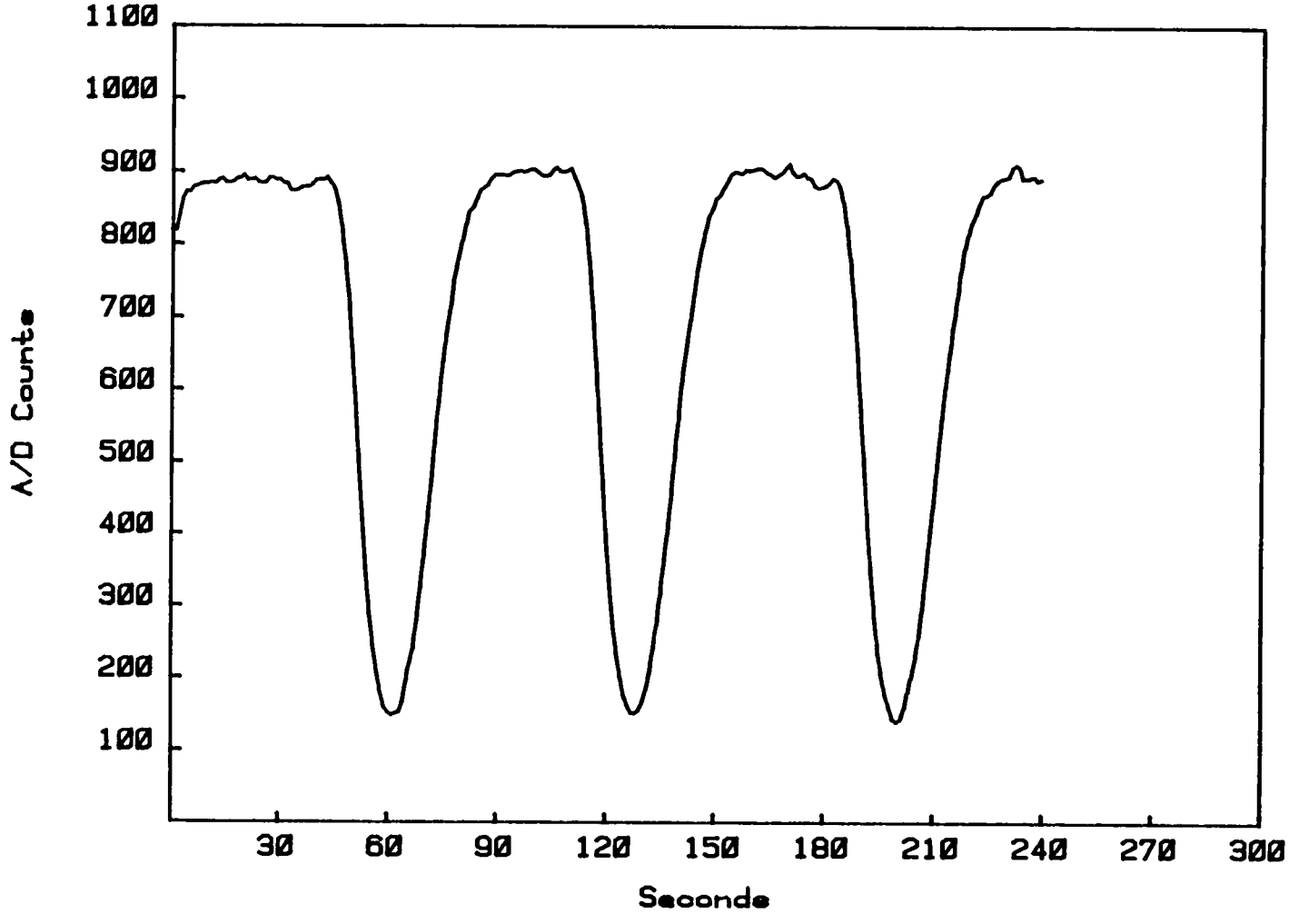

Figure 46. Three consecutive injections of NH4Cl using the Kratos cell.

technique, and to determine the feasibility of passivating the surface of the guide with a silanizing agent, the absorption of several prepared indophenol solutions was measured. A 1 millimolar stock indophenol solution was prepared from indophenol[112], and buffered in a pH 8.5 borax buffer. Four other solutions, ranging in concentration from 0.1 to 0.8 millimolar indophenol were prepared from the stock solution by volumetric dilution with the borax buffer. Although the logarithm of the absorption coefficient at pH 8.5 is 3.95 vs ~4.5 at pH 12.5, the lower pH buffer was chosen to prevent hydrolysis of the siloxane modified surface.

The waveguide was prepared by immersing a microscope slide[113] in a molten 10 mole % $AgNO_3/NaNO_3$ bath at 310 °C for 10 minutes. This waveguide supported four modes of propagation at 632.8 nm and had similar index properties as the guide used in the FIA experiments. To prepare the guide for silanization, it was ultrasonically cleaned in detergent, rinsed in distilled water, and then immersed in warm 1N HCl for 30 minutes. The HCl bath hydrolyzes the surface of glass slide thus increasing the reactivity of the surface with the silanizing agent. After treatment, the slide was rinsed with deionized distilled water, immersed wet in neat trimethylchlorosilane and refluxed for 12 hours.

Following this treatment, the slide was rinsed with toluene, dried and cured at 120 °C for 2 hours.

As the silanizing reagent possessed only one reactive group (monochloro), surfaces treated with this molecule yield films that are mono or submonolayer in coverage. This treatment produced a uniformly hydrophobic surface as observed by comparing the contact angle for several drops of water placed on the treated surface versus the contact angle for an untreated surface. Furthermore, an untreated slide immersed in methylene blue was heavily stained, whereas the treated slide resisted staining by methylene blue. As the film coverage for this treatment was expected to be submonolayer, no appreciable change in optical properties of the waveguide was expected (i.e. coupling angles). This was verified by subsequent experiments.

The absorbance measurements were made with the same optical setup as previously used with the flow experiments. For each determination, a sample was manually injected into the cell, allowed to settle for 30 seconds, and then the intensity of the signal acquired for an additional 30 seconds. After flushing the cell with 2 ml of borax buffer, the absorbance of the buffer solution was recorded and subtracted as the blank. The results for a waveguide that had not been treated with trimethylchlorosilane are presented in Table 13 and Figures 47-48.

Table 13. Response of an untreated Ag^+ diffused Waveguide to Indophenol.

Mode 0 TE

O.D. = 161.15*[Indophenol] + 5.87e-4

Correlation Coefficient:	.9947
Standard Error of Estimate:	.0051
Std. Dev. of Blank:	.0056 (absorbance)
Minimum Detectable Qty.:	1.02e-4 M

Mode 0 TM

O.D. = 222.04*[Indophenol] + 1.23e-4

Correlation Coefficient:	.9919
Standard Error of Estimate:	.0088
Std. Dev. of Blank:	.0021
Minimum Detectable Qty.:	2.83e-5 M

Mode 3 TE

O.D. = 221.48*[Indophenol] - 4.90e-4

Correlation Coefficient:	.9979
Standard Error of Estimate:	.0042
Std. Dev. of Blank:	.0035
Minimum Detectable Qty.:	4.84e-5

Mode 3 TM

O.D. = 227.13*[Indophenol] - 2.6e-3

Correlation Coefficient:	.9808
Standard Error of Estimate:	.0137
Std. Dev. of Blank:	.0037
Minimum Detectable Qty.:	6.10e-5

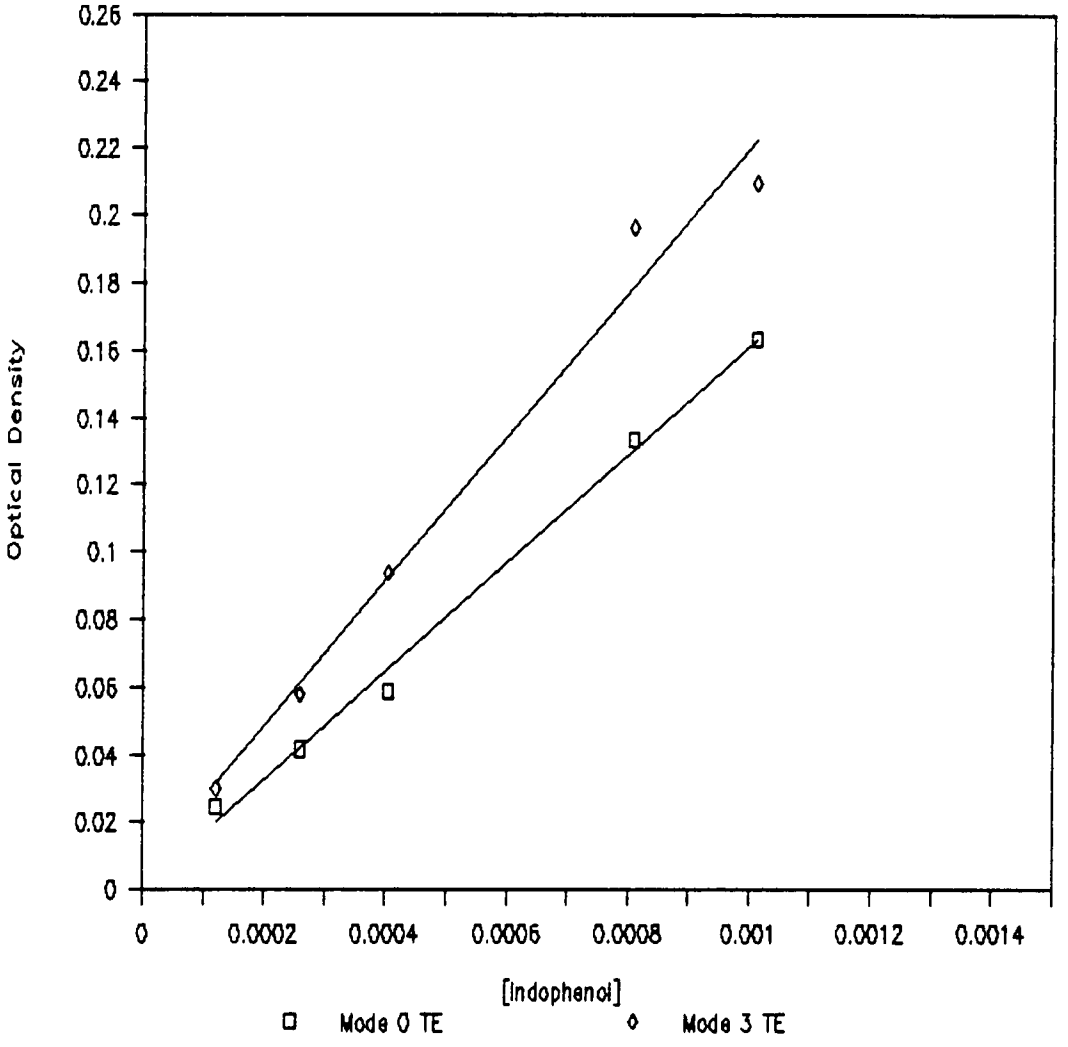

Figure 47. Calibration curve for the absorbance of Indophenol Blue using an untreated Ag^+ diffused waveguide with TE polarization.

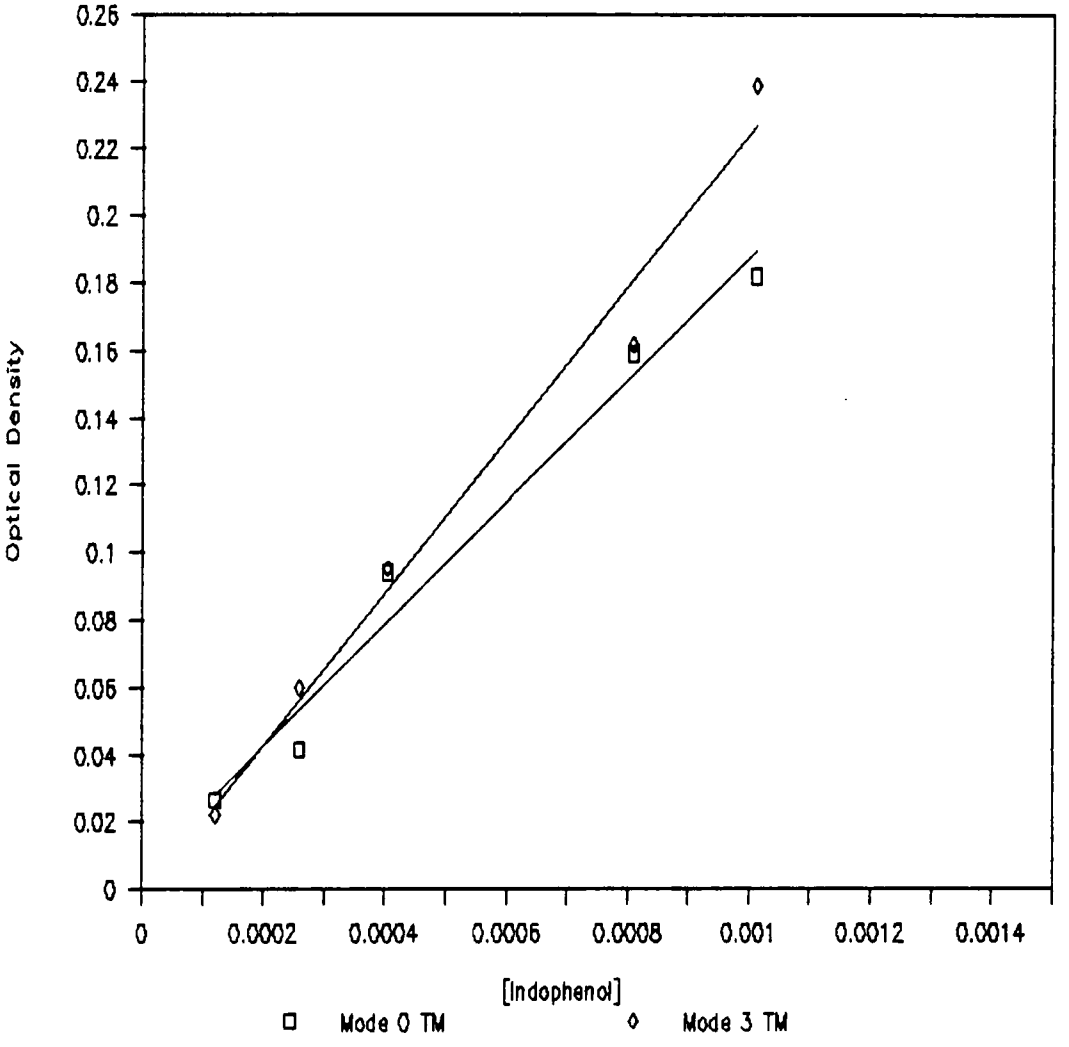

Figure 48. Calibration curve for the absorbance of Indophenol Blue using an untreated Ag^+ diffused waveguide with TM polarization.

With the untreated guide, the sensitivity increases with mode number and is in general higher for TM polarization (perpendicular to the surface of the guide) than TE. However, the most sensitive modes are also attenuated more severely than the lower order modes and therefore require a proportionally higher amplification to match the input requirements of the ADC. This leads to greater variance in the baseline and, as a result, ultimately limits the minimum detectable quantity. As can be seen from Table 13, sensitivity and baseline stability are conflicting goals. Thus, optimal operation of the waveguide is necessarily a compromise. Based on these measurements either mode three TE or mode zero TM could be used to maximize sensitivity and yet retain a relatively stable baseline. However, for subsequent measurements, mode three with TE polarization was preferentially chosen as it typically exhibited lower attenuation losses than mode zero with TM polarization.

The results for the treated guide are shown in Figures 49-50 and Table 14. The general trend in sensitivity is not altered by treating the waveguide with a silanizing agent although the sensitivity of the treated guide is somewhat lower. Silanization of the waveguide however considerably reduced the variability of the baseline (blank), and as a result, the minimum detectable quantity for the treated guide is at least one order of magnitude lower than that of

Table 14. Response of a silanized Ag^{+} diffused Waveguide to Indophenol.

Mode 0 TE

O.D. = 136.40*[Indophenol] + 3.21e-3

Correlation Coefficient:	.9936
Standard Error of Estimate:	.0047
Std. Dev. of Blank:	.0001
Minimum Detectable Qty.:	1.93e-6

Mode 0 TM

O.D. = 164.90*[Indophenol] + 1.83e-3

Correlation Coefficient:	.9975
Standard Error of Estimate:	.0036
Std. Dev. of Blank:	.00006
Minimum Detectable Qty.:	5.15e-7

Mode 3 TE

O.D. = 162.27*[Indophenol] + 1.73e-2

Correlation Coefficient:	.9957
Standard Error of Estimate:	.0046
Std. Dev. of Blank:	.0053
Minimum Detectable Qty.:	6.17e-6

Mode 3 TM

O.D. = 186.69*[Indophenol] + 5.75e-3

Correlation Coefficient:	.9993
Standard Error of Estimate:	.0022
Std. Dev. of Blank:	.0038
Minimum Detectable Qty.:	3.15e-5

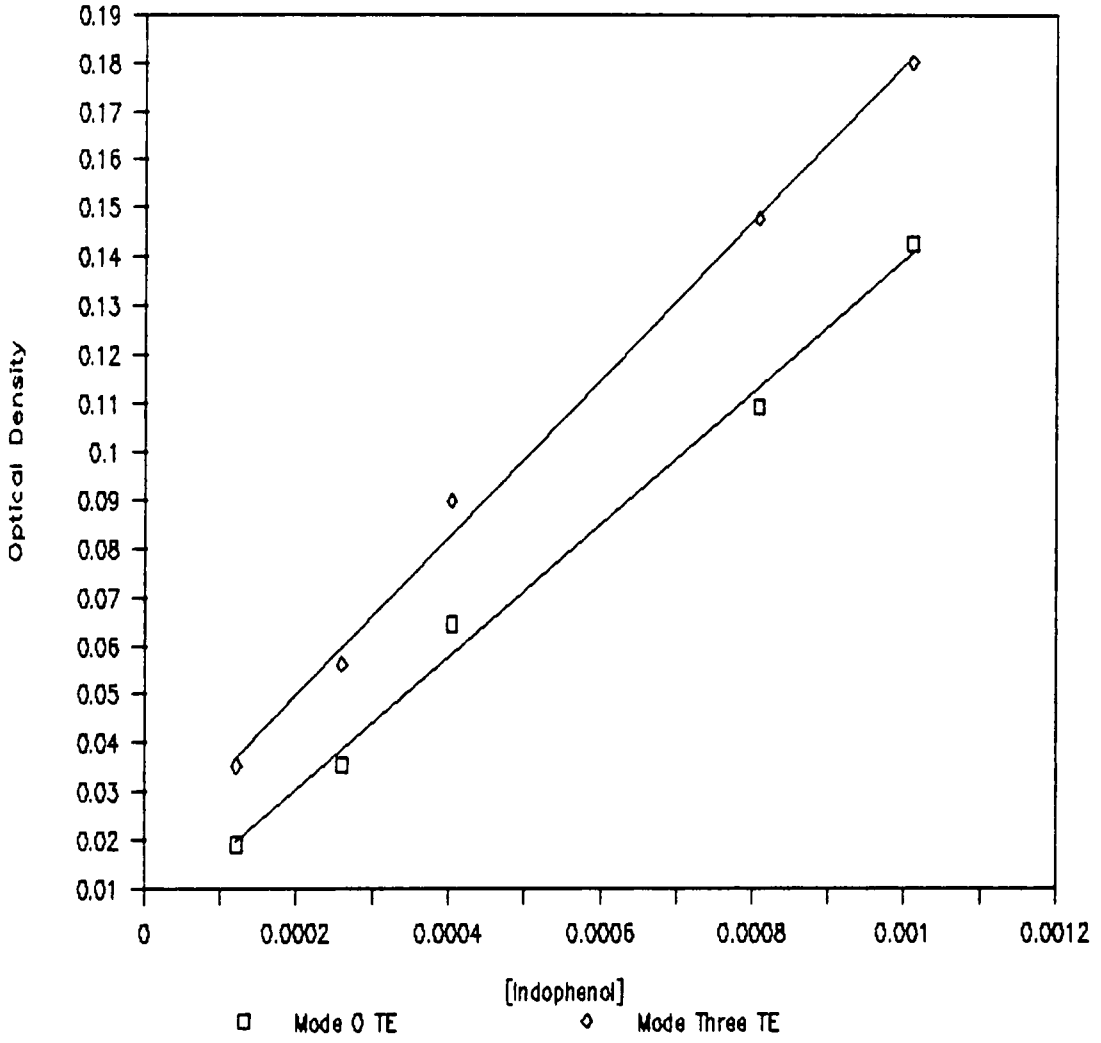

Figure 49. Calibration curve for the absorbance of Indophenol Blue using a silanized Ag^+ diffused waveguide with TE polarization.

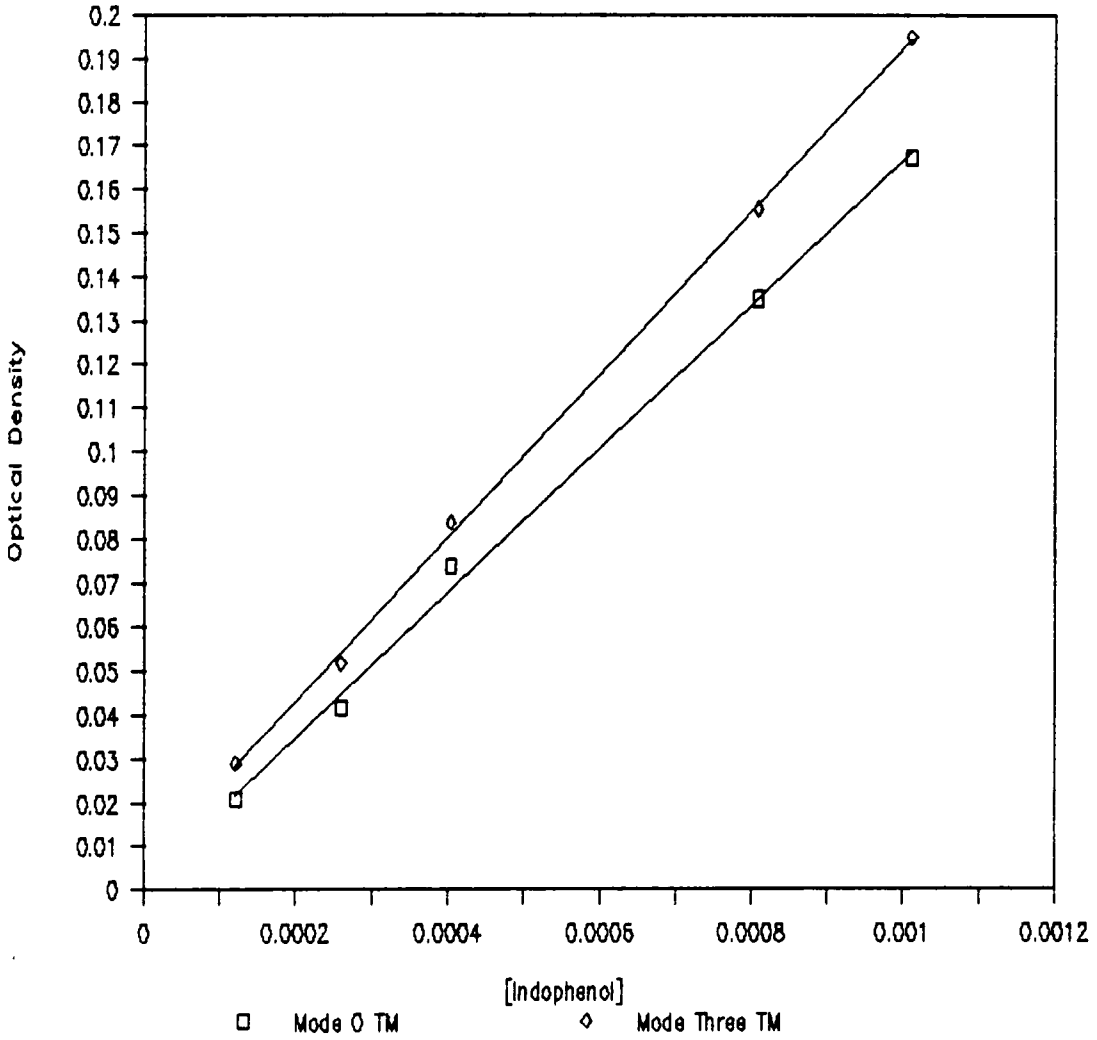

Figure 50. Calibration curve for the absorbance of Indophenol Blue using a silanized Ag^+ diffused waveguide with TM polarization.

the untreated waveguide. For the reasons listed above, operation of the waveguide in mode three with TE polarization, would still be the best compromise for sensitive and stable operation. Passivating waveguides with nonpolar monofunctional silane groups would be beneficial for solution use at pH lower than 9, as the treated waveguides have similar sensitivities yet vastly improved stabilities over the untreated waveguides.

F. FIA of UREA

The FIA of urea was used as the final test of the planar waveguide as an absorbance detector. Urea is hydrolyzed by the enzyme urease to ammonia and carbon dioxide; the ammonia subsequently produced is conveniently determined using Berthelot's reaction. Although free enzymes were, in the past, used extensively in analytical determinations, the current trend is to immobilize the enzyme on an inert carrier. This usually enhances the stability of the enzyme, increases recovery, and generally lowers the unit cost of the analysis. Urease may be conveniently immobilized on nylon with the bifunctional coupling reagent glutaraldehyde. The reaction scheme is shown in Figure 51.

In the first step, the amide linkages of Nylon 6 are cleaved with HCl, leaving a free primary amine and a carboxylic acid. Glutaraldehyde, a difunctional aldehyde, then reacts with the free amine to form a Schiff base, or imine linkage. The remaining aldehyde group is then free to react with another primary amine, usually a lysine group from the enzyme, to form the di-imine immobilized enzyme.

The immobilization of urease in a Nylon tube was adapted from the method of Sundaram and Hornby[114]. Sections of 0.034" i.d. Nylon 6 tubing[115] were cut into 1.5 meter lengths. The interior of the Nylon tubes were hydrolyzed

Enzyme Immobilization

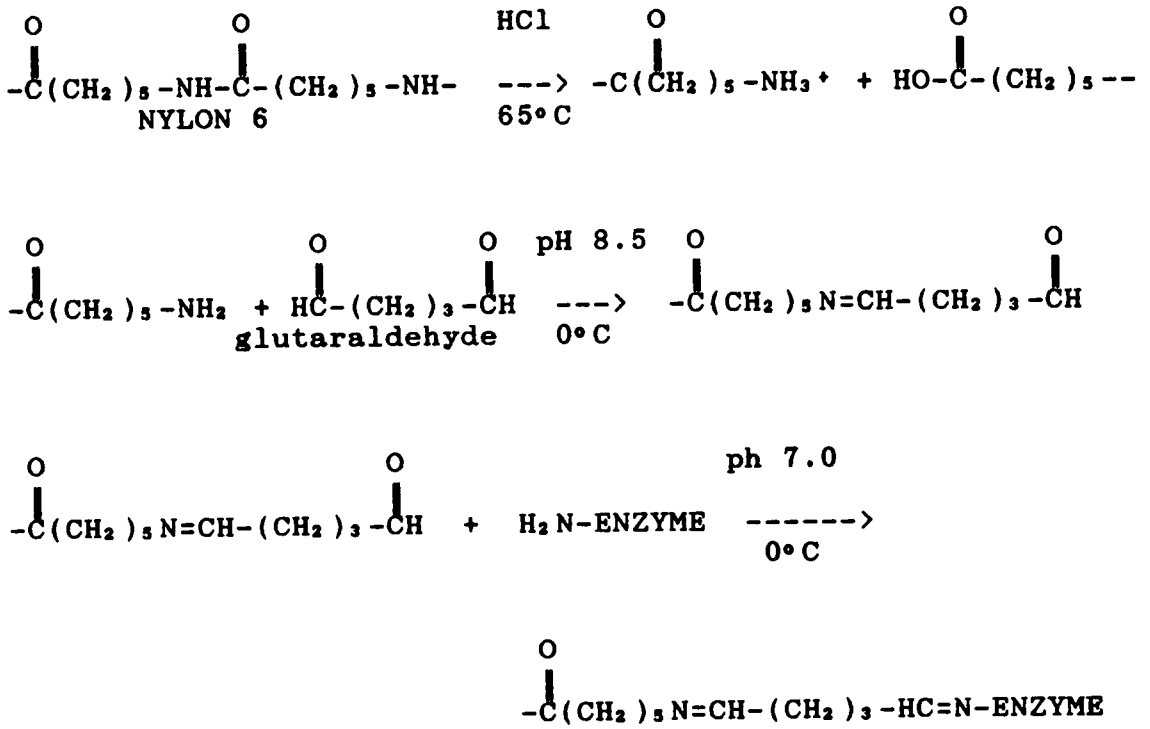

Figure 51. Reaction scheme for the immobilization of urease on Nylon 6 tubing.

with a 65 °C, 4 M HCl solution pumped through the tubes at 1 ml/min for 1 hour. After hydrolysis, the tubes were rinsed with 300 ml of de-ionized water. Next, the tubes were filled with a 12.5% (w/v) solution of glutaraldehyde in .01 M sodium borate buffer. This solution was circulated through tubes at 1 ml/min for 30 minutes at 0 °C. Following this coupling step, the excess glutaraldehyde was rinsed from the tubes with 200 ml of the sodium borate buffer.

The enzyme solution was prepared from 10 mg of Sigma type IX Jack Bean Urease. The activity was reported to be between 50,000 - 80,000 units per gram of enzyme, where 1 unit will liberate 1 micromole of ammonia per minute in a pH 7 solution incubated at 25 °C. The urease was dissolved in 5 ml of a .1 M, pH 7.0 phosphate buffer solution which also contained 2.5 e-5 M EDTA and 5.0 e-6 M mercaptoethanol, a reversible denaturing agent which facilitates enzyme immobilization. The Nylon tubes were filled with this solution, which was then allowed to circulate at 2 ml/min for 16 hours at 4 °C. After immobilization, the tubes were rinsed with 500 ml of 0.2 M NaCl solution to remove any noncovalently bound enzyme. The immobilized enzyme reactors were then filled with a pH 7, 0.1 M phosphate buffer and stored refrigerated (4 °C) until used.

The activity of the enzyme reactors were initially characterized by injecting a 1 milliliter aliquot of urea solution, ranging in concentration from 3 to 93 millimolar,

into the tube, and allowing the aliquot to react for times varying between 1 and 10 minutes. A 3.0 meter enzyme reactor was used in these determinations. It was thermostatted at 37 °C in a water bath. After the urea solutions were allowed to react for the specified time, the sample was removed, and the ammonia produced quantitated by a manual Berthelot determination. The solutions were diluted by a factor of 6 before the absorbance was measured with a Perkin Elmer UV-VIS 330 spectrometer. All samples were corrected for a blank, which was a 1 ml phosphate buffer aliquot prepared in a similar manner as the urea sample. The results are shown in Figure 52 and indicate that the linear working range is approximately 0 to 40 mM urea. Typically, a working range of 0 to 20 mM is adequate for most serum urea determinations[116].

The FIA manifold used for the NH_4Cl determinations was modified to include the 1.5 meter enzyme reactor, which was inserted between the sample injector and the phenol mixing tee. The manifold was thermostatted to 37 °C, while the secondary development coil was thermostatted to 75 °C. The flow rates for each of the reagent streams was set to 0.7 ± 0.05 ml/min with an overall flow rate of 1.93 ml/min. The detector was the silver ion diffused waveguide used during the NH_4Cl determinations, mounted in the 9.2 microliter flow cell. A Helium Neon laser beam was coupled into the wave guide which was tuned to mode three with TE polarization.

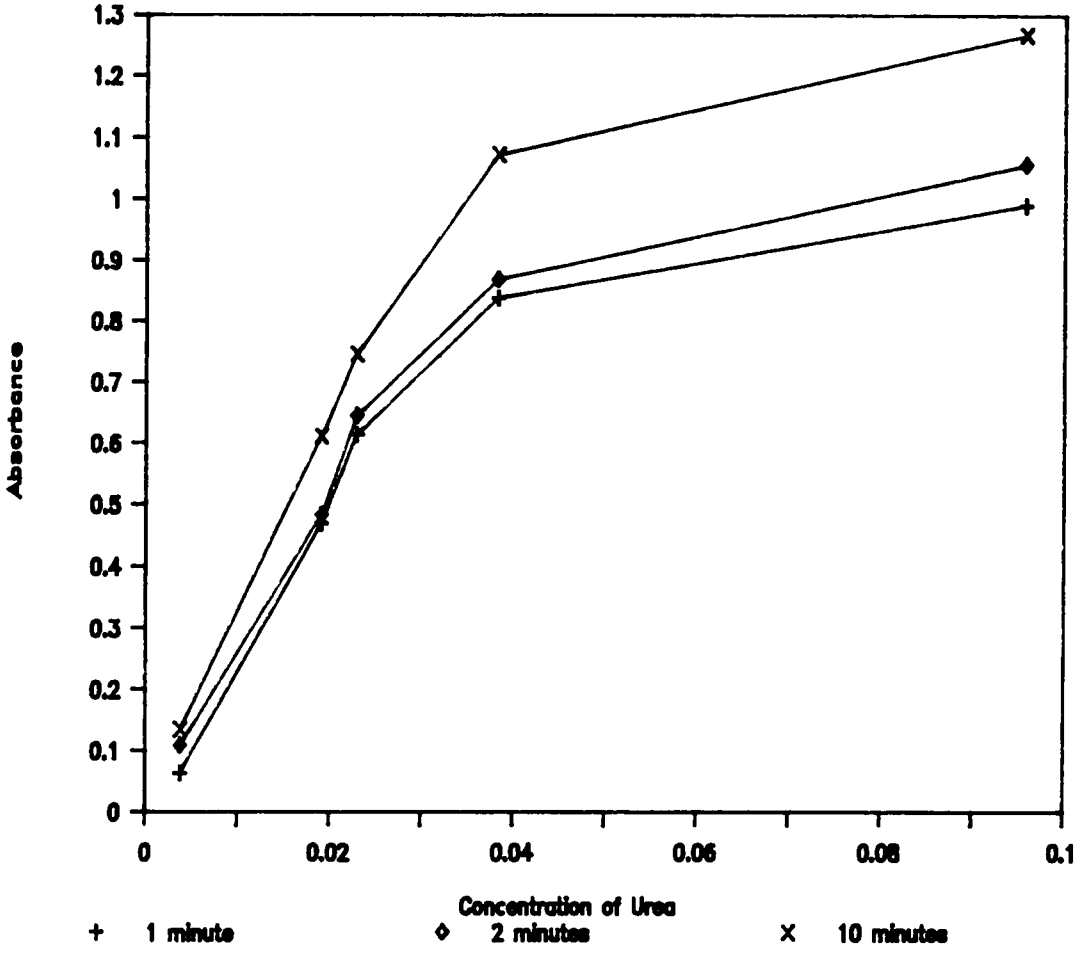

Figure 52. Calibration curve for immobilized urease reactor tube.

A 20.87 mM urea stock solution was prepared from Sigma ACS reagent grade urea in a solution of 0.1 M, pH 7 phosphate buffer with 25 micromolar EDTA. The urea standards, ranging in concentration from 1.6 to 20.87 millimolar were prepared by volumetric dilution from this stock solution. Quadruplicate 60 microliter samples of each of the standards were injected onto the manifold and the response measured. The results are compiled in Table 15 and Figure 53.

The results for the FIA of urea indicate that for the current method the working range is 1mM to approximately 21 mM. The correlation coefficient of .9937 indicates a linearity comparable to the calibration curves obtained for the ammonium chloride determinations. Although the precision appears to be poorer than the ammonium chloride results, the standard deviation of the sample absorbance is constant at approximately 0.002, indicating that as a result of the low absorbance values, the variability of the baseline (± 0.003 Absorbance units) becomes the limiting factor in the precision of the measurements.

Due to the increased volume of the manifold, the residence time of the sample was increased from 75 seconds, to approximately 180 seconds. The peak width was correspondingly increased from 45 to 120 seconds and the

Table 15. FIA of Urea using the Ag^{+} Diffused Waveguide.

[Urea]	$A_{632.8}$ Std.Dev. (%RSD)
.02087	.0854 ± .0019 (2.30)
.00835	.0371 ± .0017 (3.74)
.0050	.0249 ± .0032 (12.77)
.0016	.0101 ± .0014 (14.12)

O.D. = 3.88*[Urea] + .0046

Correlation Coefficient: .9936
Standard Error of Estimate: .0024
Minimum Detectable Quantity: 9.96e-4 M

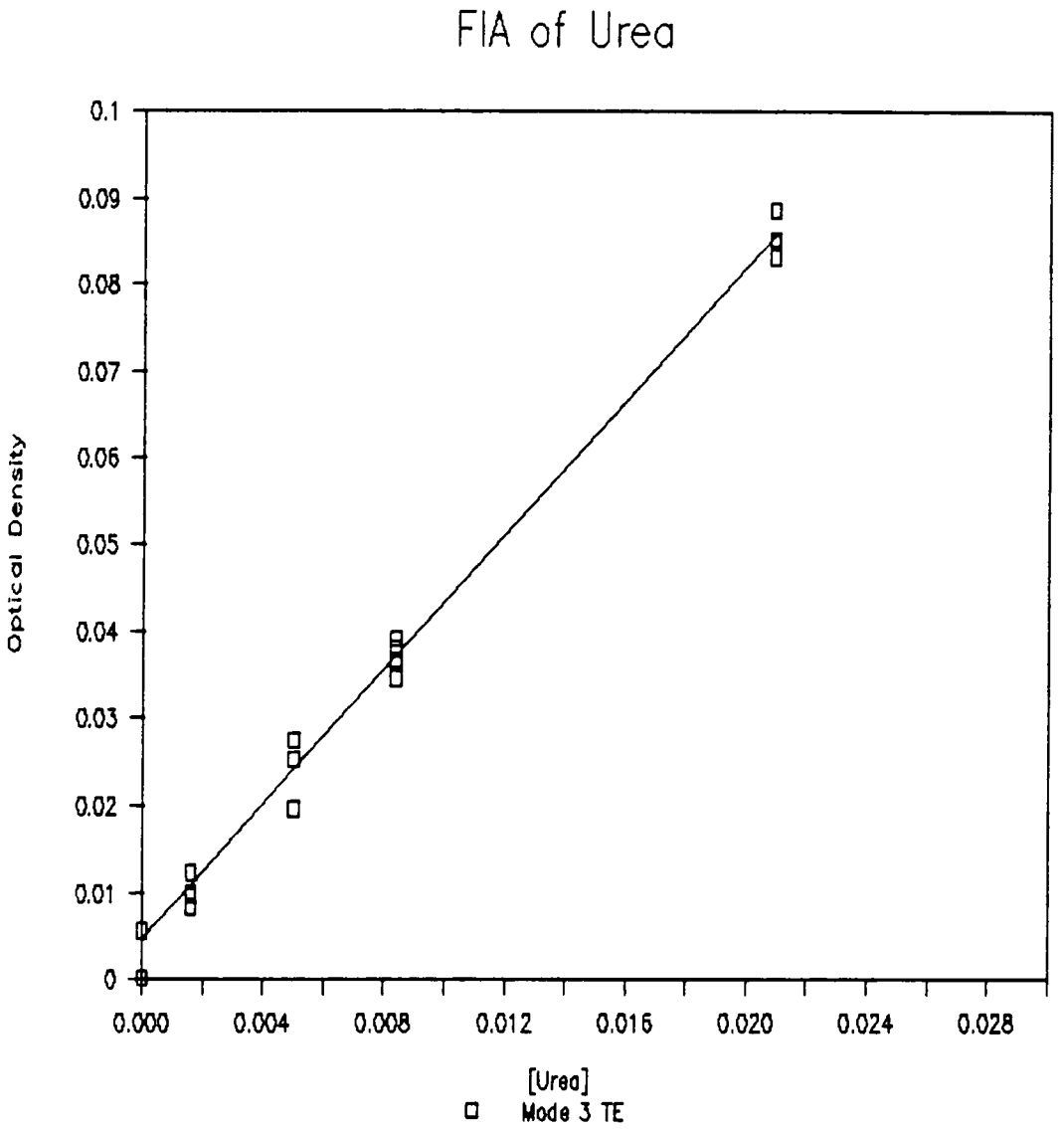

Figure 53. Calibration curve for FIA of urea using the 9.2 µl temperature isolated flow cell. The sensor was a Ag^+ diffused waveguide operated in mode 3 with TE polarization.

sample rate decreased from >60 samples per hour to 30 samples per hour. A 20 % conversion of urea to ammonia was determined by comparing the absorbance of the urea solutions to a calibration curve prepared under similar conditions with NH_4Cl standards. In comparison, Inman and Hornby report an 80% conversion of urea with their immobilized reactors. These numbers agree fairly well given that their 3 meter tubes were calibrated at lower sample rates (20 samples/hour) and with urea concentrations at least a factor of 10 lower than those used in this study.

It is well known that urea is hydrolyzed to ammonia by alkaline solutions at elevated temperatures[118]. Because the sample was not quantitatively converted to ammonia by the enzyme reactor, it was possible that hydrolysis of the excess urea could significantly contribute to the blank and the absorbance measured for the sample. As a check, the enzyme reactor was removed from the manifold and the response to several 60 microliter injections of the urea solutions were measured. No appreciable response was recorded for any concentration of urea. Ngo[119] reported similar results in a study of possible interferences for the analysis of ammonia with Berthelot's reaction. He found that urea concentrations of 10 millimolar had no affect upon the final absorbance of solutions that were 0.5mM in NH_4Cl.

The working range of this method is ultimately limited by the Michaelis constant (K_m) of the immobilized enzyme.

As the substrate concentration approaches Km, the reaction begins to deviate from first order kinetics and the working curves become nonlinear[120]. The Michaelis constant is an inverse measure of the affinity of the enzyme for the substrate and its value is approximately 4 mM for urease in solution[121]. Immobilization of the enzyme, however affects the physical and chemical environment of the enzyme and may act to either increase or decrease this affinity. In order to determine the upper limits of the present method, the Michaelis constant was calculated from the FIA data using a Lineweaver-Burke plot[122].

In this method the inverse reaction rate is plotted versus the inverse substrate concentration. The reaction rate of this hydrolysis reaction is measured by the quantity of ammonia produced for a specified reaction time. This is conveniently determined by measuring the absorbance of the indophenol produced divided by the resisdence time of the urea sample in the immobilized enzyme reactor. The slope of this plot is proportional to the Michaelis constant and the intercept is equal to the inverse maximum velocity. The data is plotted in Figure 54.

The Km calculated using this method was 19.03 ± 7.6 mM urea, indicating that the upper limit of the analytical range is approximately 20 mM urea. As a comparison, Sundaram[123] calculates Km's between 17 and 28 mM for urease immobilized on nylon tubes using several different synthetic

Table 16. Lineweaver Burke Plot for Immobilized Urease.

$[Urea]^{-1}$	Time/[Optical Density]
47.92	14.69
119.76	33.87
200.	50.22
625	124.92

$[v]^{-1} = .186*[S]^{-1} + 9.77$

Correlation Coefficient: .9955
Standard Error of Estimate: 3.94

K_m = 19.03 ± 7.65 mM
Vmax = .1023 ± .0491 min^{-1}

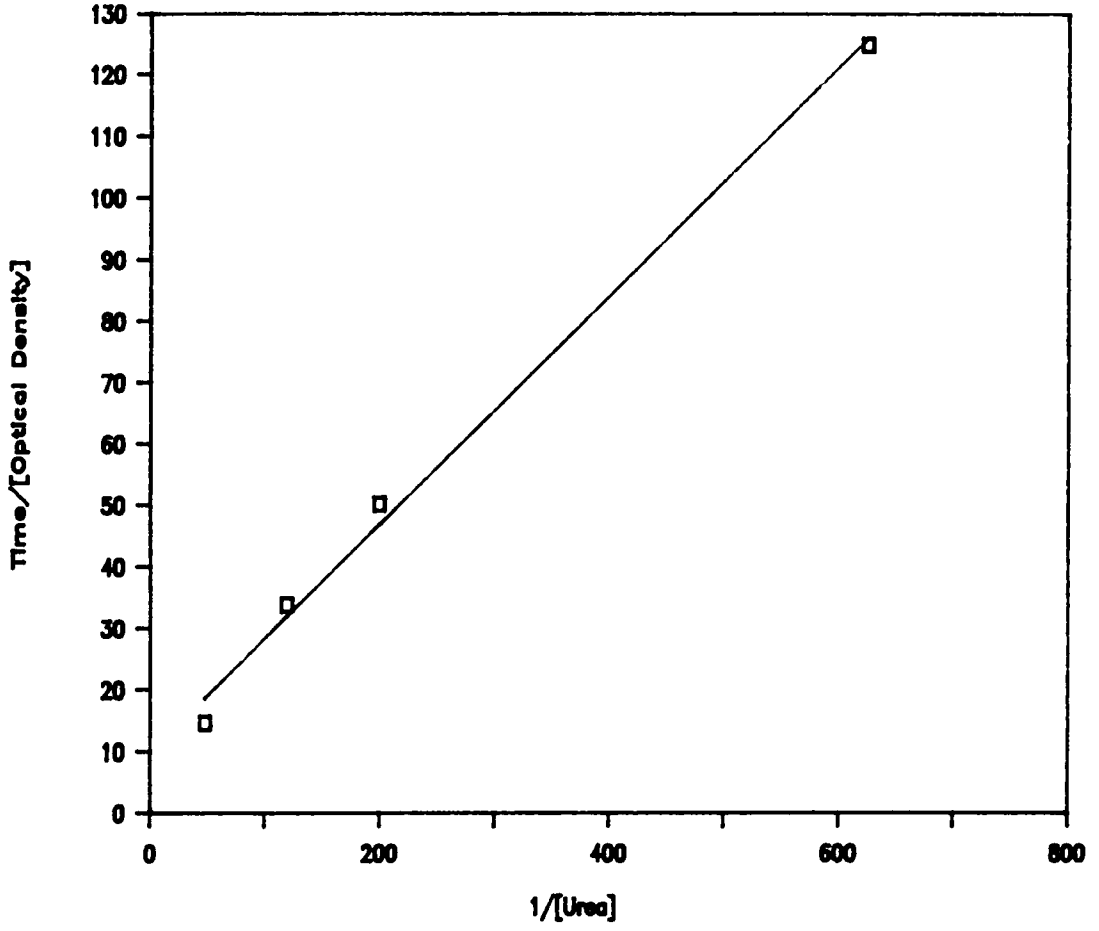

Figure 54. Lineweaver Burke plot for an immobilized urease enzyme reactor.

methods. Urease immobilized on Nylon powder or in Nylon mesh commonly have measured Km's of approximately 3.5 mM to 4 mM, essentially the same as that of the unbound enzyme[9]. The observed increase of Km for immobilization of urease in nylon tubes has been shown to be a result of the stationary diffusion layer present at the surface of the open tubular reactor. The rate of reaction is limited by the diffusion of the substrate across the diffusion layer to the immobilized enzyme[124]. Onyezili, showed that the Michaelis constant of tubular reactors decrease as the flow rates increase. The Michaelis constant for immobilized urease in Nylon tubes was observed to decrease from 20 mM at 3 ml/min to 10 mM at 24 ml/min. These results suggest that the analytical working range could be extended by decreasing the flow rate and thus increasing the apparent Michaelis constant.

VI. Discussion

A. Evaluation of the Planar Waveguide as an Absorption Sensor

Comparing the results obtained from the planar waveguide with the data obtained from a conventional transmission cell brings several important pieces of information to light. The first is that these planar waveguides are approximately .8 to 1.0% as sensitive as the conventional 1 centimeter path length transmission cell. Second, given a constant concentration of an absorbing species, as depicted in Figure 55, the attenuation of the waveguide increases monotonically as a function of mode number. Typically, mode three was approximately 1.4 times more sensitive than mode 0 for a waveguide fabricated in a 10 mole % $AgNO_3/NaNO_3$ solution at 310 °C. Also, TM (parallel) polarization exhibited a slightly higher sensitivity than TE (perpendicular) polarization.

All of these trends can be qualitatively explained using the ray optics model developed in Section 3. The calculated effective depth of penetration of the evanescent wave, as a function of the internal angle (effective index), for the waveguide used in Figure 55, was shown in Figure 8. Note that the highest value of the internal angle

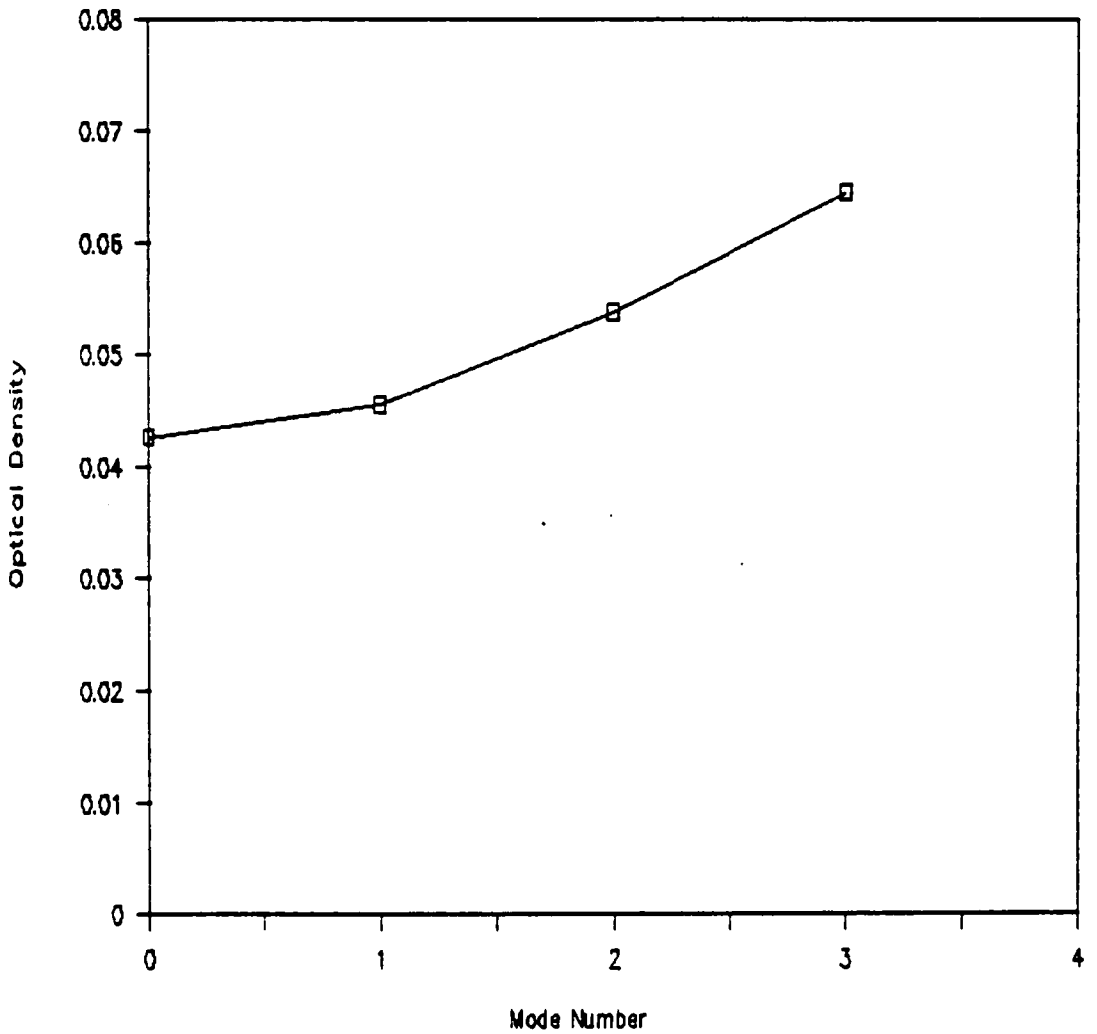

Figure 55. Guide response to indophenol as a function of the mode number.

corresponds to the lowest mode number. As was shown previously, the depth of penetration increases as the incidence angle decreases (or as the mode number increases) and is deeper for TM polarization than TE polarization. The ratio of the depth of penetration for mode 3 compared to mode 0 is approximately 2.

Utilizing the ray optics model, the attenuation of the waveguide can be calculated using equation 3.46. Absorption data for a Ag^+ waveguide is shown in Table 17. The thickness of the waveguide,~5.9 microns, was calculated using equation 4.2. The calculated absorbances are .024 and .031 for mode 0 and mode 3, respectively. The measured values were .143 and .18, respectively. The differences arise from two limitations of the ray optics model derived in section 3. The first limitation, as previously discussed, was the assumption of discrete interactions with the surface of the guide. As a result of this assumption the calculated absorbance was expected to be too low. The second, and most significant limitation, is the application of this model to a gradient index waveguide.

If a waveguide is formed by a diffusion process, the index profile of the guiding film is not a step function. As discussed in section 4, the index decreases continuously from a maximum value at the surface of the glass slide to the index of the substrate. As a consequence of this gradient index profile, it was shown in section 3 that the

Table 17. Measured and Calculated Absorbance Using the Ray Optics Model.

Mode	0	3	
Neff	1.5782	1.5168	
θ(rad)	1.449	1.266	
Length	2 cm	2 cm	
A measured	.143	.180	
[Indophenol]	1.01 mM	1.01 mM	
Step Index Profile			
Guide Width	5.9	5.9	microns
Bounces	205	526	
Absorbance	.024	.030	
Polynomial Profile			
Guide Width	1.5	4.0	microns
Bounces	816	786	
Absorbance	.096	.116	
Parabolic Profile			
Guide Width	2.3	5.1	microns
Bounces	532	616	
Absorbance	.0627	.091	

effective width of the guide was dependent upon the effective index of the guided mode and was typically much smaller than the actual width measured or calculated from the diffusion conditions. Furthermore, if the index profile can be approximated by a parabolic approximation (equation 3.37), it was shown that ray trajectories had the same periodicity or essentially the same number of "bounces" per unit length. Therefore, the absorbance calculated from equation 3.46, which assumes a constant film thickness, and an increasing number of interactions with the surface as a function of the mode number, should be in considerable error.

Included in Table 17 are values of the absorbance calculated using both a second order polynomial profile (equation 4.1) and a parabolic profile (equation 3.37). The number of interactions for a specific mode was calculated from the measured effective index and then compared to the appropriate profile to determine the corresponding effective depth. Both profiles are graphed in Figure 56. Unfortunately, there is still a considerable difference between the measured and calculated values of the absorbance. However, the use of the second order polynomial distribution gave somewhat better results than the parabolic profile, which is consistent with Stewart's[57] findings. The limitations of these calculations arise from the uncertainty of the shape of the index profile and the effect of this

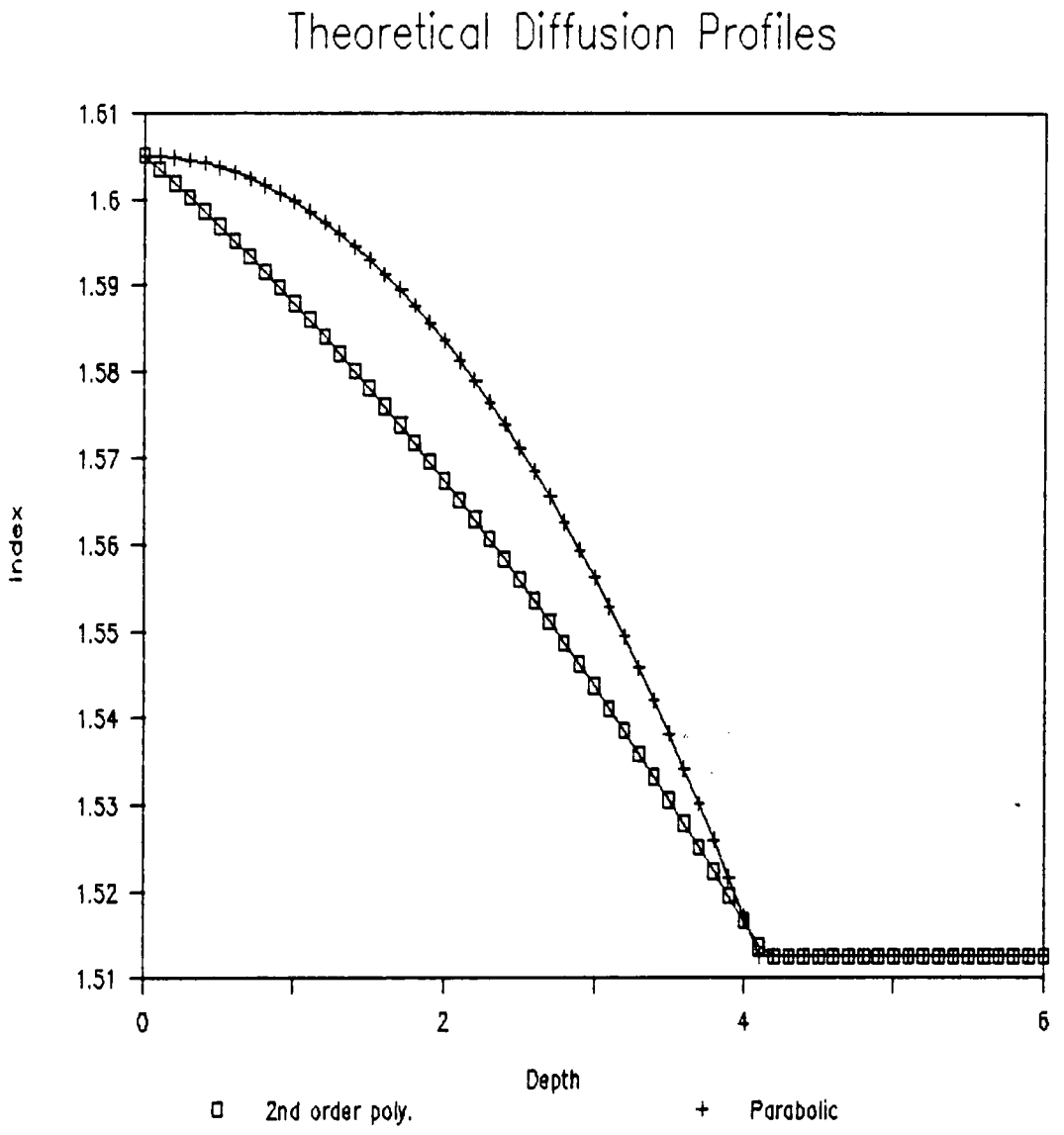

Figure 56. Theoretical diffusion profiles for Ag^+ diffused waveguides.

gradient index profile on the effective penetration depth. The inverse WKB approximation[125] has been used extensively to calculate the shape of the index profile from the measured effective indices. However, around 10 guided modes (rather than the 4 present in these guides) are needed to adequately define the index profile.

As a first approximation, the penetration depth could be considered the same for the step index and the gradient index guide since an abrupt dielectric interface occurs at the cladding Ag^+ diffused waveguide interface. Difficulties arise with this calculation, however, in determining the index at the surface of the waveguide, calculating the index matching term, and the propagation angle for this interface. Therefore, even if the index profile was explicitly known, use of the ray optics model to obtain anything other than qualitative information concerning the absorption behavior of the waveguide would meet with considerable difficulties.

The absorption data for the passivated waveguides (section 5, Figure 49) is replotted as the attenuation coefficient of the waveguide versus the attenuation coefficient of the dye in Figure 57. This allows the comparison of the measured and calculated values of the interaction ratio, R, as shown in Figure 9.

If one ignores the n(x) dependence of the waveguide in the interaction ratio derivation, the calculated results indicate that for a normalized guide thickness of ~10, the 4

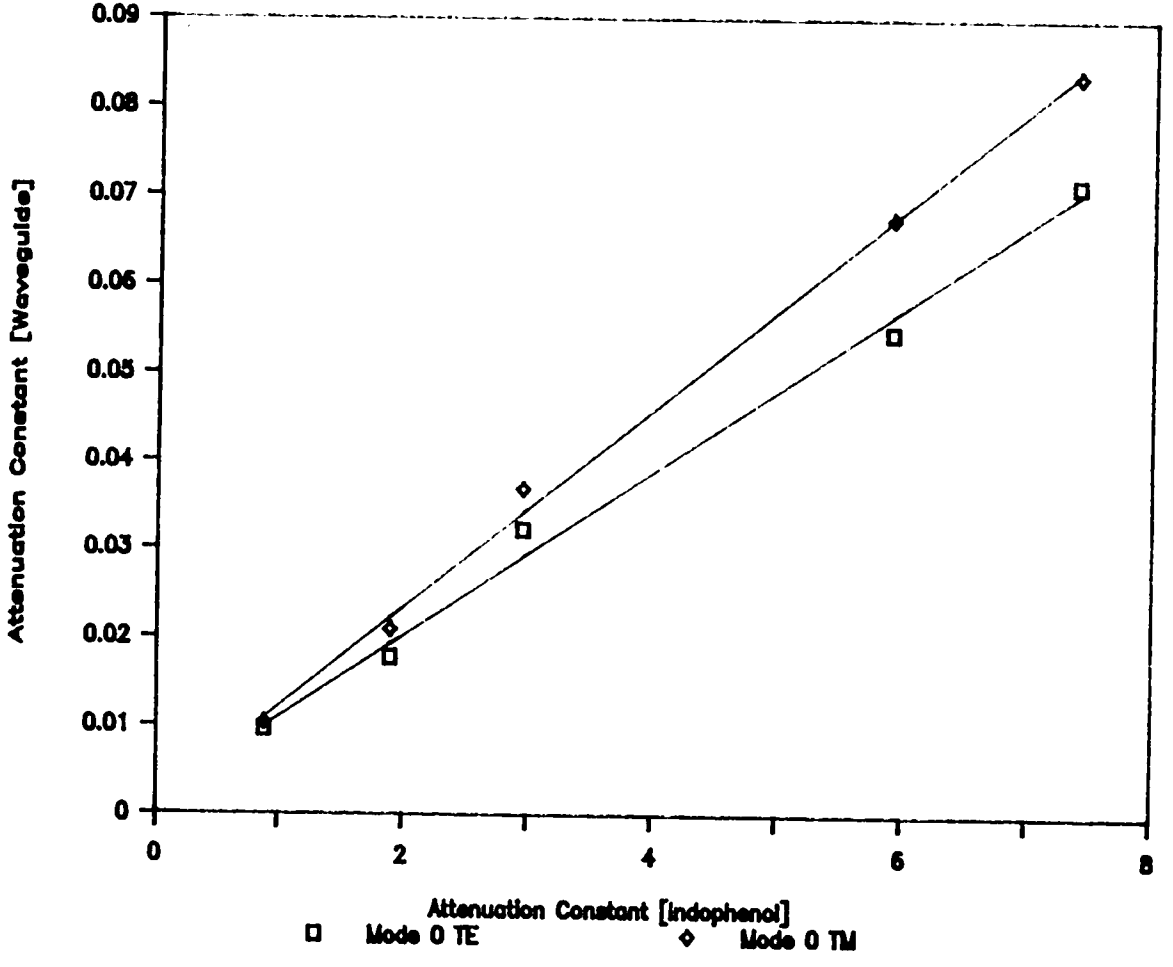

Figure 57. Relative attenuation of a Ag^{+} waveguide at mode zero.

supported modes of the guide should exhibit very little sensitivity to absorption. However, if the index profile of the guide is assumed to be of the form of the second order polynomial displayed in Figure 56, then the width of the guide changes, as a function of the mode number, as previously discussed. Using the data from Table 17, the calculated normalized effective width of mode 0 is 2.2 and 6.3 for mode 3. The results of calculating R using these effective depths, is tabulated in Table 18. R calculated for mode 0 and 3 is .3% and .41% respectively, whereas the measured values are .93% and 1.11 %. Although the absolute values differ, the R ratio for mode 3 to mode 0 is consistent between the measured and calculated data.

The calculated interaction ratio should only be considered as a rough guide of the sensitivity of the planar waveguide. In the derivation of R, only attenuation due to a homogeneous absorbing layer was considered. Surface phenomena such as adsorption and double layer effects were not considered, and are potential sources of major deviations of the sensitivity of the planar guide. Harris and Polky[20], using a step index guide, calculated a value of .8% for R at mode zero. But they also reported measured values of up to 40% using methylene blue as the absorbing media. They demonstrated that surface adsorption of the dye dominated the attenuation of the waveguide, and in some cases irreversibly attenuated the beam in the guide.

Table 18. Interaction Ratio Calculations for the Ag+ Waveguide.

	Mode 0 TE		Mode 3 TE
R Measured	.93 ± .04 %		1.11 ± .04 %
R M_3/M_0		1.2	
R Calculated	.3%		.41 %
R M_3/M_0		1.37	
Normalized Width	2.2		6.3

Recently this affect has been reversed by introducing heavy metals such as the Pb^{2+} into the reagent stream[126]. Apparently, the heavy metal has a greater affinity for the negatively charged glass surface, and displaces the methylene blue dye. Clearly attenuation in the waveguide is related in a complex fashion to not only the surrounding dielectric media but the specific physical and chemical interactions at the waveguide solution interface. Future models of the attenuation of the guided beam will necessarily include these system dependent parameters.

B. Evaluation of Literature Results

Two other workers have reported using a planar waveguide as a sensor for chemical analysis; one as an absorption sensor, and the other as a differential refractometer. Mitchell[21] described the use of a sputtered glass waveguide as an enhanced attenuated total reflection sensor for bilirubin determinations in whole blood. Unfortunately no quantitative data was published, but from the calibration curve reported, it appears that the interaction ratio for the guide was approximately .3% This value is very close to what Mitchell predicted using his R calculations. This was not a flow sensor and no information was presented concerning the precision of the device, but it represents an important contribution since it demonstrated

that absorption data could be obtained in a highly scattering media using a planar waveguide.

Seifert et. al.[127] described the use of a planar optic waveguide as a differential refractometer for the determination of urea. The reaction products of the hydrolysis of urea produced a measurable change in the index of refraction of the solution. Their guide was a 180 nm thick SiO_2-TiO_2 waveguide with a refractive index of 1.76. Light was coupled into the waveguide using a grating coupler embossed into the surface of the guide. It was the grating coupler that was the actual sensor. Solutions of differing indices of refraction were allowed to flow over the grating which then modulated the coupling efficiency of the grating. The intensity of the beam was then monitored by measuring the light scattered from the guide with a fiber optic probe. An analogous experiment would be to allow an analyte solution to flow between the prism waveguide air gap and modulate the input coupling efficiency of a laser beam into a planar waveguide.

The sensitivity obtained with their device was impressive. They calculated a minimum detectable index change of $5*10^{-5}$ index units. Unfortunately this was not related to a concentration of urea, but it was clear that from their published results that the device could measure concentrations as low a 1 millimolar urea. No calibration curves were presented or any data concerning the precision

of the measurements, and they indicated difficulties with baseline stabilities. This is not surprising given the probable high R value of the guide (R > 10%) and the low coupling efficiencies of embossed grating couplers[128]. As the minimum peak width published was somewhat greater than 3 minutes, the overall analysis rate would be limited to less than 20 samples per hour. Nevertheless, perturbation of the coupling efficiency of the input coupling grating appears to hold considerable promise as a sensor mechanism, given the theoretically calculated detection limits.

In comparison with the above work it was determined in this study that a reasonably sensitive and precise sensor could be developed using a gradient index waveguide. Using a 60 microliter sample size and 9.2 microliter flow cell, the Ag ion waveguide sensor could easily support an analysis rate of 30 samples per hour with sufficient sensitivity to cover the desired analytical working range of 1 to 20 millimolar urea. The calibration curves obtained for the analysis of urea and ammonia consistently had correlation coefficients of better than 0.99 and precisions of ±5% RSD. Although the uncertainties of these analyses are probably attributable in a large part to Berthelot's reaction, rather than any mechanistic fault of the waveguide sensor, their remain many areas in which the sensitivity and precision of these planar waveguide absorption sensors could be improved.

C. Sensitivity Improvements

Although silver ion diffusion into glass substrates is a convenient and economical method of producing durable waveguides, the utility of these guides is severely limited. As previously discussed in Section IV, the maximum index change is limited by the sodium ion concentration of the glass substrates. Presently, for commercially available substrates, this is limited to about 12-15%, which limits the index increase (for silver ions) to approximately 0.1. Although it is possible to fabricate a diffused waveguide with a higher index using specialty glasses, this does not come without a price. As a result of the reducing agents present in commercial glass, increased silver ion concentrations result in a larger number of agglomerated metal particles in the waveguide. These particles contribute greatly to scattering loss, which increases dramatically as a function of the laser frequency. Compounding this problem, silver ion diffused waveguides fluoresce intensely at and below the 514.5 nm. As a result of the scattering and fluorescence, operation of these metal exchanged guides is limited to laser lines between 632.8 nm and the near IR.

To reliably achieve higher sensitivities, inorganic glass films are an obvious candidate for waveguiding films. Many techniques, such as sputtering[129], vacuum deposition[44],

and chemical vapor deposition, amongst other common techniques used in the semiconductor industry, can be used to deposit a thin film on a suitable substrate. The advantage of these techniques is that a wide range of high index materials may be deposited in accurately controlled film widths. An excellent candidate material would be silicon oxynitride[130], SiON, deposited using chemical vapor deposition. This material is highly inert (it is used as a passivation layer on silicon semiconductors), transparent from the near UV into the IR, and has an index variable from 1.45 for pure silica to 2.008 for pure Si_3N_4. Unfortunately, the disadvantage for many of these techniques is that they are extremely expensive to implement.

A more economical technology may be the use of inorganic sol-gel films. Organometallic solutions of silicon and titanium can be mixed and upon oxidation form thin durable films with indices varying from 1.5-2.0[131]. Although these films were initially marketed as antireflection coatings for optics, Tiefenthaler et al[132] have been successful in implementing these thin films as planar waveguides. By dip or spin coating the liquid organometallic solution onto a substrate and then subsequently baking it, a thin, durable, high index glass film results. Unfortunately, several repeated dippings are required to produce a film thick enough to produce a waveguide and, at least in this laboratory, extensive

scattering caused by these layers and surface cracks prevent waveguiding in these films. Annealing these films with a much slower temperature ramp (~ 1 °C/min) might possibly eliminate the tensions developed in these films gel process, and produce much higher quality waveguides[133].

Finally, the sensitivity of these measurements can be considerably enhanced if the noise due to the baseline variation can be reduced. The most serious noise contribution is adsorption on the surface of the waveguide. This results in a constant diminution of the intensity of the guided beam and eventually renders the waveguide inactive. Passivation of the waveguide through the use of nonpolar surface silanizing agents is a viable means of reducing surface adsorption in acidic or neutral solutions. This technique requires further study and could be optimized through the use of either longer chain alkane silanol groups, or possibly monolayer Langmuir-Blodgett films.

In an attempt to compensate for the effects of adsorption on the surface of the waveguide, a two wavelength experiment was conceived. By using the optical arrangement depicted in Figure 58, two laser lines could be independently coupled into the planar waveguide. Each line has a unique coupling angle, due to the phase match requirements of the propagating beam, and therefore is also coupled out of the waveguide at a unique angle. As a result the two lines are spatially resolved and can be individually

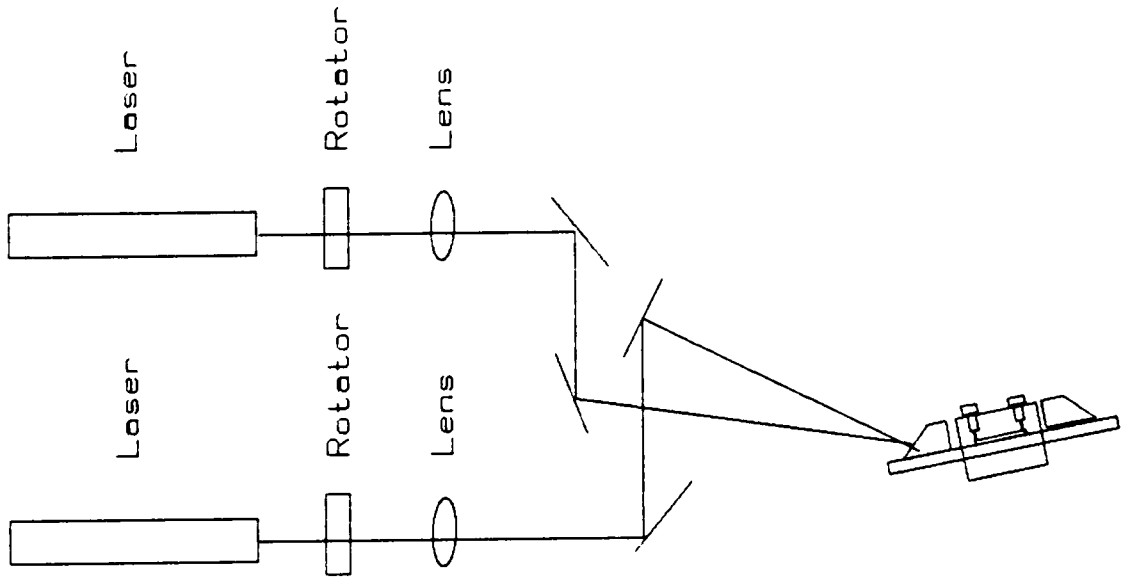

Figure 58. Optical setup for launching two beams in a planar waveguide.

detected using separate photodiodes or a diode array. If one of the laser lines is matched to the absorption frequency of the analyte, while the other, a reference line, is far removed from the absorption band, it should be possible to ratio the intensities of the two beams and attempt to correct for attenuation due to adsorption. While the analytical line will be attenuated by both absorption of the analyte and the adsorbed species, the reference line should be attenuated only by the adsorbed species. This scheme admittedly, is likely to work only if the adsorbed species is not the analyte, and the attenuation of the guide due to the adsorbed species, is solely a result of a refractive index variation(i.e. not an absorption).

Unfortunately, the analyte in this study, indophenol blue, was the major adsorbant on the waveguide. As a result, the attenuation of the guide by absorption of the adsorbed analyte was significant. Consequently, the slope of the baseline for the analytical and reference line could not be correlated in a simple fashion and therefore could not be easily used as a correction for surface adsorption. However, as an aside, considerable fluorescence was observed when the 488 nm line of the argon laser was coupled into the Ag^{+} waveguide. Although most of the fluorescent light was scattered out of the guide, a portion was confined to the waveguide and observed to couple out in the characteristic mode pattern, spatially resolved from the exciting line.

Harrick[38] observed guided wave fluorescence with ATR devices and a obvious extension of this study would be to examine the possible applications of thin film waveguides to fluorescence spectroscopy.

The effect of temperature variations on the coupling efficiency of the prisms is also a major source of baseline instability. Because this is a single beam instrument any variation in the coupling efficiencies of the input or output prism will cause a significant baseline deviation. Swalen[25] has explored several double beam optical arrangements in which the beam is rastered across the face of the input prism, causing the guided wave to propagate in a reference and sample region in the waveguide. These were rejected, however, as it was too difficult to maintain a constant coupling efficiency across the base of the input coupling prism. A fiber optic probe was placed just after the input coupling prism to measure the scattered light from the guided beam in an attempt to quantify the intensity variations of the input beam. Variation of the output coupling efficiency was significant enough though to make this small correction, essentially useless.

The ideal correction would be to eliminate the input coupling prisms for either a grating or endfire coupler, whose coupling efficiencies are independent of temperature variations. As the sensitivity of these guides is maximized by using a thin, high index, single mode guide, the utility

of the technique would not be compromised by using these types of couplers. Indeed, the true advantage of using a planar guide would be the opportunity for miniaturization and incorporation of the source, waveguide and detector on a single substrate. This type of sensor would then necessarily use an endfire coupler to mate the source and waveguide. Using modern semiconductor fabrication techniques a completely integrated, dual beam sensor, such as that depicted in Figure 1, could then be realized.

VII. CONCLUSION

The object of this research was to investigate the use of planar waveguides as analytical sensors in flowing streams. Since these devices were not commercially available, several fabrication techniques were explored. Polymer and inorganic sol gel glasses offer the largest selection of materials with the widest range of refractive index and optical properties. However, durability and fabrication difficulties precluded their use in this study. Nevertheless, these materials certainly merit further attention as thin film planar waveguide absorption sensors. Waveguides made by silver ion diffusion were found to be durable, cheap and relatively easy to fabricate. Additionally, these gradient index waveguides were found to be equally as sensitive as step index waveguides with similar waveguide parameters.

The sensitivity of the planar waveguides were found to be 2 to 3 orders of magnitude more sensitive than conventional total internal reflection elements. While the silver ion waveguides used in this study were approximately 1% as sensitive as a conventional 1 cm transmission cell, the sensitivity of these devices can be readily increased by reducing the film thickness and increasing the film index of refraction. Although this may require using other fabrication techniques, it is theoretically possible to

construct waveguides with sensitivities varying from the standard total internal reflection element to a conventional transmission flow cell.

Application of this device to Flow Injection Analysis provided a rigorous test of the capabilities of the Ag^{+} waveguide. It was found to operate reliably over the course of a typical FIA experiment. The sensitivity of the sensor was adequate for the determination of urea over the entire analytical working range, using the standard FIA method. Passivating the surface of these waveguides with silane coupling agents was found to be an effective method for preventing sample adsorption and maintaining a stable baseline.

The use of these waveguides as absorption sensors will be the most beneficial for those methods in which scattering prevents the use of conventional transmission flow cells. It had been previously shown that if the size of the scattering particle was less than the depth of penetration of the evanescent wave, attenuation of the guided beam by scattering was insignificant. Several potential applications might be in the areas of chemical process stream and wastewater analysis.

Future research should concentrate on several areas. Either dual beam designs or the use of an alternate method of exciting the waveguide, such as a grating coupler, should be explored to eliminate the variability of the baseline due

to the temperature dependence of the coupling efficiencies of the prisms. Other optical phenomena, such as fluorescence, which could take advantage of the high surface energies present in the waveguide should be exploited. The integration of a laser source, waveguide, and photodetector on a single substrate and the feasibility of a "spectrometer on a chip", should also be explored. In conclusion, the use of planar waveguides as chemical sensors provides a rich opportunity for the study of conventional optical techniques on a two dimensional substrate.

VIII. REFERENCES.

1 Harrick, N.J. *Phys. Rev. Letters.*, **1960**, 4, 224.

2 Fahrenfort, J. *Spectrochim. Acta.*, **1961**, 17, 698.

3 Sabo, M; Gross, J; Wang,J.; Rosenberg, I.E. *Anal.Chem.* **1985**, 57, 610.

4 Stryer, Lubert. "Biochemistry"; W.H. Freeman: San Francisco,1975.

5 Kaplan, Alex and Szabo, Laverne. "Clinical Chemistry: Interpretations and Techniques"; Lea & Febiger: Philadelphia, 1979.

6 Henry, R. In "Clinical Chemistry: Principles and Technics", 2nd Ed,; Cannon,D.C.; Winkelman,W., Eds.; Harper Row: Hagerstown,Md., 1974.

7 Tamir, T. In "Topics in Applied Physics Integrated Optics" 2nd ed., Tamir, T. Ed.; Springer-Verlag: Berlin, 1982,Chapter 1.

8 Osterberg, H.; Smith, L.W. *J. Opt. Soc. Am.* **1964**, 54, 1073-1078.

9 Osterberg, H.; Smith, L.W. *J. Opt. Soc. Am.* **1964**, 54, 1078-1084.

10 Anderson, D.B.; In " Optical and Electro-Optical Information Processing" Tippett,J., Ed.; M.I.T. Press: Cambridge, Mass.; 1965, 221-234.

11 Miller, S.E. *Bell Sys. Tech. J.* **1969**, 48, 2059.

12 Shubert, R,; Harris, J.H. *IEEE Trans. Microwave Theory Tech.* **1968**, MTT-16, 1048.

13 Kondo, M. *IEEE Trans. Microwave Theory Tech.* **1982**, MTT-30, 1747-1753.

14 Kaminow, I.P.; Carruthers, J.R.; Turner, E.H.; Stulz, L.W. Appl. Phys. Letters **1973**, 22, 540.

15 Valette, S. *Electron. Lett.* **1983**, 19, 883-885.

16 Johnson, L.M.; Leonberger, F.J.; Pratt, G.W. *Appl. Phys. Lett.* **1982**, 41, 134.

17 Izutsu, M.; Enokihara, A.; Sueta, T. In "Technical Digest, Second European Conference on Integrated Optics" Firenze Italy, 1983, 144.

18 Izutsu, M.; Enokihara, A.; Sueta, T. *Electron. Lett.* **1982**, 18, 867.

19 Midwinter,J.E. *IEEE J. Quant. Elec.* 1971, QE-7, 339-344.

20 Polky, J.N.; Harris, J.H. *J. Opt. Soc. Am.* **1972**, 62, 1081-1087.

21 Mitchell, G.L. *IEEE J. Quant. Elec.* **1977**, QE-13, 173-176.

22 Levy, Y.;Imbert, C.; Cipriani, J.; Racine, S.; Dupeyrat, R. *Opt. Comm.* **1974**, 11, 66-69.

23 Rabolt, J.F.; Santo, R.; Swalen, J.D. *App. Spect.* **1979**, 33, 549-551.

24 Rabolt, J.F.; Santo, R.; Schlotter, N.E.; Swalen, J.D. *IBM. J. Res. Develop.* **1982**, 26, 209-216.

25 Swalen, J.D.; Tacke, M.; Santo, R.; Rieckoff, K.E.; Fischer, J. *Helv. Chim. Acta.* **1978**, 61, 960-977.

26 Swalen, J.D., Schlotter, N.E.; Santo, R.; Rabolt, J.F. *J. Adhesion* **1981**, 13, 189-194.

27 Tiefenthaler, K.; Lukosz, W. *Opt. Lett.* **1984**, 10, 137-139.

28 Bohn, P.W. *Anal. Chem.* **1985**, 57, 1203-1208.

29 Miller, D.R.; Han, O.H.; Bohn, P.W. *App. Opt.* **1987**, 41(2), 245-249.

30 Hecht, E.; Zajac, A. "Optics"; Addison Wesley: Reading, Mass., 1979, p.74.

31 Newton,I. "Opticks"; Dover Publications: New York, 1952.

32 Goos, F.; Hänchen,H. *Ann.Physik* **1943**, 43, 383.

33 Tien, P.K. *App.Opt.* **1971**, 10, 2395.

34 Swalen, J.D.; Tacke, M.; Santo,R.; Rieckhoff,K.E.; Fisher,J. *Hel.Chem.Acta.* **1978**, 61, 960.

35 Kogelnick, H. In "Integrated Optics", 2nd ed.; Tamir,T., Ed.; Springer-Verlag:Berlin, 1979; Vol.7, Chapter 2.

36 Haliday, D.; Resnick,R. "Physics"; John Wiley: New York, 1978.

37 Lee,D., In "Electromagnetic Principles of Integrated Optics", John Wiley:New York, 1986; Chapter 5.

38 Harrick, N.J. "Internal Reflection Spectroscopy"; John Wiley:New York, 1979.

39 Hansen, W. *Spec.Chim.Acta.* **1965**, 21, 815-833.

40 Tamir,T. In "Integrated Optics" 2nd ed.; Tamir,T. Ed., Springer Verlag:Berlin, 1979; Vol.7, Chapter 3.

41 Tien,P.K.; Ulrich,R.; Martin,R.J. *Appl.Phys.Lett.* **1969**, 14, 291.

42 Harris,J.H.; Shubert,R.; *IEEE Trans. MMT.* **1968**, 16, 1048.

43 Lee,D., In "Electromagnetic Principles of Integrated Optics", John Wiley: New York, 1986; Chapter 6.

44 Zernike, F. In "Integrated Optics" 2nd ed.; Tamir,T. Ed., Springer Verlag:Berlin, 1979; Vol.7, Chapter 5.

45 Harris,J.H.; Schubert,R.; Polky,J.N. *J.Opt.Soc.Am.* **1970**, 60, 1007.

46 Ulrich,R.; Weber, H.P. *App.Opt.* **1972**, 11, 428-433.

47 Polystyrene, Catalog # 18,242-7 Aldrich Chemical Co. Milwaukee, Wisconsin, 53233.

48 Strictly qualitative test to determine relative strength of adhesion.

49 Shipley Company Inc., 1457 MacArthur Rd., Newton, Mass., 02162, MicroPosit products, Sept.1983.

50 The spin coater was designed and built with the help of Glen Wollenburg.

51 7 Micro Laboratory Cleaner, International Products Corp., P.O. Box 118, Trenton N.J.,08601-0118.

52 Giallorenzi, T.G.; West, E.J.; Kirk, R.; Ginther, R.; Andrews, R.A. *App.Opt.* **1973**, 12, 1240-1245.

53 Chartier,G. In "Integrated Optics Physics and Applications"; Martellucci, S.; Chester, A.N.,Eds.; Plenum Press: New York, 1983; Chapter 3.

54 Findakly, T. *Opt.Eng.* **1985**, 24, 244-250.

55 Doremus, R.H. *J.Phys.Chem.* **1964**, 68, 2212-2218.

56 Stewart, G.; Millar, P.J.R.; Laybourn, C.D.; Wilkinson, C.D.W.; DeLaRue, R.M. *IEEE J.Quant.Elec.* **1977**, QE-13, 192-200.

57 Kaufmann Glass Co., 1301 Northeast Blvd., Wilmington De., 19899.

58 Coutaz, J.L.; Jaussaud, P.C. *App.Opt.* **1982**, 21, 1063-1065.

59 Coutaz, J.L.; Jaussaud,P.C.; Chartier, G.H. *App.Opt.* **1982**, 21, 1066-1068.

60 Zsigmondy, R. *Dingler Polytechnisches J.*, **1897**, 306, 91.

61 United Detector Technology, 12525 Chadron Ave., Hawthorne, Ca., 90250.

62 Optics for Research, Box 82, Caldwell, N.J.,07006, Model RA-½-632.8.

63 Hecht, E.; Zajac, A.; "Optics"; Addison-Wesley:Reading, Mass., 1979; pg. 248.

64 Rofin Limited, Winslade House, Egham Hill, Surrey England.

65 Ulrich,R.; Torge,R. *App.Opt.* **1973**, 12, 2901-2908.

66 Precomp, Inc. 17 Barstow Road, Great Neck, New York 11021.

67 Precision Optical,Inc. 869 W. 17th Street, Costa Mesa,Ca.

68 Edmund Scientific Co. Edison N.J. Catalog part # 30143.

69 Schott Optical Glass Inc., 400 York Avenue, Duryea, Penn. 18642, Catalog 3111.

70 Mitchell, G.L. *App. Opt.* **1980**, 19, A114.

71 Buehler, 41 Waukegan Rd.,Lake Bluff, Illinois, 60044.

72 Jenkins,F.; White,H.; "Fundamentals of Optics", 4th ed.; McGraw-Hill:New York, 1976; pg. 30-31.

73 Conder,W.S.; Ph.D. Dissertation, Virginia Polytechnic University and State Institute, Blacksburg, Va., 1985.

74 United Detector Technology, 12525 Chadron Ave., Hawthorne, Ca., 90250, Technical Brochure "Planar-Diffused Silicon Photodiodes".

75 O'Haver, T.C. *J.Chem.Ed.* **1972**, 49, A131-134.

76 Burgess, L.W.; Ph.D. Dissertation, Virginia Polytechnic University and State Institute, Blacksburg, Va.,1984.

77 Benchmark Technical Sales, P.O. Box 756, Lewes, Delaware 19958.

78 Carr, P.W.; Bowers,L.D. "Immobilized Enzymes in Analytical and Clinical Chemistry"; John Wiley: New York; 1978.

79 Dow Corning, Midland, Michigan.

80 Weber, F.; M.S. Thesis, Virginia PolyTechnic University and State Institute, Blacksburg, Va., 1985.

81 Burden, R.L.; Faires, J.D.; Reynolds, A.C. "Numerical Analysis"; 2nd ed.; Prindle, Weber and Schmidt: Boston, Mass., 1981; Chapter 2.

82 Stewart, G.; Laybourn, P.J.R. *IEEE J.Quantum Electron.* **1978**, QE-13, 930-934.

83 Ruzicka, J.; Hansen, E.H. *Anal.Chim.Acta.* **1980**, 114, 19-44.

84 Smith, W.F. *Tetrahedron* **1964**, 20, 671.

85 Berthelot, M.P. *Repert. Chim. Appl.* **1859**, 1, 284.

86 Bolleter, W.T.; Bushman, C.J.; Tidwell, P.W. *Anal. Chem.* **1961**, 33, 592.

87 Chapin, R.M. *J. Am. Chem. Soc.* **1929**, 51, 2112.

88 Patton, C.J.; Crouch, S.R. *Anal. Chem. 1977, 49, 464-469.*

89 Crowther, A.B.; Large, R.S. *Analyst* **1956**, 81, 64-65.

90 Russell, J.A. *J. Biol. Chem.* **1944**, 156, 457-461.

91 Soloway, S.; Santoro, A. *Anal. Chem.* **1955**, 27, 798.

92 Lubochinsky, B.; Zalta, J.P. *Bull. Soc. Chim. Biol.* **1954**, 36, 1363-1366.

93 Weichselbaum, T.E.; Hagerty, J.C.; Mark, H.B. *Anal. Chem.* **1969**, 41, 848-850.

94 Corbett, J.F. *J. Chem. Soc.(B)* **1970**, 1502-1509.

95 Ngo, T.T.; Yam, C.F. Anal. Lettr. 1984, 17(A15), 1771-1782.

96 "Standard Methods for Examination of Water and Wastewater", 15th ed. American Public Health Association:Washington D.C., 1980, pg. 351-361.

97 Sawyer, R.; Grissley, L. In " Technicon Symposia-Automation in Analytical Chemistry", Vol 1., Mediad. Inc.:New York, pg. 347-350.

98 Harwood, J.E.; Huyser, D.J. *Water Res.* **1970**, 4, 501-515.

99 Chaney, A.L.; Marbach, E.P. *Clin. Chem.* **1962**, 8, 130-132.

100 Mann, L.T. *Anal. Chem.* **1963**, 35, 2179-2182.

101 Kratos model SFA-201 8 microliter flow cell.

102 Weatherburn, M.W. *Anal. Chem.* **1967**, 39, 971-974.

103 Searcy, R.L.; Simms, N.M.; Foreman, J.A.; Bergquist, L.M. *Clin. Chim. Acta.* **1965**, 12, 170.

104 Swinehart, J.H.; Rock, P.A. *Inorg. Chim.* **1966**, 5, 573.

105 Swinehart, J.H.; *Coord. Chem. Rev.* **1967**, 2, 385-402.

106 Scheiner, D. *Water Res.* **1976**, 10, 31-36.

107 Stewart, B.M. *Water Res.* **1985**, 19, 1443-1445.

108 Bruce, J., Malcolm In" Rodd's Chemistry of Carbon Compounds" 2nd ed.; Coffey,S., Ed.; American Elsevier: New York, 1974; Vol.III, Chapter 8, pg. 133.

109 Ruzicka, J.; Hansen, E.H. "Flow Injection Analysis"; John Wiley & Sons: New York, 1981; p 16-17.

110 Plueddemann, E. In "Silane Coupling Agents" Plueddeman, E. Ed.; Plenum Press:New York, 1982; Chapter 3.

111 Long, G.L.; Winefordner, J.D. *Anal.Chem.* 1983, 55, 712-724A.

112 Kodak 3487, Indophenol Salt. Eastman Kodak, Rochester N.Y. 14650.

113 Clay Adams, Gold Seal. Fisher Scientific Co., Pittsburgh, Pa. 15219.

114 Sundaram, P.V.; Hornby,W.E. *FEBS Letters* **1970**, 10, 325.

115 Atlantic Plumbing Supply Roanoke, Va. USA.

116 Henry, R. In "Clinical Chemistry Principles and Techniques"; Cannon, J.; Winkelman,W.,EDs.; Harper Row: Hagerstown, Md., 2nd Ed., 1974.

117 Hornby, W.E.; Inman,D.J. *Biochem J.* **1972**, 129, 255-262.

118 Morrison, R.T.; Boyd, R.N. "Organic Chemistry", 3rd ed.; Allyn and Bacon Inc.: Boston; 1973.

119 Ngo,T.T.; Phan, A.P.H.; Yam, C.F.; Lenhoff,H.M. *Anal. Chem.* **1982**, 54, 46.

120 Moore, J.W.; Pearson, R.G. "Kinetics and Mechanism", 3rd ed.; John Wiley:New York, 1981.

121 Carr,P.W.; Bowers,L.D. "Immobilized Enzymes in Analytical and Clinical Chemistry Fundamentals and Applications",v.56, John Wiley: New York, 1980.

122 Lineweaver, H.; Burke, D. *J.Am.Chem.Soc.* **1934**, 56, 658.

123 Sundaram, P.V.; Igloi, M.P.; Wassermann, R.; Hinsch, W.; Knoke, K.J. *Clin. Chem.* **1978**, 24, 234.

124 Onyezili, F.N.; Onitiri, A.C. *Biochim. Biophy. Acta* **1981**, 659, 244.

125 Gedeon, A. *Opt.Comm.*,**1974**, 12, 329-332.

126 Private communictation with Jim Petersen.

127 Seifert, M.; Tienfenthaler, K.; Hewberger, K.; Lukosz, W.; Mosbach,K. *Anal. Lett.* **1986**, 19, 205-216.

128 Tiefenthaler, K.; Briquet, V.; Buser, E.; Horisberger, M.; Lukosz, W. *SPIE*, **1984**, 514, 215.

129 Goell, J.E.; Standley, R.D.; *Bell Sys. Tech. J.*, **1969**, 48, 3445-3448.

130 Baak, T. *Appl.Opt.* **1982**, 21, 1069.

131 Liquicoat. E.M.Merck, Darnstadt, W.Germany.

132 Lukosz,W.; Tienfenthaler,K. *Opt.Lett.*, **1983**, 8, 537-539.

133 Private communication, Dr. Thomas Ward.

IX. APPENDIX 1. Software Appendix.

Single Channel Interrupt Driven Data Acquisition Routine

Glossary

Take.Data

Requires the number of points, the address of the data buffer, and the data acquisition rate, on the stack. This word starts the interrupt driven terminal task to acquire data from a single analog to digital channel.

Start.Clk

Requires the clock rate on the stack. Initializes and starts the real time clock.

T

Requires the number of points to acquire on the stack. Acquires data at 10 Hz.

GO

Requires the number of points to acquire on the stack. Acquires data at 1 Hz.

.1HZ , 1HZ, 10HZ, 100HZ, 1KHZ, 10KHZ, EXTERNAL

Clock rates for the real time clock.

```
220 Block

0 ( Single Channel Terminal Task Data Acq.)    BASE @ OCTAL
1 176770  CONSTANT CSRADC      170000  CONSTANT CLKCSR
2 176772  CONSTANT ADCBUF      VARIABLE DATUM    10000 ALLOT
3 VARIABLE CLOCK               VARIABLE SPEED
4.0 CLOCK !          DATUM 10000 ERASE
5 (Interrupt routine starts, tests and stores data at the
6  rate of SPEED.  Trigger A/D with external source. )
7
8 ASSEMBLER  BEGIN    R -) U  MOV    U CLOCK  MOV
9    CSRADC 400 #  MOV                          (enble a/d)
10   BEGIN CSRADC    TST B 0<  END    PTR U) )  ADCBUF  MOV
11          PTR U) 2 #  ADD    CNT U)  DEC  0= IF  CLKCSR CLR
12          U )  WAKE #  MOV    THEN  U  R )+    MOV
13          CSRADC  0 #  MOV B           200 200 INTERRUPT
14 BASE !
15



221 BLOCK
0 ( Data acquisition - Terminal task )    BASE @ OCTAL
1
2   : .1HZ  107;    : 1HZ  106;    :10HZ  105;    : 100HZ;
3   : 1KHZ  103;    : 10KHZ  102;    : EXTERNAL  101;
4
5  : START.CLK ( speed -- )    CLKCSR !  ;
6
7  : TAKE.DATA ( #pnts,addr,speed--)  CLOCK GET
8         SPEED !    PTR !    CNT !    SPEED @    START.CLK
9         STOP       CLOCK RELEASE  ;
10
11 ( To start run #pnts, addr, speed TAKE.DATA )
12
13  : T (#pnts )  2000 MS    7 EMIT  DATUM  10HZ  TAKE.DATA ;
14  : GO (#pnts ) 2000 MS    7 EMIT  DATUM  1HZ  TAKE.DATA ;
15  BASE !
```

Non-Terminal Task Scope Display Routines

Glossary

SCOPE-TASK

Word to define scope task.

1SCAN

Requires the data address, and the number of points to display on the stack. Takes the data array(s) and outputs them to the digital to analog converter

SCOPE

Requires the address and number of points to display on the stack. Activates the scope task and begins displaying the data on the oscilloscope.

SUSPEND

Suspends the scope task.

```
274 BLOCK
0 ( Scope Display Non-terminal task )    BASE @ OCTAL
1 176760 CONSTANT 0DAC   176762 CONSTANT 1DAC
2 VARIABLE  DATA-ADDR          VARIABLE #POINTS
3  : SCOPE-TASK   TASK ;       <CONSIGN>   SCOPE-TASK
4
5  CODE 1SCAN  ( addr, cnt --)   1 S )+  MOV   0  S )+  MOV
6    2  CLR   0DAC  CLR   1DAC  CLR
7    BEGIN    0DAC 0 )+  MOV   1 SOB  0DAC  CLR    NEXT
8
9
10  : SCOPE ( addr, cnt --)
11        #POINTS !   DATA-ADDR  !   SCOPE-TASK   ACTIVATE
12             BEGIN  DATA-ADDR @   #POINTS @  1SCAN  60 MS
13             0  END ;
14  : SUSPEND ( TASK --)  ACTIVATE STOP ;
15  BASE !



275 BLOCK
0 ( Dual channel scope display task )   BASE @ OCTAL
1 176760 CONSTANT 0DAC   176762 CONSTANT 1DAC
2 VARIABLE  0DATA   VARIABLE 1DATA    VARIABLE #POINTS
3  : SCOPE-TASK   TASK ;       <CONSIGN>   SCOPE-TASK
4
5  CODE 1SCAN  ( addr1,addr2, cnt --)
6    2  S )+  MOV   1  S )+  MOV  0  S )+  MOV   0DAC  CLR
7    1DAC CLR   BEGIN   0DAC 0 )+  MOV   1DAC  1 )+  MOV
8    2  SOB   1DAC CLR   0DAC CLR   NEXT
9
10 : SCOPE (addr1,addr2,cnt--)
11        #POINTS !  1DATA !  0DATA !  SCOPE-TASK  ACTIVATE
12        BEGIN  0DATA @  1DATA @   #POINTS @  1SCAN  60 MS
13        0  END ;
14 : SUSPEND ( TASK---)  ACTIVATE STOP ;
15 BASE !
```

RETICON DIODE ARRAY ACQUISITION ROUTINES

ACQUIRE

Requires the data buffer address and #points to acquire on the stack. This routine acquires data from the reticon diode array. The first data point is synchronized with the REQ A signal from the parallel port.

GO

Begins acquiring data continuously from the reticon array. Use ESCAPE to terminate this program.

```
240 BLOCK
0 ( Reticon Diode Array Acquisition Routines ) BASE @ OCTAL
1  167770 CONSTANT  P_CSR   176770  CONSTANT  CSRADC
2  176772 CONSTANT   CSRADC   CREATE TEMP  1000 ALLOT
3  TEMP 1000 ERASE
4
5 CODE ACQUIRE ( addr, #pnts)  0 S )+  MOV      ( ctr to RO)
6     1 S )+  MOV   CSRADC 402 #  MOV
7     BEGIN  P_CSR  TST   0<  END
8     BEGIN  BEGIN  CSRADC  TST B  0< END
9            1 )+  BUFADC  MOV    0  DEC  0=  END
10    BUFADC  0 # MOV  NEXT
11
12 BASE !
13
14 : GO  BEGIN TEMP  256 ACQUIRE  10 MS ESCAPE 0 END ;
15
```

REPORT GENERATOR

AVERAGE

Requires the data buffer address and the number of points on the stack. This routine finds the average of a data array, prints the results and stores the average in the floating variable DATA_AVERAGE.

MINIMUM

Requires the data buffer address and number of points on the stack. This routine finds the minimum in an array of numbers, prints the value and stores the result in 1TEMP.

SUM.OF.SQUARES

This routine squares the individual points of an array and then calculates the sum of the squares. The result is stored in SQUARES.

STD.DEV

Requires the address of the data array and the number of points. This routine calculates the standard deviation of a data array, prints the results and stores the value in the floating variable SIGMA.

REPORT

This routine generates a report for the indicated data blocks. It calculates the standard deviation of the baseline, the peak height and absorbance for the input FIA peak data. This routine has the capability of filtering the data before determining the absorbance values with a variable width Savitsky Golay digital filter.

FILTER_WIDTH

Requires the filter width, 9,13,or 19 on the stack. This routine stores the appropriate address in the vectored variable 'SAVITSKY.

SAVITSKY

Requires the address of the data array and the number of points on the stack. This routine filters the input data array with a variable width Savitsky Golay digital filter. The results are stored in the floating array FD.ARRAY.

```
205 BLOCK
0 ( Average routines)
1
2 VARIABLE #PNTS                          0 #PNTS !
3 VARIABLE DATA_ARRAY_ADDR                0 DATA_ARRAY_ADDR !
4 2VARIABLE SUM.OF.X                      0.0 E 0 SUM.OF.X F!
5 2VARIABLE DATA_AVERAGE                  0.0 E 0 DATA_AVERAGE F!
6
7  : AVERAGE ( addr, #pnts--)  #PNTS !  DATA_ARRAY_ADDR !
8    #PNTS @ 0 DO  DATA_ARRAY_ADDR @ I 2* + @  ( get addr)
9    0 FLOAT  SUM.OF.X  F@  F+  SUM.OF.X  F!  ( add to temp)
10     LOOP    SUM.OF.X  F@  #PNTS @ 0  FLOAT  F/
11             DATA_AVERAGE  F!   ." The Average is."
12             DATA_AVERAGE  F@  F.  CR  ;
13
14 : CLEAR.ALL  0.0 E 0  SUM.OF.X  F!   0.0 E 0
15    DATA_AVERAGE F!  0  #PNTS !  ;



206 BLOCK
0  ( Routines to find minimum of array)
1       VARIABLE 1TEMP   32767  1TEMP !   2VARIABLE  SIGMA  0.0 E 0 SIGMA !
2       2VARIABLE MEAN   0.0 E 0 MEAN !   2VARIABLE SQUARES 0.0 E 0 SQUARES !
3
4  : RESTORE  32767 1TEMP ! ;
5
6  : MINIMUM ( data addr, #pnts)  #PNTS !  DATA_ARRAY_ADDR !
7               #PNTS @ 0   DO   DATA_ARRAY_ADDR @  I 2* + @ 1TEMP @ MIN
8                                1TEMP ! LOOP
9               ." The minimum value of the array is " 1TEMP @ . RESTORE ;
10
11  : SUM.OF.SQUARES ( --result)
12              #PNTS @ 0  DO   DATA.ARRAY.ADDR @ I 2* + @  0 FLOAT 2DUP   F*
13                                      SQUARES  F@  F+  SQUARES  F!
14                               LOOP ;
15
```

```
207 BLOCK
0 (Standard deviation calc. contd)
1
2  : (STD.DEV)  ( -- result)
3               ( Calculate n*mean^2)  #PNTS @ 0 FLOAT  DATA_AVERAGE F@ 2DUP F* F*
4
5               (Calculate 2meanx)  DATA_AVERAGE F@  2E0  F* SUM.OF.X  F@  F*  F- SQUARES  F@  F+
6               #PNTS @  0 FLOAT  1E0  F-  F/  SQRT  SIGMA  F!  ;
7
8  : STD.DEV ( data addr, #pnts)  CR  AVERAGE  SUM.OF.SQUARES  (STD.DEV)
9                       ." The Standard Deviation is " SIGMA F@ E.  ;
10
11  : CLEAR.ALL  0.0 E 0 SQUARES  F!  CLEAR.ALL ;
12
13
14
15


208 BLOCK
0 ( Report generator)
1       VARIABLE  START                 VARIABLE  #BLK/SMP                VARIABLE  #SAMPLES
2       VARIABLE  #AVG                  VARIABLE  ?FILTER          VARIABLE #PTS/SEC
3       VARIABLE  PEAK_LOCATION
4  : REPORT  CR  CR
5       ." Number of samples to analyze ? "       ASK  #SAMPLES !  CR
6       ." Number of data blocks per sample? "    ASK  #BLK/SMP !  CR
7       ." Starting data block ? "                ASK  START !     CR
8       ." Number of points to average for the baseline ?"  ASK #AVG !  CR
9       ." Do you wish to filter the data (1 = yes, 0 = no)?" ASK DUP FILTER? !
10              IF CR. ." Input filter width"  ASK  FILTER_WIDTH   ELSE  THEN CR
11
12      ." Number of points acquired/sec?"        ASK  #PTS/SEC !  CR
13      ." Peak location in seconds?"             ASK  PEAK_LOCATION !  CR
14
15                                                                    [ -->
```

```
209 BLOCK
0 ( Report generator cont'd)
1 ]
2       #PTS/SEC @  PEAK_LOCATION @ * 2*  PEAK_LOCATION !
3       #SAMPLES @ #BLK/SMP @ *  START @  + START @  DO
4               CR CR ." BLOCK #"  I .
5               #BLK/SMP @ 0 DO                    ( move data to pad)
6                                       J I +  BLOCK PAD 80 + 1024 I * 1024 MOVE
7                                       LOOP
8               ?FILTER @
9       IF  PAD 80 + #BLK/SMP @  512 *  SAVITSKY    ( filter data)
10         FD.ARRAY  PAD 80 + #BLK/SMP @ 512 * MOVE ( move to pad)
11      THEN PAD 98 +  #AVG @ STD.DEV                                          ( find baseline)
12         CLEAR.ALL   CR   ." Peak height "
13         PAD 70 +  PEAK_LOCATION @ + 10 AVERAGE   ( find peak ht)
14         CLEAR.ALL   #BLK/SMP @   +LOOP
15         CR  ." END OF DATA" ;


214 BLOCK
0 (SAVITSKY GOLAY FILTER ROUTINES )
1       VARIABLE FD.ARRAY  2048 ALLOT    FD.ARRAY  2048 ERASE
2       VARIABLE  RAWDATA    VARIABLE 'SAVITSKY    (  9 - 19 pt routines)
3  215 LOAD  216 LOAD  217 LOAD
4
5  : FILTER_WIDTH  ( # of data pts in window)
6               DUP   9 - 0= IF ['']    9.POINT  'SAVITSKY !
7       ELSE DUP  13 - 0= IF ['']   13.POINT  'SAVITSKY !
8       ELSE DUP  19 - 0= IF ['']   19.POINT  'SAVITSKY !
9       ELSE DUP  1 ABORT" not a valid filter width "
10      THEN THEN THEN  ;
11
12  : SAVITSKY    'SAVITSKY @ EXECUTE ;
13
14
15
```

```
215 BLOCK
0 ( SAVITSKY GOLAY)
1  : 9.POINT  ( rawdata, #pnts --)  SWAP  RAWDATA !
2       5 - 4 DO
3                       RAWDATA @  I  2* + @ 59 M*                ( pt 5 )
4                       RAWDATA @  I 4 - 2*  +  -21 M*            ( pt 1 )
5                       RAWDATA @  I 3 - 2*  +   14 M*            ( PT 2 )
6                       RAWDATA @  I 2 - 2*  +   39 M*            ( PT 3 )
7                       RAWDATA @  I 1 - 2*  +   54 M*            ( PT 4 )
8                       RAWDATA @  I 1 + 2*  +   54 M*            ( PT 6 )
9                       RAWDATA @  I 2 + 2*  +   39 M*            ( PT 7 )
10                      RAWDATA @  I 3 + 2*  +   14 M*            ( PT 8 )
11                      RAWDATA @  I 4 + 2*  +  -21 M*            ( PT 9 )
12                      D+ D+ D+ D+ D+ D+ D+ D+ 231 M/
13                        FD.ARRAY  I 2*  +  !
14              LOOP ;
15


216 BLOCK
0 ( 13.POINT SAVITSKY GOLAY FILTER )
1  : 13.POINT   ( rawdata, #pnts )  SWAP   RAWDATA !
2  7 - 6 DO   RAWDATA @ I  2* + @  25  M*                ( PT 7 )
3                RAWDATA @  I 6 - 2*  +  @  -11  M* D+          ( PT 1 )
4                RAWDATA @  I 5 - 2*  +  @    0  M* D+          ( PT 2 )
5                RAWDATA @  I 4 - 2*  +  @    9  M* D+          ( PT 3 )
6                RAWDATA @  I 3 - 2*  +  @   16  M* D+          ( PT 4 )
7                RAWDATA @  I 2 - 2*  +  @   21  M* D+          ( PT 5 )
8                RAWDATA @  I 1 - 2*  +  @   24  M* D+          ( PT 6 )
9                RAWDATA @  I 1 + 2*  +  @   24  M* D+          ( PT 8 )
10               RAWDATA @  I 2 + 2*  +  @   21  M* D+          ( PT 9 )
11               RAWDATA @  I 3 + 2*  +  @   16  M* D+          ( PT 10 )
12               RAWDATA @  I 4 + 2*  +  @    9  M* D+          ( PT 11 )
13               RAWDATA @  I 5 + 2*  +  @    0  M* D+          ( PT 12 )
14               RAWDATA @  I 6 + 2*  +  @  -11  M* D+          ( PT 13 )
15               143 M/   FD.ARRAY I 2*  +  !  LOOP ;
```

```
217 BLOCK
0 ( 19.POINT SAVITSKY FILTER )
1
2  : 19.POINT ( rawdata, #pnts )  SWAP  RAWDATA !
3     10 - 9  DO
4                RAWDATA @ I         2* + @ 269     M*
5                RAWDATA @ I   9 -  2* + @ -136    M*  D+
6                RAWDATA @ I   8 -  2* + @  -51    M*  D+
7                RAWDATA @ I   7 -  2* + @   24    M*  D+
8                RAWDATA @ I   6 -  2* + @   89    M*  D+
9                RAWDATA @ I   5 -  2* + @  144    M*  D+
10               RAWDATA @ I   4 -  2* + @  189    M*  D+
11               RAWDATA @ I   3 -  2* + @  224    M*  D+
12               RAWDATA @ I   2 -  2* + @  249    M*  D+
13               RAWDATA @ I   1 -  2* + @  264    M*  D+
14               RAWDATA @ I   1 +  2* + @  264    M*  D+
15                                                [ -->
```

```
218 BLOCK
0 (19.POINT CONT'D )
1]
2                RAWDATA @ I   2 +  2* + @  249    M*  D+
3                RAWDATA @ I   3 +  2* + @  224    M*  D+
4                RAWDATA @ I   4 +  2* + @  189    M*  D+
5                RAWDATA @ I   5 +  2* + @  144    M*  D+
6                RAWDATA @ I   6 +  2* + @   89    M*  D+
7                RAWDATA @ I   7 +  2* + @   24    M*  D+
8                RAWDATA @ I   8 +  2* + @  -51    M*  D+
9                RAWDATA @ I   9 +  2* + @ -136    M*  D+
10               2261  M/ FD.ARRAY I 1 -  2* + !
11               LOOP ;
12
13
14
15
```

```
C
C       WAVEGUIDE ANALYSIS PROGRAM USING SECANT ANALYSIS
C         follows Rabolt's treatment
C
C
        REAL INDEX(3),K1(3),K2(3),INDEXA,INDEXB
        INTEGER POLARIZATION
        REAL NPRISM,K,NEWINDEX,GAMMA
C
C
C*************** INPUT VARIABLES ******************************
C
C
C
        PI       = 3.14159
C
        GAMMA = 1.00
        INDEX(2)=1.5100
C
        TYPE 10
10      FORMAT(1X,' ENTER THE PRISM INDEX ',$)
        ACCEPT 11,NPRISM
11      FORMAT(F6.4)
        TYPE 20
20      FORMAT(1X,' ENTER THE ACUTEANGLE OF THE PRISM ',$)
        ACCEPT 21,ACUTEANG
21      FORMAT(F4.1)
        TYPE 30
30      FORMAT(1X,' ENTER THE SUBSTRATE INDEX ',$)
        ACCEPT 31,INDEX(3)
31      FORMAT(F6.4)
        TYPE 40
40      FORMAT(1X,' ENTER THE CLADDING INDEX ',$)
        ACCEPT 41,INDEX(1)
41      FORMAT(F6.4)
        TYPE 50
50      FORMAT(1X,' ENTER INITIAL GUESS FOR FILM INDEX, LOWER BOUND ',$)
        ACCEPT 51,INDEXA
51      FORMAT(F6.4)
        TYPE 60
60      FORMAT(1X,' ENTER INITIAL GUESS FOR FILM INDEX,UPPER BOUND ',$)
        ACCEPT 61,INDEXB
61      FORMAT(F6.4)
C
        TYPE 100
100     FORMAT ( ' INPUT MODE NUMBER AND COUPLING ANGLE ',$)
C
C
        ACCEPT 150,M1,EXANG1
150     FORMAT ( I1,1X,F6.3 )
        TYPE 175 , M1, EXANG1
175     FORMAT(1X, I1,1X,F6.3 )
C
C
C
C
        TYPE 200
```

```
200     FORMAT( ' INPUT SECOND MODE NUMBER AND COUPLING ANGLE ',$ )
C
        ACCEPT 250,M2,EXANG2
250     FORMAT ( I1,1X,F6.3)
C
C
C
        TYPE 300
300     FORMAT(' LASER WAVELENGTH IN NANOMETERS ? ')
C
        ACCEPT 305 , WAVELENGTH
305     FORMAT ( F7.2 )
C
        TYPE 310
310     FORMAT ( ' TE OR TM POLARIZATION enter 0 OR 1 ?' )
C
C
        ACCEPT 315 , POLARIZATION
315     FORMAT (  I2 )
C
C ************** INITIALIZE VARIABLES *********************
C
C
        TYPE 400 ,M1,M2,EXANG1,EXANG2,WAVELENGTH
400     FORMAT (1X, I1,1X,I1,1X,F6.2,1X,F6.2,1X,F7.2 )
C
C
C
        K = 2.00 * PI/(WAVELENGTH * 1.0E-9)
C
C ***************** CONVERT ANGLES TO RADIANS ***************
C
        EXANG1 = EXANG1 * PI/180.0
        EXANG2 = EXANG2 * PI/180.0
        ACUTEANG = ACUTEANG * PI/180.0
C
C
C ***************** CALCULATE BETA FOR EACH MODE **************
C
C
        TEMP = K * NPRISM
        TEMP1 = COS( ACUTEANG + EXANG1)/NPRISM
        TEMP2 = COS( ACUTEANG + EXANG2)/NPRISM
C
        BETA1 = TEMP * SIN( ACUTEANG + ASIN(TEMP1) )
        BETA2 = TEMP * SIN( ACUTEANG + ASIN(TEMP2) )
C
        X1 = BETA1/K
        X2 = BETA2/K
        TYPE 426,X1,X2
426     FORMAT(1X,'BETA1/K=',F5.3,1X,'BETA2/K=',F5.3)
C
        IF ((BETA1/K .GT. INDEXA ).AND.(BETA1/K .LT.INDEXB)) GO TO 449
        TYPE 430
430     FORMAT(1X,' Beta out of range , input is incorrect ')
C
C
C ***************** CALCULATE K NUMBERS ************************
C
```

```
C
449     IF ( POLARIZATION .EQ. 0 ) GAMMA = 1.00
        IF ( POLARIZATION .EQ. 1 ) GAMMA = 1.51**2
        TYPE 435, GAMMA
435     FORMAT( ' GAMMA IS ',F5.2 )

C
        DO 450 I = 1,3
C
        K1(I) = SQRT( ABS(BETA1**2 - (INDEX(I) * K)**2))/GAMMA
        K2(I) = SQRT( ABS(BETA2**2 - (INDEX(I) * K)**2))/GAMMA
C
450     CONTINUE
C
C
C ****************** CALCULATE THICKNESS OF THE FILM ***************
C                     AND INDEX USING THE SECANT METHOD
C A*********************************************************************
C
        J = 2
        N0 = 20
CA
C

        X01 = SQRT(ABS( BETA1**2 - (INDEXA*K)**2))
        X02 = SQRT(ABS( BETA2**2 - (INDEXA*K)**2))
        X11 = SQRT(ABS( BETA1**2 - (INDEXB*K)**2))
        X12 = SQRT(ABS( BETA2**2 - (INDEXB*K)**2))
C
C
C ***************** CALCULATE F(X0_) AND F(X1_) *****************
C
C
        Y0  = (1/X01)*(M1*PI + ATAN(K1(1)/X01) + ATAN(K1(3)/X01) )
C
        Y0  = Y0 - (1/X02)*(M2*PI +ATAN(K2(1)/X02) +ATAN(K2(3)/X02))
C
        Y1  = (1/X11)*(M1*PI +ATAN(K1(1)/X11) + ATAN(K1(3)/X11))
C
        Y1  = Y1 - (1/X12)*(M2*PI + ATAN(K2(1)/X12) + ATAN(K2(3)/X12))
C
C
C
600     NEWINDEX = INDEXB - Y1*(INDEXB-INDEXA)/(Y1-Y0)
C
C
        IF( ABS( NEWINDEX - INDEXB).LT. 1.0E-5) GO TO 2000
C
C
C******************** UPDATE VALUES OF X0,X1,Y0,Y1 ******************
C
C
        INDEXA = INDEXB
        Y0     = Y1
        INDEXB = NEWINDEX
        IF ( POLARIZATION  .EQ. 1 ) GAMMA  = NEWINDEX **2
C
C ******************* CALCULATE F(NEWINDEX) FOR Y1 ******************
C
```

```
C
        T1 = SQRT( ABS ( BETA1**2 - (NEWINDEX * K)**2) )/GAMMA
        T2 = SQRT( ABS ( BETA2**2 - (NEWINDEX * K)**2) )/GAMMA
C
C
        T3 = (1/T1)*(M1*PI + ATAN(K1(1)/T1) + ATAN(K1(3)/T1) )
C
        Y1 = T3 - (1/T2)*(M2*PI + ATAN(K2(1)/T2) + ATAN(K2(3)/T2) )
C
        TYPE  650,NEWINDEX,T3
650     FORMAT(1X,F7.4,3X,E12.4)
C
C
        J = J + 1
        IF (J - N0) 600,600,3000
C
2000    TYPE 2010,NEWINDEX
2010    FORMAT( ' THE INDEX OF THE FILM = ',1X,F7.5)
C
C ***** CALCULATE THE NEW VALUE OF THE THICKNESS *****
C
        T1 = SQRT(ABS(BETA1**2 - (NEWINDEX * K)**2))
        T2 = SQRT(ABS(BETA2**2 - (NEWINDEX * K)**2))
        T3 = (1/T1)*(M1*PI + ATAN(K1(1)/T1) + ATAN(K1(3)/T1))
        T4 = (1/T2)*(M2*PI + ATAN(K2(1)/T2) + ATAN(K2(3)/T2))
C
        TYPE 2020,T3,T4
2020    FORMAT( 1X,' THE THICKNESS OF THE FILM =',1X,E12.4,2X,E12.4 )
C
C
        STOP
3000    TYPE 3010
3010    FORMAT( ' TOO MANY ITERATIONS ')
        END
C
C
C ********************************************************************

C       FUNCTION ASIN
C ********************************************************************
        FUNCTION ASIN(A)
        ASIN = ATAN(A/SQRT(1-A**2))
        RETURN
        END
```

```
C
        T1 = SQRT( ABS ( BETA1**2 - (NEWINDEX * K)**2) )/GAMMA
        T2 = SQRT( ABS ( BETA2**2 - (NEWINDEX * K)**2) )/GAMMA
C
C
        T3 = (1/T1)*(M1*PI + ATAN(K1(1)/T1) + ATAN(K1(3)/T1) )
C
        Y1 = T3 - (1/T2)*(M2*PI + ATAN(K2(1)/T2) + ATAN(K2(3)/T2) )
C
        TYPE  650,NEWINDEX,T3
650     FORMAT(1X,F7.4,3X,E12.4)
C
C
        J = J + 1
        IF (J - N0) 600,600,3000
C
2000    TYPE 2010,NEWINDEX
2010    FORMAT( ' THE INDEX OF THE FILM = ',1X,F7.5)
C
C ***** CALCULATE THE NEW VALUE OF THE THICKNESS *****
C
        T1 = SQRT(ABS(BETA1**2 - (NEWINDEX * K)**2))
        T2 = SQRT(ABS(BETA2**2 - (NEWINDEX * K)**2))
        T3 = (1/T1)*(M1*PI + ATAN(K1(1)/T1) + ATAN(K1(3)/T1))
        T4 = (1/T2)*(M2*PI + ATAN(K2(1)/T2) + ATAN(K2(3)/T2))
C
        TYPE 2020,T3,T4
2020    FORMAT( 1X,' THE THICKNESS OF THE FILM =',1X,E12.4,2X,E12.4 )
C
C
        STOP
3000    TYPE 3010
3010    FORMAT( ' TOO MANY ITERATIONS ')
        END
C
C
C ***************************************************************

C       FUNCTION ASIN
C ***************************************************************
        FUNCTION ASIN(A)
        ASIN = ATAN(A/SQRT(1-A**2))
        RETURN
        END
```

```
C
C       CALCULATION OF OPTICAL FIELD INTENSITIES FOR A SINGLE FILM
C       ASYMMETRIC WAVEGUIDE .
C       Based on Bohn's analysis Anal. Chem. v57,#7,1985,p1203
C       Steve Choquette v2 October 1985
C       Normalization constant A.Yariv Fiber and Int. optics
C       pg 228.
C
        REAL WAVELENGTH,NFILM,NSUB,NAIR,NPRISM,THICKNESS
        REAL EXTANG(5)
        DOUBLE PRECISION OFI(5,70)
        DOUBLE PRECISION K,K1,K2,K3,B,B1,BETA
        DOUBLE PRECISION RTEMP,DENOM,NORML,NUMER,MU
        INTEGER T1,MODNUM(5),COUNTER
        DATA C/'C'/
        LOGICAL * 1 FNAME(11)
C
C
C ****** Fname is the name of the data disk output file. *****
C
        PI      = 3.14159
        COUNTER = 70
        MU      = 4.0 * PI * 1.0 E -7
C
C ***** mu ,the permeability of free space ,has units of *****
C       meters kg Coulombs-2
C
C ***** ACCEPT VARIABLES ***************
C
        TYPE 1
1       FORMAT(1X,' ENTER THE INDEX OF THE PRISM ',$)
        ACCEPT 2,NPRISM
2       FORMAT(F6.4)
        TYPE 10
10      FORMAT(1X,' ENTER THE ACUTE ANGLE OF THE PRISM ',$)
        ACCEPT 11,ACUTEANG
11      FORMAT(F4.1)
        TYPE 20
20      FORMAT(1X,' ENTER THE INDEX OF THE SUBSTRATE',$)
        ACCEPT 21,NSUB
21      FORMAT(F6.4)
        TYPE 30
30      FORMAT(1X,' ENTER THE INDEX OF THE CLADDING ',$)
        ACCEPT 31,NAIR
31      FORMAT(F6.4)
C
        TYPE 100
100     FORMAT(1X,' ENTER THE NUMBER OF MODE CALCULATIONS .',$)
C
        ACCEPT 150,NMODES
150     FORMAT(I1)
C
        DO 300 I=1,NMODES
C
                TYPE 200
200             FORMAT(1X,' INPUT MODE NUMBER AND COUPLING ANGLE ',$)
C
                ACCEPT 250,MODNUM(I),EXTANG(I)
250             FORMAT(I1,1X,F5.2)
```

```
      TYPE 255 , EXTANG(I)
255   FORMAT(1X,' ANGLE ',1X, F5.2 )
C
300   CONTINUE
C
      TYPE 400
400   FORMAT( ' LASER WAVELENGTH IN NANOMETERS ? ',$)
C
      ACCEPT 450,WAVELENGTH
450   FORMAT( F7.2)
C
      TYPE 500
500   FORMAT(1X,' ENTER FILM INDEX AND THICKNESS ',$)
C
      ACCEPT 550,NFILM,THICKNESS
550   FORMAT( F6.4,1X,E12.4)
C
      TYPE 551,NFILM,THICKNESS,WAVELENGTH
551   FORMAT ( 1X,F6.4,1X,E12.4,1X,F7.2)
      TYPE 552 ,  NPRISM,ACUTEANG,NAIR
552   FORMAT(1X,F6.4,1X,F4.1,1X,F6.4)
C
C
C
C ****** INITIALIZE ALL VARIABLES *****
C
C
      K = 2*PI/(WAVELENGTH * 1.0E-9)
C
C
C ****** CONVERT ANGLES TO RADIANS ****
C
      DO 600I = 1,NMODES
C
            EXTANG(I) = EXTANG(I)*PI/180.0
C
600   CONTINUE
C
      ACUTEANG = ACUTEANG*PI/180.0
C
C
C ****** CALCULATE OFI FOR EACH MODE *****
C
C
C
      DO 650 I = 1,COUNTER
C
            DEPTH(I) = -.5E-6 + (I-1)*.05E-6
C
650   CONTINUE
C
C
      DO 700 I = 1,NMODES
C
C     CALCULATE BETA
C
            B = K* NPRISM
            B1 = COS(ACUTEANG + EXTANG(I))/NPRISM
C
```

```
                BETA = B * SIN(ACUTEANG + ASIN(B1))
C
C  ***** If Beta is greater than nfilm, stop the calculation *****
C
      IF( (BETA / K) .GT.NFILM) GO TO  10000
C     CALCULATE K NUMBERS
C
                K1  =  SQRT( ABS(BETA**2 -(NAIR*K)**2))
                K2  =  SQRT( ABS(BETA**2 -(NFILM*K)**2))
                K3  =  SQRT( ABS(BETA**2 -(NSUB *K)**2))
C
C  ***** Calculate normalization factor *****
C
                DENOM = BETA*(THICKNESS + 1/K1 +1/K3)*(K2**2+K3**2)
                NUMER = K * 3.0 E 8 * MU
                NORML = 2*K2*SQRT(NUMER/DENOM)

              TYPE 672,NORML
672           FORMAT(1X,'NORML = ',E12.4 )
C
C             CALCULATE  OFI IN SUBSTRATE
C
                DO 675 J= 1,10
C
                        OFI(I,J) = NORML *  EXP(K3*DEPTH(J))
C
675             CONTINUE
C
C
C       INDEX INTO DEPTH ARRAY
C
                T1 = INT(THICKNESS*1E6/.05) + 12
         TYPE 801,T1,DEPTH(T1)
801      FORMAT (1X,I3,1X,E12.4)
C       CALCULATE OFI IN THE FILM
C
C
                DO 680 J = 11,T1
C
                 OFI(I,J) =  COS(K2*DEPTH(J)) + (K3/K2)*SIN(K2*DEPTH(J))
                 OFI(I,J) =  NORML * OFI(I,J)
C
680             CONTINUE
C       CALCULATE OFI FOR AIR
C
                DO 690 J = T1+1,COUNTER
C
               RTEMP = COS(K2*THICKNESS) + (K3/K2)*SIN(K2*THICKNESS)
C
               OFI(I,J) = RTEMP*EXP(-K1*(DEPTH(J)-THICKNESS))
               OFI(I,J) = NORML * OFI(I,J)
C
690             CONTINUE
C
700     CONTINUE
C ***** PRINT OUT RESULTS *****
C
        DO 750 I = 1,NMODES
C
```

```
                TYPE 710
710             FORMAT(1X,' DEPTH ',10X, ' OFI ' )
C
C
                DO 720 J = 1,70
C
                        TYPE 730, DEPTH(J),OFI(I,J)
730                     FORMAT(1X,E12.4,5X,E12.4 )
C
C
720             CONTINUE
C
741             TYPE 740
740             FORMAT(1X,' TYPE C TO CONTINUE ')
C
                ACCEPT 745 ,AA
745             FORMAT( A1 )
                IF(AA.EQ.C)GO TO 750
                GO TO 741
C
C
750     CONTINUE
C
C
C ********** WRITE DATA TO A DISK FILE ********
C
C ********** GET FILE NAME 10 CHARACTERS ONLY *****
C
        TYPE 1000
1000    FORMAT( 1X,' Enter the file name ',$)
C
        ACCEPT 1010,LFN,( FNAME(I),I=1,LFN )
1010    FORMAT(Q,10A1)
C
C
C
        OPEN ( UNIT = 1,NAME = FNAME ,TYPE='NEW')
        WRITE ( 1,820 ) COUNTER
820     FORMAT(1X,I2)
C
        DO 800 I = 1,NMODES
            DO 850 J = 1,COUNTER
               WRITE(1,810) DEPTH(J),OFI(I,J)
810            FORMAT (1X,E12.4,',',E12.4)
850         CONTINUE
800     CONTINUE
C
C
        CLOSE ( UNIT = 1 )
        STOP
C
10000     TYPE 10010,BETA/K,NFILM
10010     FORMAT(1X,'Stop calculation beta=',F6.5,2X,'nfilm ='F6.5)
C
          END
C
C ********** FUNCTION AREA **********
C
        FUNCTION ASIN(X)
```

```
      DOUBLE PRECISION X
C
      ASIN = ATAN(X/SQRT(1-X**2))
C
      RETURN
      END
```

The vita has been removed from the scanned document